ECMWF COPERNICUS REPORT

Copernicus Atmosphere Monitoring Service

# Validation of the CAMS regional services: concentrations above the surface

## Status update for the period September-November 2020

Issued by: KNMI

Date: 19 March 2021

Ref: CAMS84_2018SC3_D4.1.1-SON2020.pdf

IMPLEMENTED BY ECMWF

# Validation of the CAMS regional services: concentrations above the surface

## Status update for the period September-November 2020

***AUTHORS:***
D. Akritidis (AUTH), T. Antonakaki (AA), Y. Bennouna (CNRS-LA), A.-M. Blechschmidt (IUP-UB), T. Bösch (IUP-UB), H. Clark (CNRS-LA), C. Gielen (BIRA-IASB), F. Hendrick (BIRA-IASB), J. Kapsomenakis (AA), S. Kartsios (AUTH), E. Katragkou (AUTH), D. Melas (AUTH), A. Mortier (MetNo), E. Peters (IUP-UB), K. Petersen (MPI), A. Piters (KNMI), A. Richter (IUP-UB), M. van Roozendael (BIRA-IASB), M. Schulz (MetNo), N. Sudarchikova (MPI), A. Wagner (MPI), P. Zanis (AUTH), C. Zerefos (AA)

***EDITORS:***
J. Douros (KNMI), H.J. Eskes (KNMI)

**REPORT OF THE COPERNICUS ATMOSPHERE MONITORING SERVICE, VALIDATION SUBPROJECT (CAMS-84).**

***CITATION:***
Douros, J., H.J. Eskes, D. Akritidis, T. Antonakaki, Y. Bennouna, A.-M. Blechschmidt, T. Bösch, H. Clark, C. Gielen, F. Hendrick, J. Kapsomenakis, S. Kartsios, E. Katragkou, D. Melas, A. Mortier, E. Peters, K. Petersen, A. Piters, A. Richter, M. van Roozendael, M. Schulz, N. Sudarchikova, A. Wagner, P. Zanis, C. Zerefos, Validation of CAMS regional services: concentrations above the surface, Status update for September - November 2020, Copernicus Atmosphere Monitoring Service (CAMS) report, CAMS84_2018SC3_D4.1.1-SON2020, March 2021, doi:10.24380/hzgz-xy79.

***STATUS:***
Version 1.0

***DATE:***
19 March 2021

***REF:***
CAMS84_2018SC3_D4.1.1-SON2020

## Executive Summary

The Copernicus Atmosphere Monitoring Service (CAMS, http://atmosphere.copernicus.eu) is a component of the European Earth Observation programme Copernicus. The CAMS service consists of two major forecast and analysis systems. First, the CAMS global near-real time (NRT) service provides daily analyses and forecasts of reactive trace gases, greenhouse gases and aerosol concentrations, and is based on the ECMWF Integrated Forecast System (called CAMS-global in this document). Secondly, nine models in Europe, perform air quality forecasts and analyses on a daily basis, nested within CAMS-global. Based on these individual forecasts and analyses, an ensemble forecast of air quality over Europe is produced and disseminated by Météo-France (called ENSEMBLE or CAMS-regional below). The regional members use the global forecasting results as boundary conditions at the sides and top of the domain.

This document reports on two validation activities, namely

- an evaluation of the consistency between the global and regional modelling components of CAMS, focussing on the boundaries of the regional domain, and
- an evaluation of the regional ENSEMBLE and the nine individual models contributing to the ensemble with independent observations, focusing on the concentrations above the surface.

The current analysis includes ozone ($O_3$), nitrogen dioxide ($NO_2$), aerosol (PM10/PM2.5/AOD) and carbon monoxide (CO) forecasts covering the period up to November 2020.

The forecasts from the regional models were compared with the following set of observations:

- aerosol lidar observations from the EARLINET network;
- aerosol AOD observations from the AERONET network;
- IAGOS routine aircraft measurements of ozone and CO;
- ozone sonde profiles;
- MAX-DOAS $NO_2$ tropospheric columns;
- GOME-2/MetOp-A $NO_2$ satellite tropospheric column retrievals (IUP-UB v1.0 product);
- high-altitude ozone surface stations;
- CO and $O_3$ from GAW mountain stations; and
- CO observations from the MOPITT satellite instrument.

These observations are available to CAMS within one month after the observations were made.

This report is based on regional model data available for the months May 2016 to November 2020, with a focus on September – November 2020 (SON2020). The report is updated every 3 months. The main results are summarised below, focusing on the performance of the regional ensemble. Detailed results, also for the individual models, are presented in sections 3 to 11, and each of these sections starts with a summary of the main results. Model specific findings are summarised in section 12.

The last upgrade implemented in CAMS-global was on 6 October 2020, while the lust upgrade for the CAMS regional models happened on 25 November 2020, implementing new anthropogenic emissions and making available an additional pollen species.

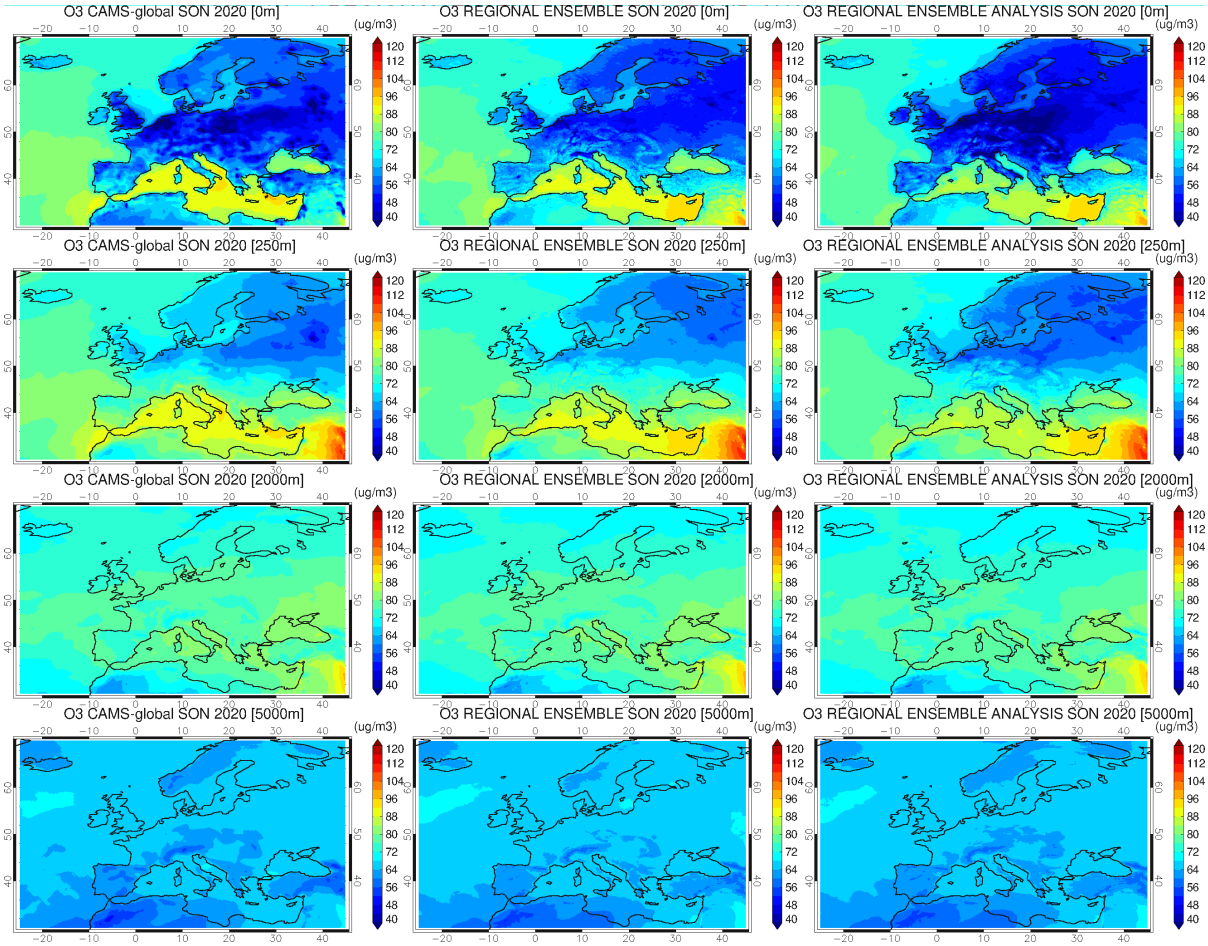


Figure S.1. CAMS global ozone forecast for day 1 (left), CAMS regional ENSEMBLE ozone forecast for day 1 (middle), CAMS regional ENSEMBLE ozone analysis (right). From top to bottom: 0, 250, 2000, 5000m altitude level. The results are averaged over the September - November 2020 period.

**General conclusions for the individual regional models**

Regional models in general appear to have efficiently implemented the use of global CAMS boundary conditions and provide 3D fields that are comparable to those of the global model.

For ozone, bias and correlation at GAW and EEA e-reporting high altitude surface stations show small spread among most of the models and improved performance by the analysis product. Comparisons with ozone sondes provide an even more favourable picture as the spread is even smaller.

For $NO_2$, validation with MAX-DOAS shows as sizeable spread between individual models, especially when considering the diurnal cycles. However, most of the simulated values probably fall within the uncertainty range of MAX-DOAS retrievals. The overall spatial distribution of tropospheric $NO_2$ as seen by GOME-2A/MetOp-A is reproduced by the regional models, but values over central European emission hotspots are underestimated by most models.

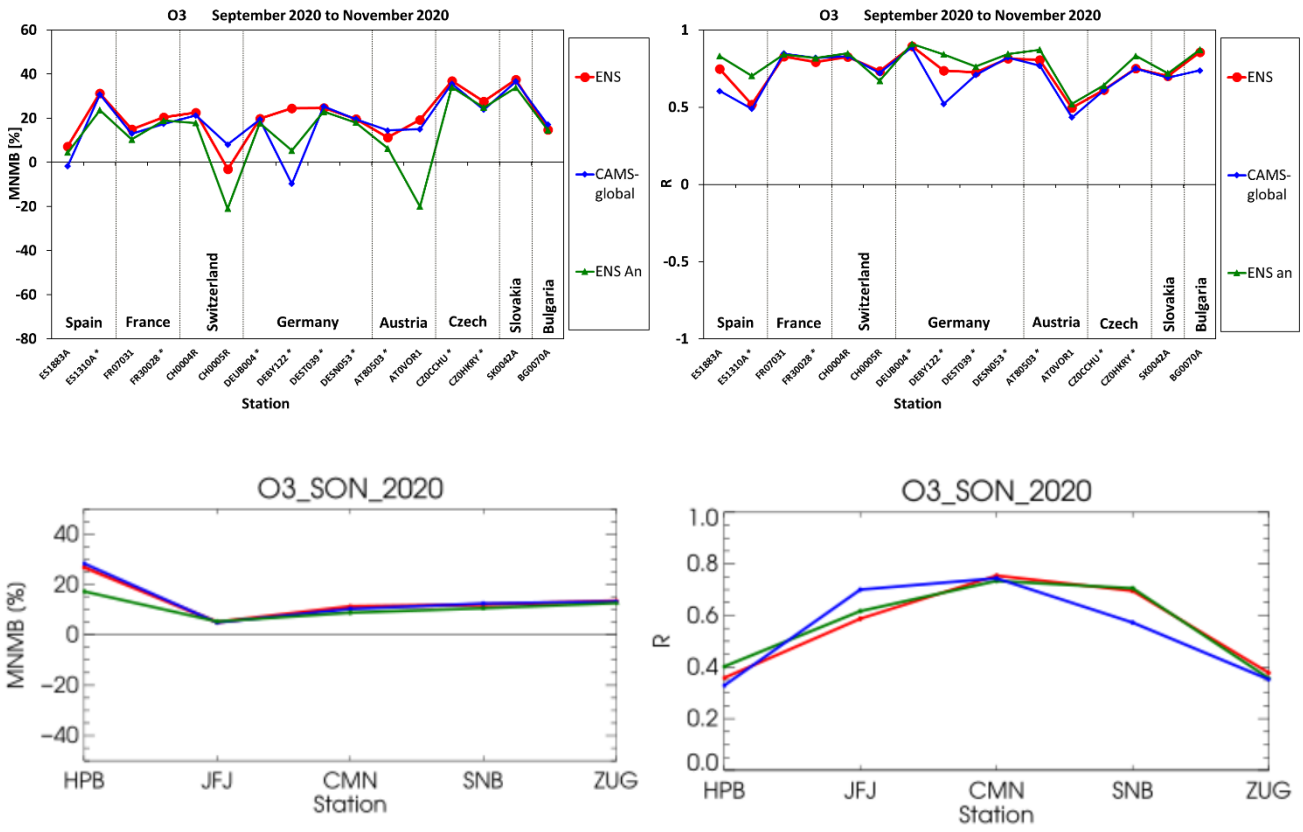


Figure S.2. Normalised bias (left) and correlation coefficient (right) for ozone for the high-altitude (above 1 km) EEA Air Quality e-reporting stations (top) and the 5 high-altitude European GAW stations (bottom). Lines represent ENSEMBLE forecast (solid red), ENSEMBLE analysis (solid green) and CAMS-global system (blue) for September - November 2020. The horizontal axis is the station identifier referring to Hohenpeissenberg (HPB), Jungfraujoch (JFJ), Monte Cimone (CMN), Sonnblick (SNB) and Zugspitze (ZUG).

For CO, comparisons at GAW mountain stations show a slightly negative bias and small model spread for the forecasts. For the analyses, bias is positive for some models and spread is quite higher. The latter is especially true for the correlation coefficient. Comparisons with MOPITT retrievals show an underestimation over land and some local overestimations over the ocean for most models.

For PM, observations from the EARLINET and AERONET networks reveal that the order of magnitude in extinction is similar between the models and the lidar profiles at most locations, while the decrease in extinction with height seems to be generally steeper in the observations.

**General conclusions for the regional ENSEMBLE**

The comparison of the European regional CAMS ENSEMBLE air quality forecasts and analyses against above-surface observations of $O_3$, $NO_2$, CO for the period up to the 1st of December 2020 demonstrates that overall, the biases observed are small, often within the uncertainty of the validation approach while temporal correlations for ozone and CO are reasonable. Performance of the ENSEMBLE analysis product is found to be generally superior to that of the ENSEMBLE forecasts. The ENSEMBLE performs generally better than any of the individual models for ozone, $NO_2$ and CO, showing the strength of the ensemble approach adopted in CAMS.

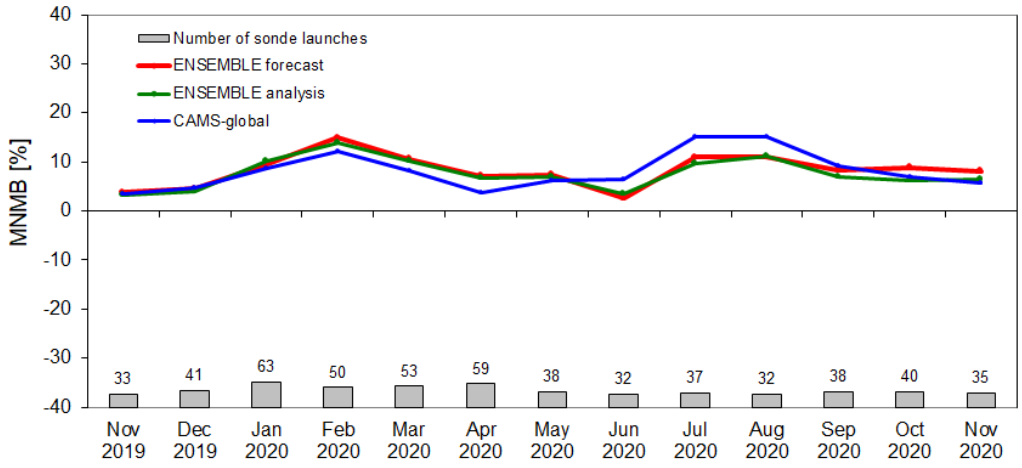


Figure S.3. Modified normalised mean bias (MNMB) against ozone sondes for the regional ENSEMBLE forecasts (red) and analyses (green) from November 2019 to November 2020 (horizontal axis). Ozone was averaged over the lower-middle free troposphere region, 500 hPa < p < 850 hPa.

**Ozone**

At the boundaries of the regional domain, the ENSEMBLE agrees well with CAMS-global, indicating that the implementation of the boundary conditions was done properly. Over the full domain there is a good match between the global and regional CAMS analyses and forecasts between 1 and 5 km altitude. These results are similar to previous quarters.

The differences between the global and regional systems reveal themselves in the boundary layer and at the surface over land, as expected. A comparison of the regional analysis product with the regional day 1 forecast (Fig. S.1) shows some differences between the regional ENSEMBLE forecast and analysis, with the analysis generally having lower concentrations near the surface.

For high altitude stations, Fig. S.2, mostly an overestimation between up to 35% is observed for the ENSEMBLE first day forecast, while comparison against ozone sondes shows a milder overestimation in the 6-25% range (also Fig. S.3). Time correlations at high-altitude and GAW stations range between 0.35 and 0.89 during this period with generally improved figures for the ENSEMBLE analyses as compared to the ENSEMBLE forecast in the case 3 out of the 5 GAW stations.

**Nitrogen dioxide ($NO_2$)**

The overall spatial distribution of tropospheric $NO_2$ as observed from space by GOME-2A is reproduced by the ENSEMBLE during SON2020 (Fig. S.4) with better results by the analysis compared to the forecast. As described in previous reports, winter values over European emission hotspots simulated by the regional ENSEMBLE analysis, forecasts and CAMS-global show significantly smaller values than GOME-2A, the observed inter-annual variability is therefore not reproduced. Values over European emission hotspots are better represented by the regional ENSEMBLE analysis and forecasts than by CAMS-global, although this difference is not so evident this quarter, possibly due to the effects of COVID19 related restrictions.

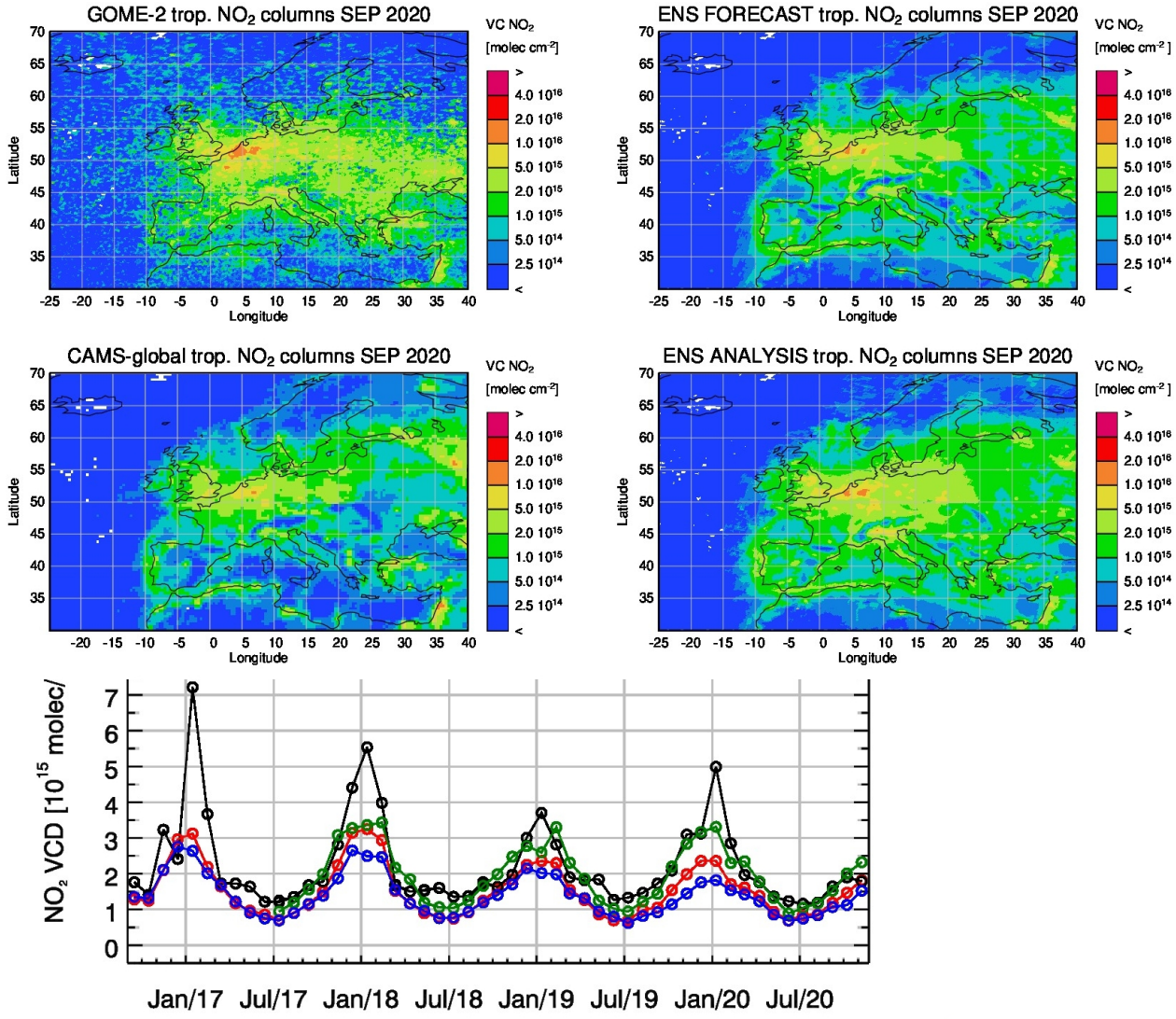


Figure S.4. Maps of satellite-retrieved and model-simulated tropospheric $NO_2$ columns [molecules $cm^{-2}$] for September 2020 for GOME-2A (top left), regional ENSEMBLE forecasts (top right) CAMS-global forecasts (middle left) and regional ENSEMBLE analyses (middle right). The panel at the bottom shows corresponding time series of average tropospheric $NO_2$ columns [$10^{15}$ molecules $cm^{-2}$] from GOME-2A (black), regional ENSEMBLE forecasts (red), CAMS-global forecasts (blue) and regional ENSEMBLE analyses (green). GOME-2A data were gridded to regional model resolution (i.e., 0.1° x 0.1°). Model data were treated with the same reference sector (25°W - 20°E) subtraction approach as the satellite data and linearly interpolated to the satellite overpass time (9:30 LT).

Systematic uncertainties in the retrievals (on average on the order of 20% – 30% over polluted regions) depend on the season, with winter values and especially January in mid and high latitudes normally associated with larger error margins. Conclusions may differ for comparisons to other satellite $NO_2$ products (e.g., TEMIS GOME-2, http://www.temis.nl). We note that since the CAMS-global upgrade of 26 June 2018, GOME-2A observations are assimilated by the global system. This is, however, a different retrieval product than the one used for validation reported here (University of Bremen retrieval).

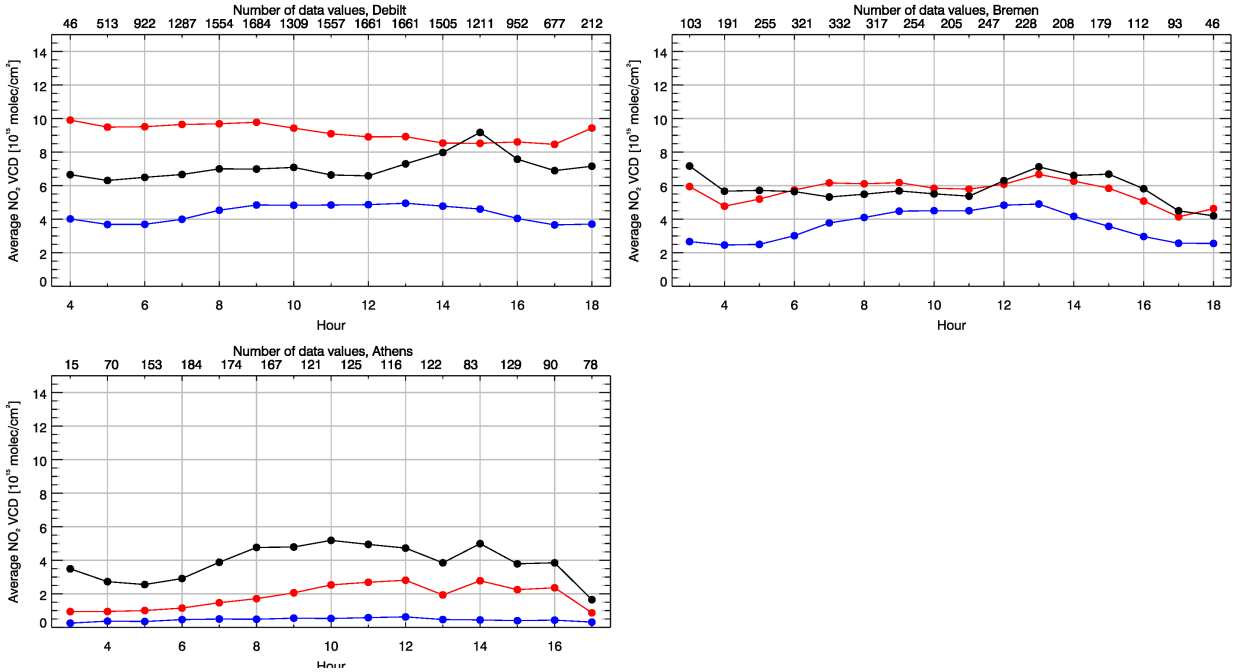


Figure S.5: Diurnal cycles (averages over hourly bins) of tropospheric $NO_2$ VCDs [$10^{15}$ molec. $cm^{-2}$] from MAX-DOAS and models for De Bilt (the Netherlands) (top left), Bremen (Germany) top right and Athens (Greece) (bottom). The coloured lines show (black) MAX-DOAS retrievals, (red) regional ENSEMBLE forecasts and (blue) CAMS-global. Period: June – November 2020.

Comparisons to ground based remote sensing MAX-DOAS retrievals at three different European stations (see Figure S.5) for the time period of SON 2020 show that regional ENSEMBLE forecasts are closer to the urban station observations of Bremen and Athens than CAMS-global, mainly attributed to the difference in spatial resolution. For De Bilt, CAMS-global performs better than the regional ENSEMBLE. However, this may change with the next reports when more months of data will be included. The performance of simulations for diurnal cycles of tropospheric $NO_2$ columns depends on the location, but generally shows a moderate performance for the ENSEMBLE products at the three stations.

**Aerosol / PM**

The regional models are compared with EARLINET climatological lidar profiles for the same season (data from 2006-2020), Fig. S.6. The standard dissemination of CAMS-regional forecasts does not include information on composition, size and humidity growth of the aerosol in the models. This introduces considerable uncertainty to the PM derived extinction, which conservatively spans a factor 10 for absolute extinction values. Relative differences among nearby stations and the form of extinction profiles are more certain. The order of magnitude in extinction is similar between the ENSEMBLE and the lidar profiles, with Ispra, Italy, close to the Alps and Granada, Spain being the most notable exceptions. The decrease in extinction with height seems to be generally steeper in the observations.

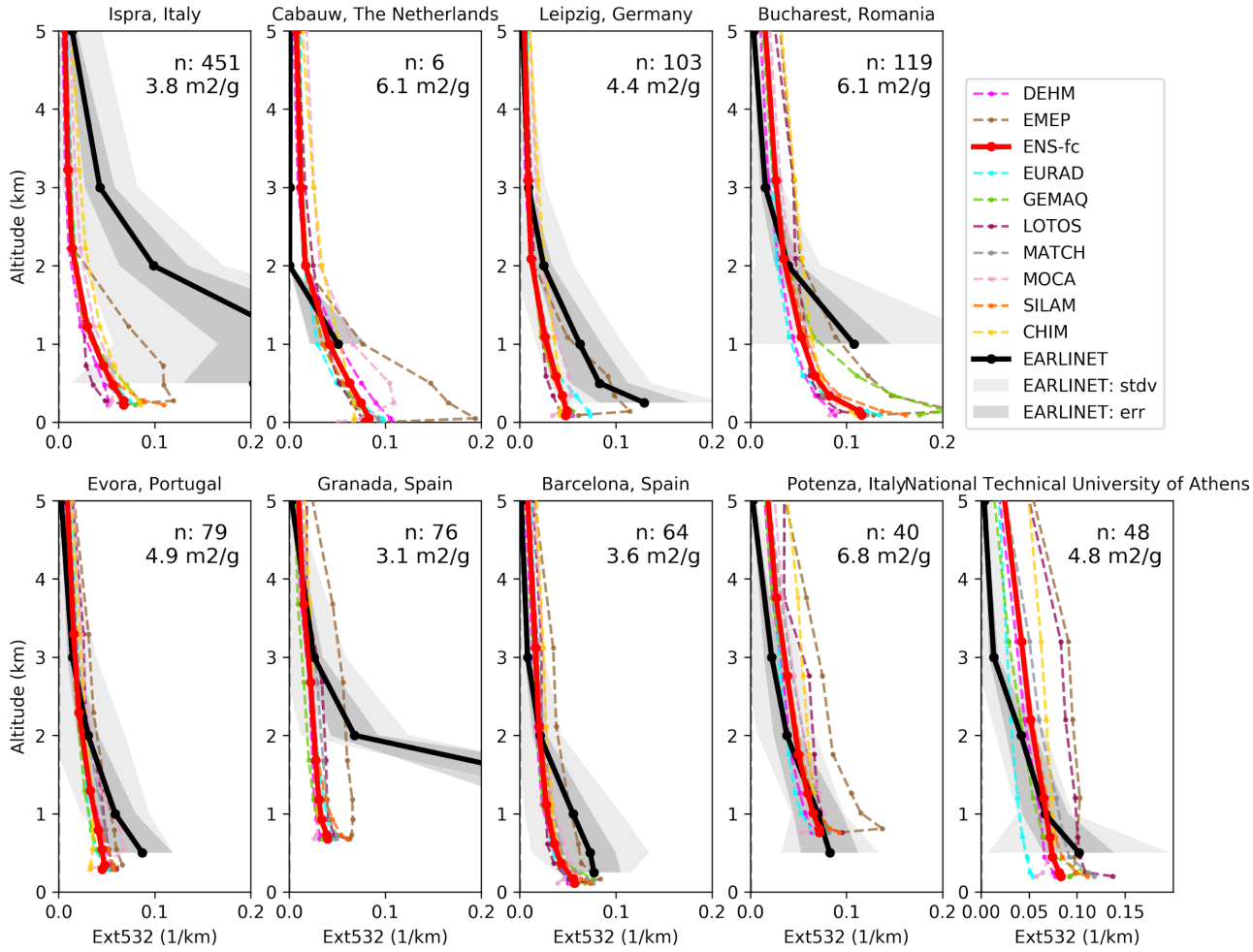


Figure S.6. Extinction profiles September - November 2020 derived from the ENSEMBLE forecast mass concentration profiles (red envelope) and from EARLINET (climatology) backscatter profiles (grey envelope: lidar ratio uncertainty, light grey: including sampling error). "n: XX means number of individual EARLINET profiles assembled (September - November 2006-2018). The EMC used for the calculation of the extinction from the concentration profiles is indicated for each station below the number of EARLINET profiles "n" used for the calculation of the climatology.

The PM10 concentrations in the regional ENSEMBLE forecasts and analyses are similar, but larger PM values are observed for the analysis over some areas of Central and Western Europe at the surface level, see Figure S.7. CAMS-global continues to show higher dust loads over the Mediterranean. The agreement between CAMS-global and the ENSEMBLE products is better for PM10 and PM2.5 in the upper layers compared to the lower layers, as expected. For PM2.5 the difference between the CAMS-global and CAMS-regional is more pronounced than for PM10 within the PBL especially for dust near the southern boundary and over the Middle East (exceeding 50 µg/m$^3$).

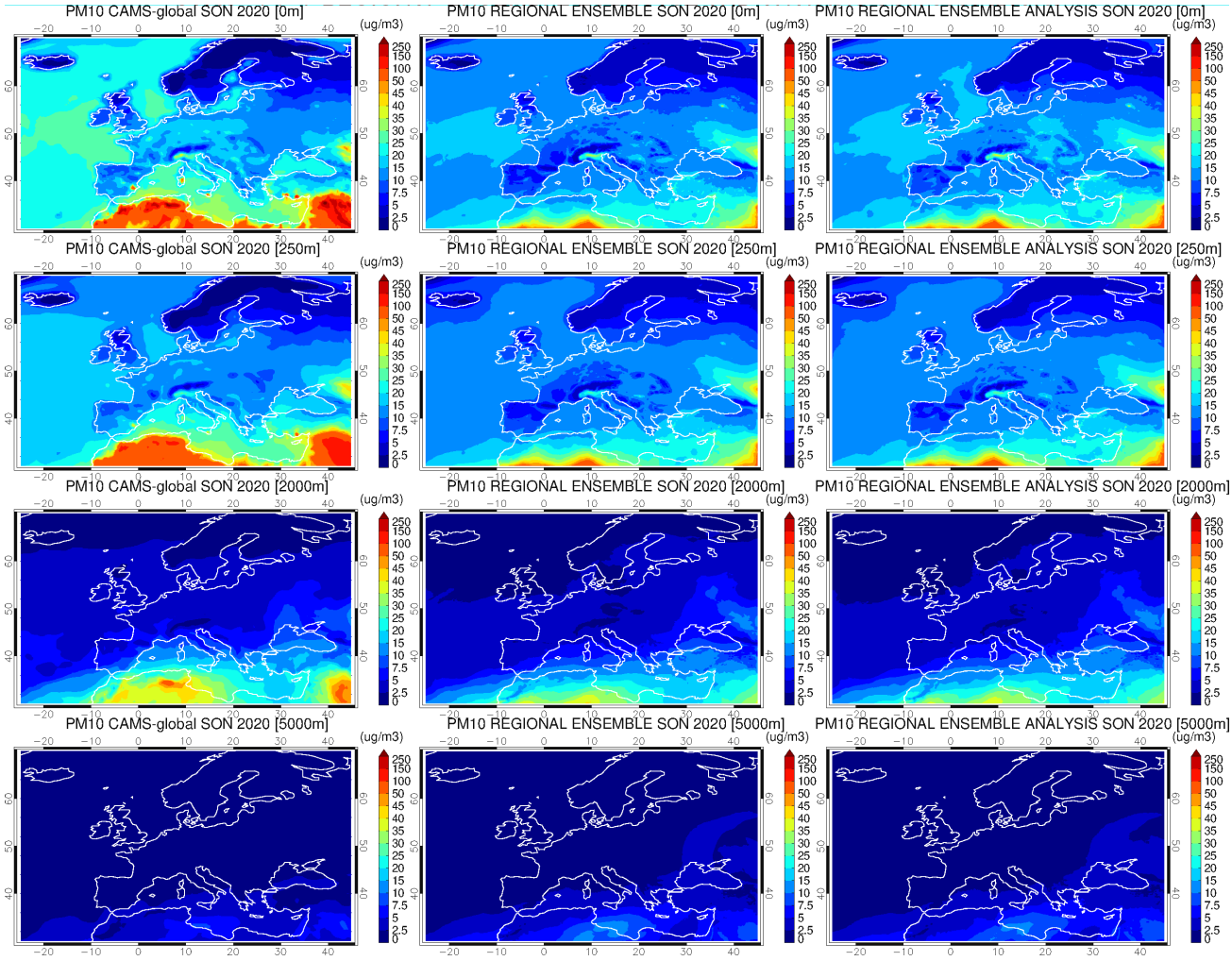


Figure S.7. CAMS global PM10 forecast for day 1 (left), CAMS regional ENSEMBLE PM10 forecast for day 1 (middle), CAMS regional PM10 analysis (right). From top to bottom: 0, 250, 2000, 5000m altitude level. Period: September to November 2020.

**Carbon monoxide (CO)**

Comparison at the GAW stations reveal biases between -8% and 10% for the analysis and between -12% and 1% for the forecast, while temporal correlations coefficients are between 0.5 and 0.79 for the analysis and between 0.7 and 0.8 for the forecast (Fig. S.8).

Comparisons with MOPITT CO satellite observations (version 8, Fig. S.9) data also show an underestimation of CO values over the land part of the domain and overestimation over the ocean part are within 20% in September and within 10% in October and November, with some regional exceptions. Relatively high CO values are seen however over several northern regions of Europe (e.g., Norwegian Sea, north of Germany, Lithuania). In October and November, the values are relatively low, especially over Spain in November. Note that due to the COVID-19 measures we may expect changes (reductions) in anthropogenic emissions which are not included in the emission inventories used by the models.

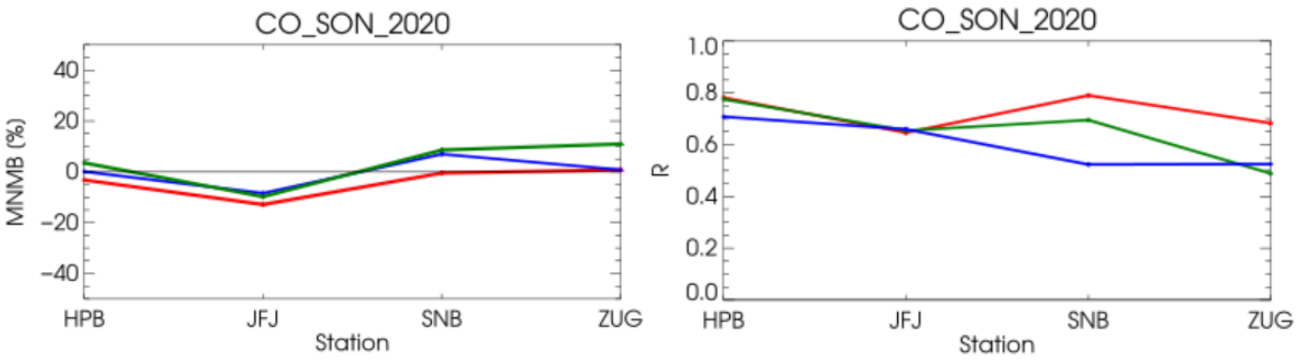


Figure S.8. MNMBs [%] (top) and correlation coefficients (bottom) for CO regional ENSEMBLE forecasts (red), analyses (green) and CAMS-global (blue) compared to observations at GAW stations. Period: September - November 2020.

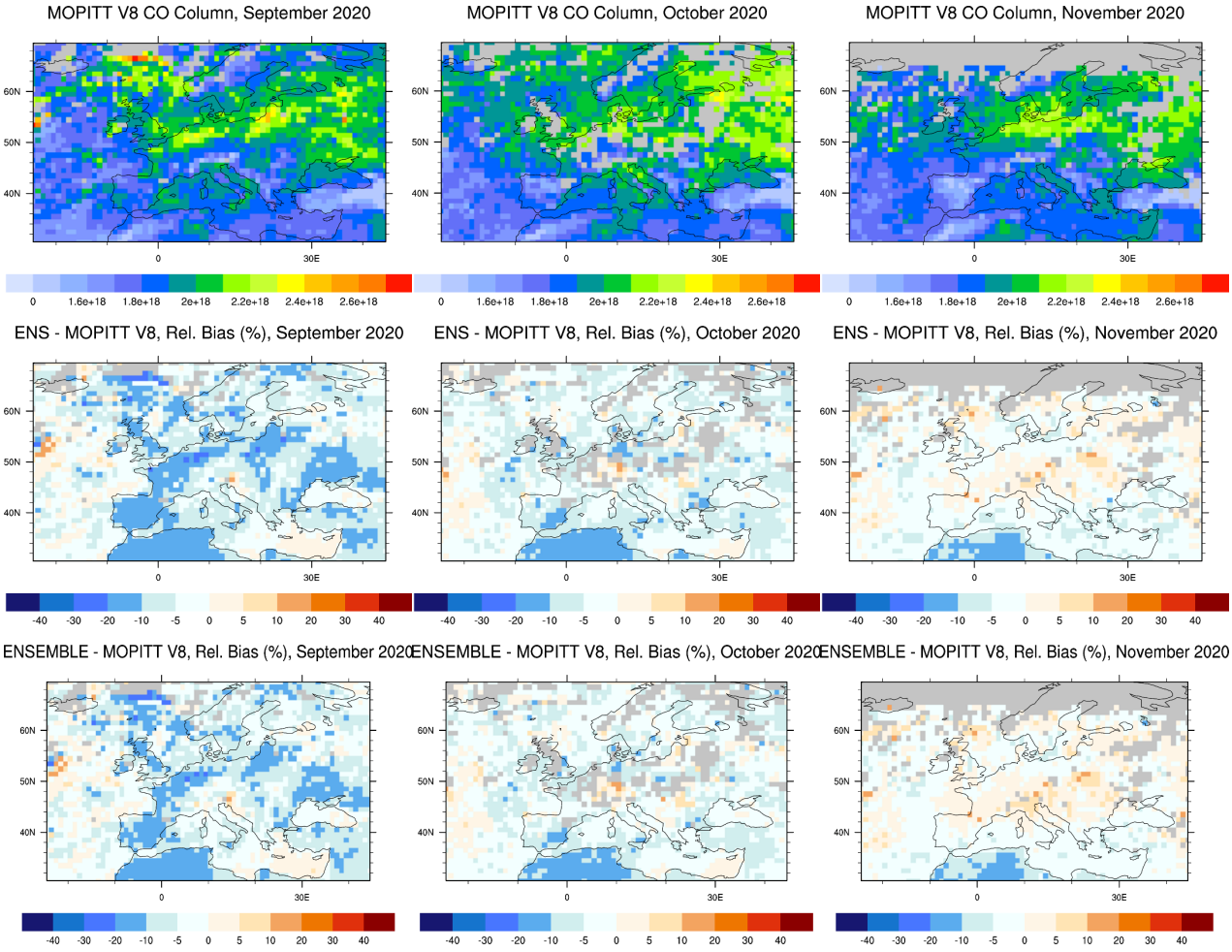


Figure S.9. CO total column for MOPITT v8 satellite retrievals (top row, in molecules/cm$^2$), relative difference between the regional ENSEMBLE forecasts and MOPITT (middle row) and regional ENSEMBLE analyses and MOPITT (bottom row) for September (left column), October (middle column) and November 2020 (right column). Grey colour indicates missing values.

# Table of Contents

# 1 Introduction

The Copernicus Atmosphere Monitoring Service (CAMS, https://atmosphere.copernicus.eu) is a component of the European Earth Observation programme Copernicus. The CAMS near-real time services consist of daily analysis and forecasts with the IFS system with data assimilation of trace gas concentrations and aerosol properties. The global modelling system is also used to provide the boundary conditions for an ensemble of more detailed regional air quality models that are used to zoom in on the European domain and produce 4-day forecasts of air quality. The regional forecasting service provides daily 4-days forecasts of the main air quality species and analyses of the day before, based on the results from 9 state-of-the-art atmospheric chemistry models. The ensemble represents the median of these 9 model forecasts.

Routine validation of the regional models against surface observations from the European member states (EEA Air Quality e-reporting) is provided for each model individually as well as the ENSEMBLE in separate quarterly validation reports. Validation reports of the CAMS regional products are available in the following portal:
https://atmosphere.copernicus.eu/regional-air-quality-production-systems.
This web page provides access to the quarterly reports on the daily analyses and forecast activities and verification of the regional ENSEMBLE. An overview of the regional air quality forecasting system is provided by Marécal et al (2015).

Validation reports (e.g. Wagner et al., 2020) for the CAMS global products are available at https://atmosphere.copernicus.eu/node/325, including the evaluation on Earth's troposphere, stratosphere, aerosols and greenhouse gases, with state-of-the art observational datasets (GAW, IAGOS, MOPPIT, EMEP, GOME-2A, OMPS-LP, BASCOE, AERONET etc.). A published overview on the validation of reactive gases and aerosols in the global analysis and forecast system can be found in Eskes et al (2015). A validation study of the global surface ozone reanalysis for Europe is provided by Katragkou et al (2015).

Details of the various observational datasets can be found in Eskes et al. (2021), "Observations characterisation and validation methods document", also available at:
https://atmosphere.copernicus.eu/eqa-reports-global-services.

This document presents an evaluation of the concentrations above the surface as modelled by the set of the 9 individual regional models and the ensemble median derived from those 9 individual forecasts and analyses, as well as the consistency between the global and regional modelling systems of CAMS.

# 2 Regional and global CAMS forecasting systems

## 2.1 Regional models

The European Air Quality products are provided from the Copernicus Atmosphere Monitoring Service (http://atmosphere.copernicus.eu/). These data are available in NetCDF or Grib-Edition2 format. The files are available each day through ftp protocol from the Météo-France server (ftp.cnrm-game-meteo.fr). Since the beginning of February 2020, the data are also available through the Atmosphere Data store (https://ads.atmosphere.copernicus.eu), although the reliability of data retrievals from was relatively low during this quarter. The products are available in Near Real Time (NRT) for four forecast days, following the protocol below:

- Each day 96h model forecasts and 24h analyses for the previous day are provided with hourly resolution. Consistent provision of the analysis product started on the 5th of July 2017.
- Products are available at eight vertical height levels: surface, 50, 250, 500, 1000, 2000, 3000, 5000 meters.
- The pollutants are $O_3$, CO, $NO_2$, $SO_2$, PM2.5, PM10, NO, $NH_3$, NMVOC, PANs, dust aerosols (fraction below 10µm), secondary inorganic aerosols (fraction below 2.5µm), birch, grass, olive, ragweed and alder pollen. Since the upgrade of February 4$^{th}$, 2020 three new aerosol species (PM from wildfires, EC from fossil fuels and EC from wood burning) are also available.
- The regional datasets cover the longitudes 335.05°E to 44.95°E every 0.1°, and latitudes 71.95°N – 30.05°N also at 0.1° resolution (~10km).
- The forecasts until the 48$^{th}$ hour are available before 7:30 UTC
- The forecasts for the 49-96$^{th}$ hour are available before 9:30 UTC
- The analyses are provided before 12:00 UTC
- Since the February 2020 upgrade, the regional models make use of the CAMS-REG-AP_v3_1 emissions (reference year: 2016) and since November 25$^{th}$, the updated CAMS-REG-AP_v4_2 emissions dataset (reference year: 2017).

The NRT forecast and analysis regional air quality data are available for the nine air quality models and their ensemble median (CAMS-regional or ENSEMBLE):

- MOCAGE model (MFM)
- LOTOS-EUROS model (KNM)
- EMEP MSC-W model (EMP)
- MATCH model (SMH)
- EURAD-IM model (RIU)
- CHIMERE model (CHI)
- SILAM model (FMI)
- DEHM model (DEM)
- GEM-AQ model (GEM)

Before October 16th, 2019 the regional ensemble was calculated based on 7 regional models (except for DEHM and GEM-AQ). This is the second quarterly report which explicitly includes results and analysis from those two new models.

Every evening, a full download of the 96h forecasts and 24h analyses fields to KNMI at full resolution is performed. These fields are co-located to the set of surface stations used, and this largely reduced datasets is shared with all validation partners.

Documentation about the regional models may be found at the address https://atmosphere.copernicus.eu/regional-air-quality-production-systems. For the purposes of this report however, it's useful to indicate what kinds of observations are actively assimilated in each model (Table 2.1).

Table 2.1: Surface and other observations that are actively assimilated in regional models.

| **Model** | **Method** | **Surface** | **Other** |
|---|---|---|---|
| CHIMERE | Kriging | $O_3$, $NO_2$, PM10, PM2.5 | |
| EMEP | Intermittent 3D-var | $O_3$, $SO_2$, $NO_2$, CO, PM10, PM2.5 | OMI $NO_2$ |
| EURAD | Intermittent 3D-var | $O_3$, $SO_2$, $NO_2$, PM10, PM2.5 | OMI and MetOp/GOME-2 $NO_2$ and $SO_2$, MOPITT and IASI CO |
| LOTOS-EUROS | Ensemble Kalman filter | $O_3$, $NO_2$, PM10, PM2.5 | OMI $NO_2$ |
| MATCH | Intermittent 3D-var | $O_3$, $NO_2$, CO, PM10, PM2.5 | |
| MOCAGE | 3D-var | $O_3$, $NO_2$, PM10 | |
| SILAM | Intermittent 3D-var | $O_3$, $NO_2$, CO, PM10, PM2.5 | |
| DEHM | Optimal interpolation | $O_3$, $NO_2$ | |
| GEM-AQ | Optimal interpolation | $O_3$, $NO_2$, CO, $SO_2$, PM10, PM2.5 | |

Validation reports of the CAMS regional products are available in the following portal: https://atmosphere.copernicus.eu/regional-services.

Whenever possible, in this report, models follow the naming and colour scheme of Table 2.2.

Table 2.2: Naming and colour scheme followed throughout this report.

| ***Model*** | ***Short model name*** | ***Colour name*** | ***Colour*** |
|---|---|---|---|
| CAMS-global | CAMSg | Blue | |
| ENSEMBLE forecast | ENS-fc | Red | |
| ENSEMBLE analysis | ENS-an | Green | |
| CHIMERE | CHIM | Yellow | |
| EMEP | EMEP | Brown | |
| EURAD | EURAD | Cyan | |
| LOTOS-EUROS | LOTOS | Purple | |
| MATCH | MATCH | Grey | |
| MOCAGE | MOCA | Pink | |
| SILAM | SILAM | Orange | |
| DEHM | DEHM | Fuchsia | |
| GEM-AQ | GEMAQ | Light Green | |

## 2.2 Global CAMS system based on the ECMWF IFS model

The CAMS-global operational assimilation/forecast system consists of the IFS-CB05 chemistry combined with the MACC aerosol model. The chemistry is described in Flemming et al. (2015); aerosol is described by the bulk aerosol scheme (Morcrette et al., 2009). Dissemination of CAMS-global forecasts is twice a day, at about 10:00 and 22:00UTC. The forecast length is 120 h. Users can get access at https://atmosphere.copernicus.eu/catalogue. Table 2.3 provides information on the satellite data used in CAMS-global.

Table 2.3: Satellite retrievals of reactive gases and aerosol optical depth that are actively assimilated in CAMS-global.

| Instrument | Satellite | Provider | Version | Type | Status |
|---|---|---|---|---|---|
| MLS | AURA | NASA | V4 | $O_3$ Profiles | 20130107 - |
| OMI | AURA | NASA | V883 | $O_3$ Total column | 20090901 - |
| GOME-2 | Metop-A | Eumetsat | GDP 4.8 | $O_3$ Total column | 20131007 - 20181231 |
| GOME-2 | Metop-B | Eumetsat | GDP 4.8 | $O_3$ Total column | 20140512 - |
| GOME-2 | Metop-C | Eumetsat | GDP 4.9 | $O_3$ Total column | 20200505 - |
| SBUV-2 | NOAA-19 | NOAA | V8 | $O_3$ 21 layer profiles | 20121007 - 20201005 |
| OMPS | Suomi-NPP | NOAA / EUMETSAT | | $O_3$ Profiles | 20170124 - 20190409, 20201006 |
| TROPOMI | Sentinel-5P | ESA | | $O_3$ column | 20181204- |
| IASI | MetOp-A | LATMOS/ULB EUMETSAT | - | CO Total column | 20090901 - 20180621 20180622 - 20191118 |
| IASI | MetOp-B | LATMOS/ULB EUMETSAT | - | CO Total column | 20140918 - 20180621 20180622 - |
| IASI | MetOp-C | EUMETSAT | | CO Total column | 20191119- |
| MOPITT | TERRA | NCAR | V5-TIR<br>V7-TIR<br>V7-TIR Lance<br>V8-TIR | CO Total column | 20130129 -<br>20160124 - 20180626<br>20180626<br><br>20190702 |
| OMI | AURA | KNMI | DOMINO V2.0 | $NO_2$ Tropospheric column | 20120705 - |
| GOME-2 | METOP A | Eumetsat | GDP 4.8 | $SO_2$ Total column | 20150902-20200504 |
| GOME-2 | METOP B | Eumetsat | GDP 4.8 | $SO_2$ Total column | 20150902- |
| GOME-2 | METOP C | Eumetsat | GDP 4.9 | $SO_2$ Total column | 20200505- |
| TROPOMI | Sentinel-5P | ESA | | $SO_2$ Total column | 20201005- |
| MODIS | AQUA / TERRA | NASA | Col. 6 Deep Blue | Aerosol total optical depth, fire radiative power | 20090901 - 20150902 - |

| | | | | | |
|---|---|---|---|---|---|
| PMAp | METOP-A<br>METOP-B | EUMETSAT | | AOD | 20170124 -<br>20170926 - |
| GOME-2 | METOP A | Eumetsat | GDP 4.8 | $NO_2$ Tropospheric column | 20180624-20200504 |
| GOME-2 | METOP B | Eumetsat | GDP 4.8 | $NO_2$ Tropospheric column | 20180626- |
| GOME-2 | METOP C | Eumetsat | GDP 4.9 | $NO_2$ Tropospheric column | 20200505- |

The most recent upgrade relevant to this report, was the upgrade to cycle 47R1 which took place on 6 October 2020 and involved a number of changes, including an update in anthropogenic emissions, improved parametrisations sea salt and desert emissions, an improved stratospheric ozone scheme and the assimilation of volcanic $SO_2$ from the Sentinel-5p/TROPOMI.

A detailed changelog and the corresponding validation reports for this last upgrade can be found on the following page:

https://atmosphere.copernicus.eu/cycle-47r1.

Upgrade and version information is available here:
https://atmosphere.copernicus.eu/changes-cams-global-production-system.

Documentation on the global system can be found here:
https://atmosphere.copernicus.eu/global-production-system.

# 3 Consistency between the global and regional modelling components of CAMS

## 3.1 Summary

This chapter reports on the consistency between the global and regional modelling components of CAMS, and the impact of global CAMS boundary conditions on regional forecasts. The current evaluation includes ozone ($O_3$) carbon monoxide (CO) nitrogen dioxide (NO2) and aerosol (PM10/PM2.5) forecasts covering the period from September to November 2020.

**Global and regional ensemble forecasts**: The two forecast products compare well for $O_3$ and CO. Higher surface $NO_2$ concentrations are found in CAMS-global compared to the regional ENSEMBLE over Europe. Higher PM10 and PM2.5 in CAMS-global compared to the regional ENSEMBLE within the boundary layer (mostly seen at the surface) over the Atlantic (sea-salt). Higher PM10 in CAMS-global compared to ENSEMBLE over the southern and south-eastern boundaries of the domain up to 2000 m altitude.

**Regional forecast variability**: The regional ensemble members exhibit the expected regional variability for $O_3$, CO, $NO_2$ and particulate matter. MOCAGE is seen as an outlier in the boundary layer for PM10, showing a strange pattern over the Atlantic, presumably due to sea salt representation. MOCAGE, EURAD, MATCH and DEHM exhibit relatively lower PM10 levels at the south boundary. EMEP, SILAM and GEMAQ have higher PM2.5 levels in the PBL near the south boundaries compared to CAMS-global, while LOTOS-EUROS and MOCAGE have lower PM2.5. CHIMERE has a spurious feature at the $O_3$ and CO boundaries.

**Daily time series.** The temporal correlation between CAMS-global and the regional models is very good for $O_3$, CO and $NO_2$ and mediocre for aerosol.

**Regional forecast and analysis**: The comparison of regional analyses and forecasts shows strong model and species dependence.

## 3.2 Methodology for the comparisons of CAMS-global and CAMS-regional

***Operational download***

The daily regional CAMS forecasts are retrieved on a daily basis by the AUTH-server. This includes the 3-hourly (0,3,6,9 etc.) regional forecast data (ensemble members and regional ENSEMBLE) for all provided species at all vertical layers for the 5 forecast days extracted from the Météo-France ftp server, and the 3-hourly (0, 3, 6, 9 etc.) global forecast data for 5 forecast days extracted from the ECMWF CAMS ftp server

***Methodology of global-regional comparison***

The following methodology is used to a) convert CAMS-global species from mass mixing ratio (kg/kg) to concentration (μg/m$^3$) and, b) extract CAMS-global species concentrations from the vertical levels that lie closest to the regional height levels.

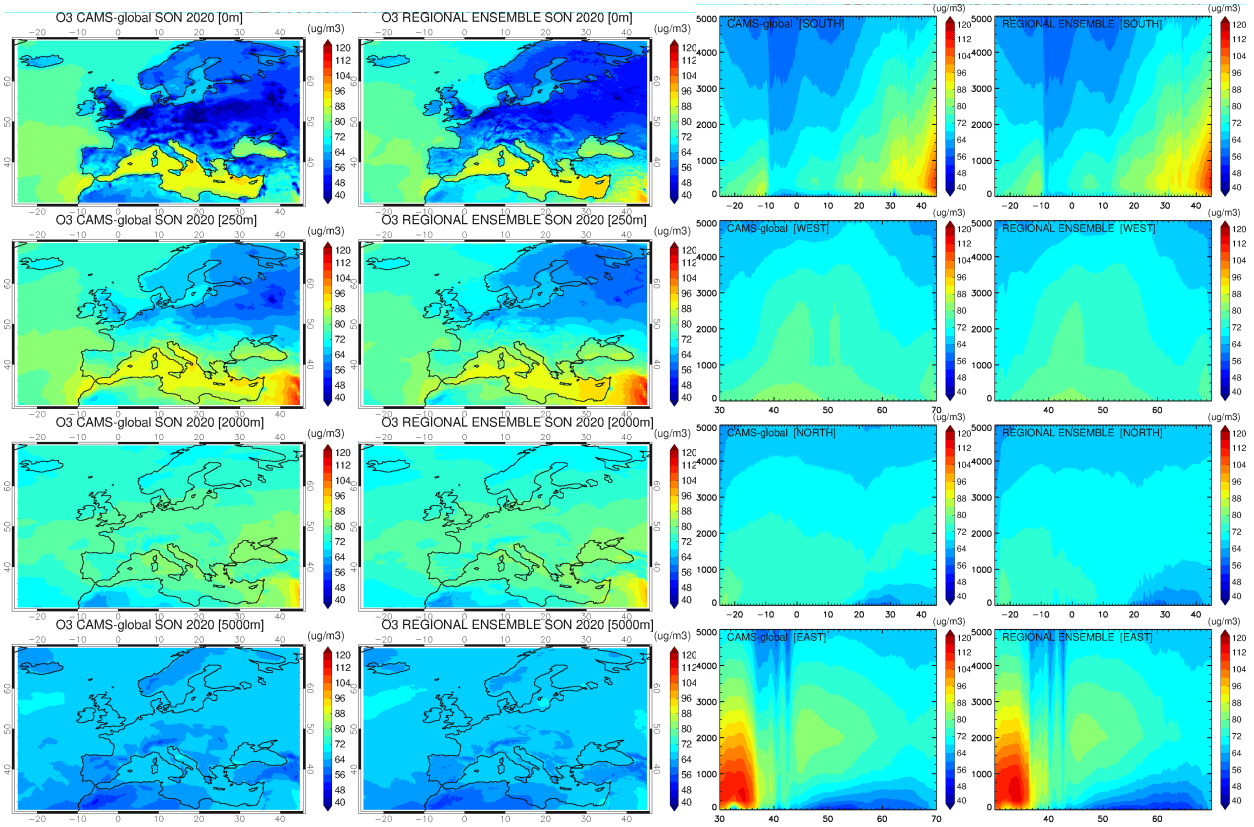


Figure 3.1. Left: Mean global and regional ENSEMBLE forecast ozone fields for four different vertical layers (0, 250, 2000, 5000 m) for SON2020. Right: Cross sections for the same period of the global and regional ENSEMBLE ozone boundaries (south, west, north, east).

The following parameters are used from the CAMS-global model: hybrid layer coefficients; temperature, surface pressure; "GEMS" ozone; carbon monoxide; "aermr01-11" and "aermr16-18" (aerosol species, kg/kg). Data from the first 78 vertical layers (from the surface) are used.

The thickness of each vertical layer Δz (m) is calculated:

$$\Delta z_k = \frac{R * T_k}{M_{air} * g} * \ln\left(\frac{p_{i_{k+1}}}{p_{i_k}}\right) \qquad (E.1)$$

where R=8.314 J/mol·K the gas constant, T the temperature at vertical layer midpoint, $M_{air}$=28.97·10$^{-3}$ kg/mol the molecular weight of air and g=9.8 m/s$^2$ the gravity acceleration.

The mass-mixing ratio (kg/kg) for ozone (go3) and carbon monoxide (CO) is initially provided. Conversion from mass mixing ratio (kg/kg) to concentration (μg/m$^3$) is performed using the following approach:

$$\rho_{O3} = mmr_{O3} * \left(\frac{p_m * M_{air}}{R * T}\right) \qquad (E.2)$$

where $\rho_{O3}$ is the ozone concentration (kg/m$^3$) and $mmr_{O3}$ the ozone mass mixing ratio (kg/kg). The expression inside the parentheses in E.2 corresponds to the air concentration (kg/m$^3$). The same approach is also used for the CO unit conversion from kg/kg to μg/m$^3$.

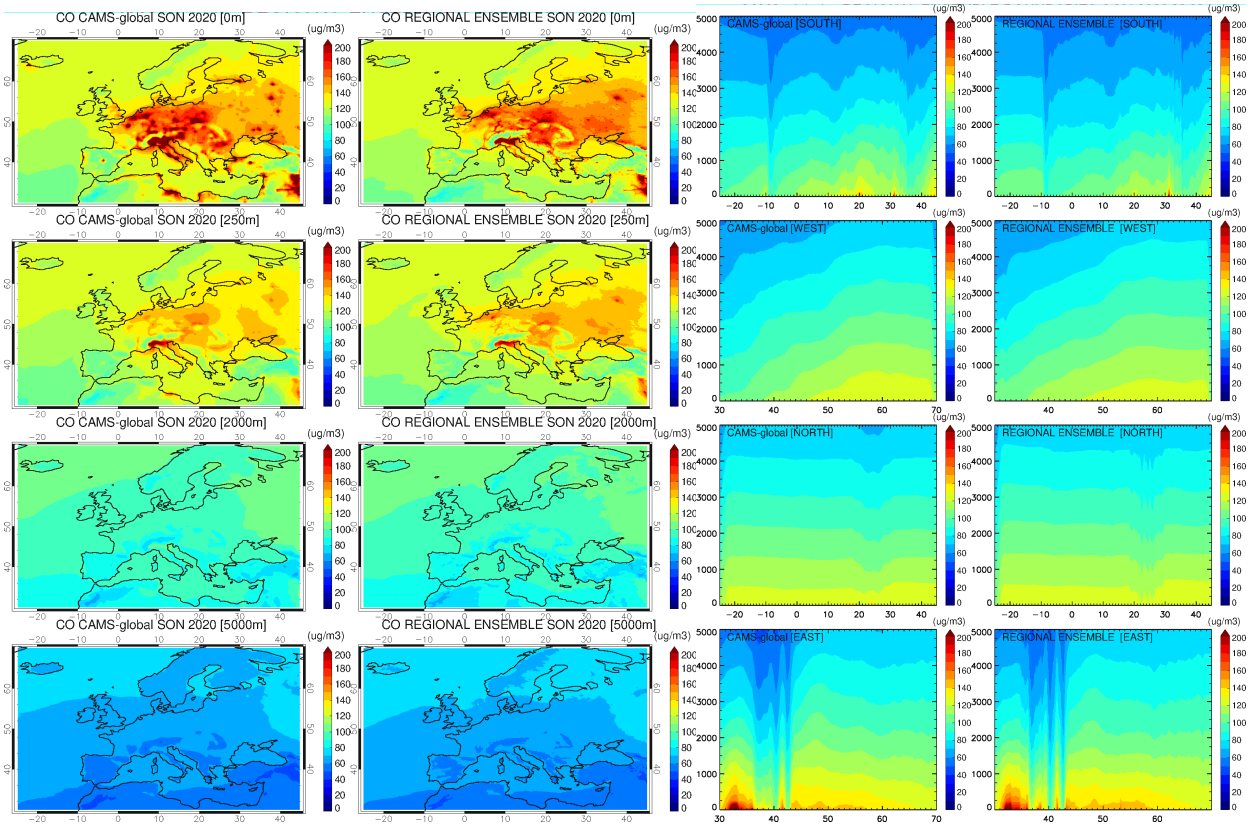


Figure 3.2. Left: Mean global and regional ENSEMBLE forecast CO fields for four different vertical layers (0, 250, 2000, 5000 m) for SON2020. Right: Cross sections for the same period of the global and regional ENSEMBLE CO boundaries (south, west, north, east).

The mass mixing ratio for all aerosol species (see Table 3.1) is initially provided. The PM10 and PM2P5 species are converted to μg/m$^3$ as follows:

$$\rho_{PM10} = \left[\frac{aermr01}{4.3} + \frac{aermr02}{4.3} + aermr04 + aermr05 + 0.4 * aermr06 + aermr07 + aemr08 + aermr11 + aerm09 + aermr10 + aermr16 + aemr17 + aermr18\right] * \left(\frac{p_m}{R_{spec} * T}\right) \quad (E.3)$$

$$\rho_{PM2P5} = \left[\frac{aermr01}{4.3} + \frac{aermr02 * 0.5}{4.3} + aermr04 + aermr05 + 0.7 * aermr07 + 0.7 * aermr08 + 0.7 * aermr11 + aermr09 + aermr10 + 0.7 * aermr16 + 0.25 * aermr17 + 0.7 * aermr18\right] * \left(\frac{p_m}{R_{spec} * T}\right) \quad (E.4)$$

where $R_{spec}$=287.058 J/(kg·K) is the specific gas constant for dry air. The expression inside the parentheses in E.3 and E.4 corresponds to the dry air concentration (kg/m$^3$).

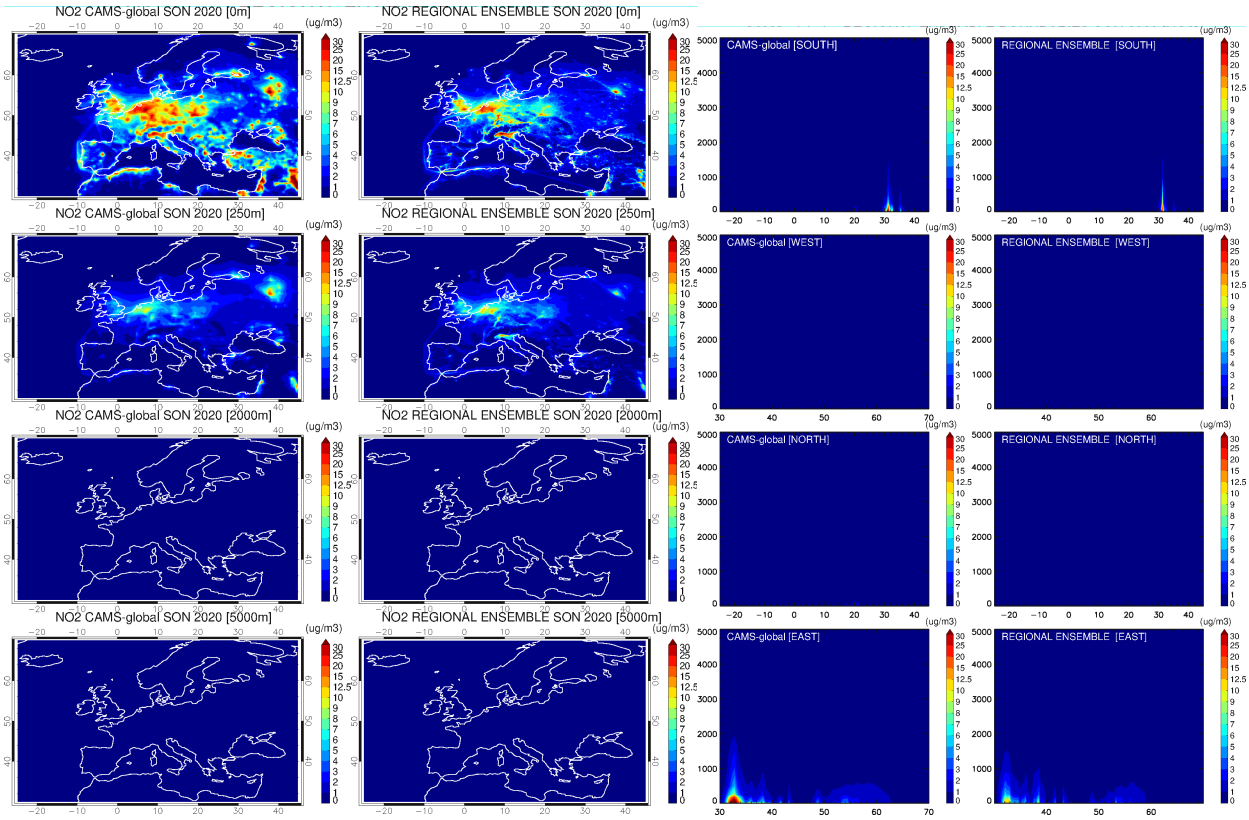


Figure 3.3. Left: Mean global and regional ENSEMBLE forecast $NO_2$ fields for four different vertical layers (0, 250, 2000, 5000 m) for SON2020. Right: Cross sections for the same period of the global and regional ENSEMBLE $NO_2$ boundaries (south, west, north, east).

Regional model products are provided at the height levels of 0, 50, 250, 500, 1000, 2000, 3000 and 5000m. For every grid point and time step of the CAMS-global model, the differences between the height of each vertical layer midpoint $z_m$ and the regional model height (e.g. 5000m) is calculated. The layer midpoint that exhibits the minimum height difference is the one that lies closest to the regional height level and is therefore selected for extraction of both chemical and aerosol species concentrations. The above procedure is performed for every regional height level. The final global product contains the $O_3$, CO, PM10 and PM2.5 concentrations in eight height levels that correspond to the CAMS-global vertical levels that lie closest to the regional height levels.

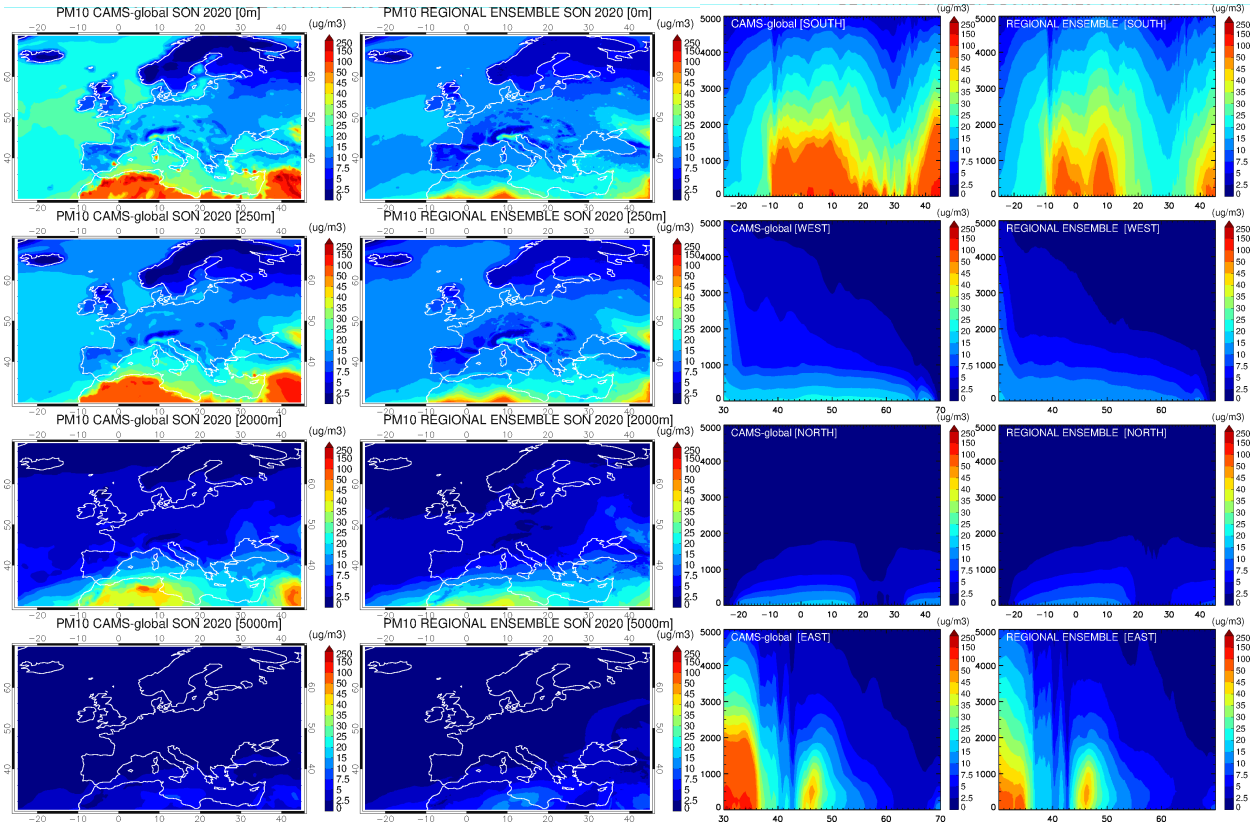


Figure 3.4 Left: Mean global and regional ensemble forecast PM10 fields for four different vertical layers (0, 250, 2000, 5000 m) for SON2020. Right: Cross sections for the same period of the global and regional ensemble PM10 boundaries (south, west, north, east).

Table 3.1: Aerosol species description.

| **Label** | | **Name** | **Size (µm)** |
|---|---|---|---|
| aermr01 | SS1 | Sea Salt Aerosol | 0.03-0.5 |
| aermr02 | SS2 | Sea Salt Aerosol | 0.5-5 |
| aermr03 | SS3 | Sea Salt Aerosol | 5-20 |
| aermr04 | DD1 | Dust Aerosol | 0.03-0.55 |
| aermr05 | DD2 | Dust Aerosol | 0.55-0.9 |
| aermr06 | DD3 | Dust Aerosol | 0.9-20 |
| aermr07 | OM1 | Hydrophobic Organic Matter Aerosol | |
| aermr08 | OM2 | Hydrophilic Organic Matter Aerosol | |
| aermr09 | BC1 | Hydrophobic Black Carbon Aerosol | |
| aermr10 | BC2 | Hydrophilic Black Carbon Aerosol | |
| aermr11 | SU1 | Sulphate Aerosol | |
| aermr16 | NI1 | Nitrate fine mode aerosol | |
| aermr17 | NI2 | Nitrate coarse mode aerosol | |
| aermr18 | NH3 | Ammonium aerosol | |

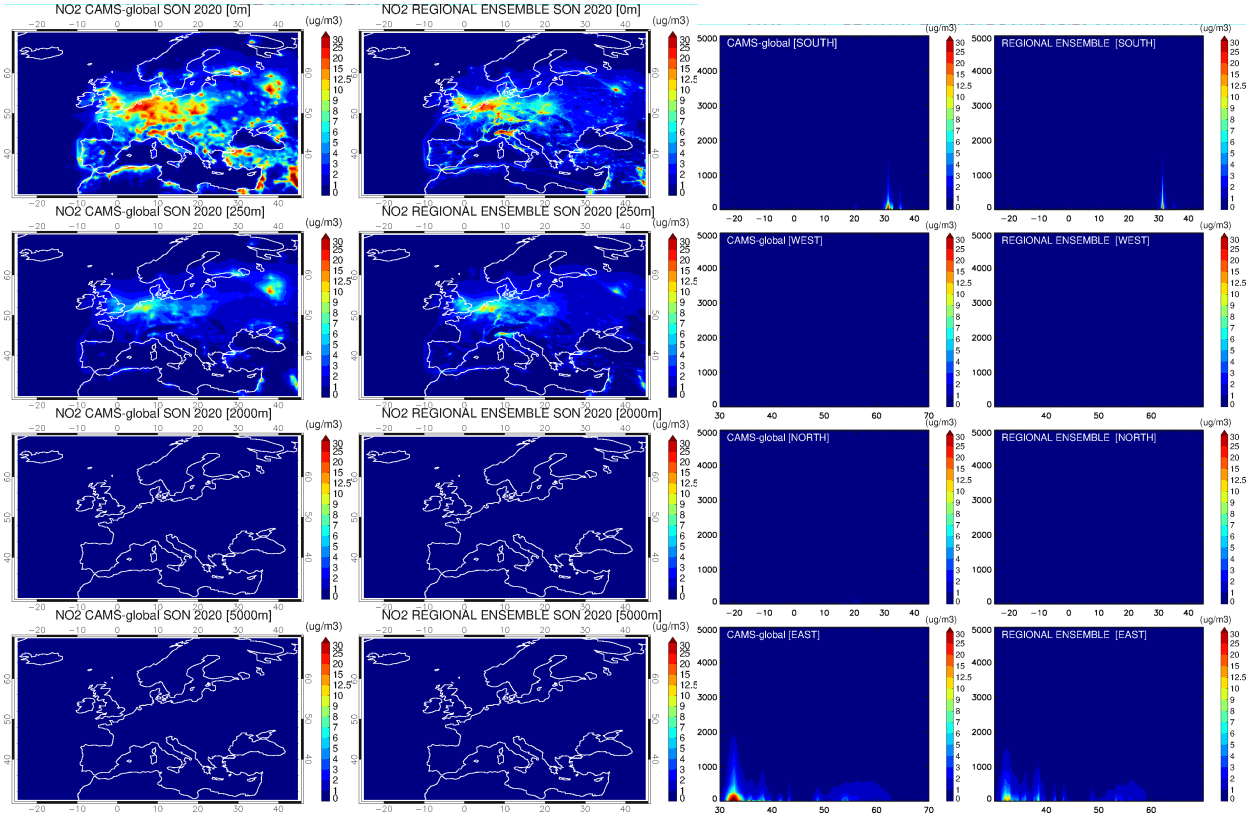


Figure 3.5 Left: Mean global and regional ENSEMBLE forecast $PM_{2.5}$ fields for four different vertical layers (0, 250, 2000, 5000 m) for SON-2020. Right: Cross sections for the same period of the global and regional ENSEMBLE ozone boundaries (south, west, north, east).

## 3.3 Consistency between the global and regional forecasts

This section reports on the consistency of the global and regional ENSEMBLE forecast. The analysis is performed for $O_3$, CO, $NO_2$, $PM_{10}$ and $PM_{2.5}$ at four levels (0, 250, 2000 and 5000 m) for the time period from September to November 2020 (SON2020).

*Ozone ($O_3$)*

Figure 3.1 shows the average SON2020 spatial distribution of $O_3$ for different vertical layers (left) and the cross sections of the lateral boundaries (right) for the CAMS-global forecast and the regional ENSEMBLE. Overall, CAMS-global and ENSEMBLE agree well for $O_3$, with CAMS-global exhibiting somehow lower ozone near the surface over continental Europe, while the opposite stands for Scandinavia. The agreement in the four boundaries is very good.

*Carbon monoxide (CO)*

Figure 3.2 illustrates the seasonal mean fields of CO and the cross sections of lateral boundaries (right) for ENSEMBLE and CAMS-global. There are more local surface CO maxima in the global forecast product, over continental Europe and the coast of North Africa. Probably, this is due to the different emissions in the two products. The comparison in the boundaries is very good.

*Nitrogen dioxide ($NO_2$)*

Figure 3.3 presents the seasonal mean fields of $NO_2$ and the cross sections of lateral boundaries (right) for ENSEMBLE and CAMS-global. In general, there are higher surface $NO_2$ concentrations in CAMS-global compared to ENSEMBLE over Europe, Middle East and North Africa. The ship emissions over the Mediterranean are mostly seen in the ENSEMBLE. Above 2000m both CAMS-global and ENSEMBLE exhibit very low concentrations (<1μg/m$^3$). The comparison in the boundaries is good, apart from the higher levels seen in CAMS-global compared to ENSEMBLE near the surface.

*Aerosols (PM10 and PM2.5)*

Figures 3.4 and 3.5 illustrate the CAMS-global and ENSEMBLE spatial distributions (left) and lateral boundary cross sections (right) of $PM_{10}$ and $PM_{2.5}$ mean fields, respectively. The main inconsistencies for particulate matter are summarized below:

- Higher PM10 and PM2.5 in CAMS-global compared to ENSEMBLE in the boundary layer (mostly seen at the surface) over the Atlantic, as well as at the western and northern boundaries.
- Higher PM10 in CAMS-global compared to ENSEMBLE over the southern and south-eastern boundaries of the domain up to 2000 m altitude.
- Some hotspots of $PM_{10}$ concentrations in CAMS-global over the Mediterranean not seen in ENSEMBLE. These are expected to disappear with the new CAMS-global version (CY47R1, see also section 3.9)
- High PM10/PM2.5 surface concentrations over Middle East seen in CAMS-global are not found in ENSEMBLE.

## 3.4 Regional variability

*Ozone ($O_3$)*

Figure 3.6 illustrates ozone mean fields for SON2020 of the individual regional ENSEMBLE members and CAMS-global (bottom panel) for selected altitudes (0, 250, 2000, 5000 m). SILAM and GEM-AQ exhibit lower surface ozone concentrations over central and north Europe (north boundary), respectively, in comparison to CAMS-global. GEM-AQ and LOTOS-EUROS models have lower $O_3$ values over the Atlantic (western boundary). MOCAGE exhibits considerably higher concentrations over the Mediterranean near the surface and over central Europe at 250m compared to CAMS-global.

*Carbon monoxide (CO)*

The SON2020 mean fields of carbon monoxide for the regional ENSEMBLE members as well as for CAMS-global are illustrated in figure 3.7 for different vertical layers. No particular outliers are found, as CO in the regional models is within the expected variability. GEM-AQ has higher CO than all other regional models within the PBL, yet being the most consistent with CAMS-global. DEHM exhibits lower CO values near the surface over central Europe than all other regional models and CAMS-global.

*Nitrogen Dioxide ($NO_2$)*

The SON2020 mean fields of nitrogen dioxide for the regional ensemble members as well as for CAMS-global are presented in Figure 3.8 for several vertical layers. LOTOS-EUROS and MATCH exhibit the lower $NO_2$ levels in the boundary layer among the regional models. Low $NO_2$ levels (< 1µg/$m^3$) above 2000m in all regional models and the CAMS-global.

*Aerosols (PM10 and PM2.5)*

The mean PM10 and PM2.5 fields for SON2020 are illustrated in Figures 3.9 and 3.10, respectively. The inconsistences noted are:

- MOCAGE is seen as an outlier in the boundary layer for PM10, showing a strange pattern over the Atlantic, presumably due to using different sea salt boundary conditions than the rest of the models.
- MOCAGE, EURAD, MATCH and DEHM exhibit relatively lower PM10 levels at the Southern boundary.
- EMEP, SILAM and GEMAQ have higher PM2.5 levels in the PBL near the Southern boundaries compared to CAMS-global, while LOTOS-EUROS and MOCAGE have lower PM2.5.

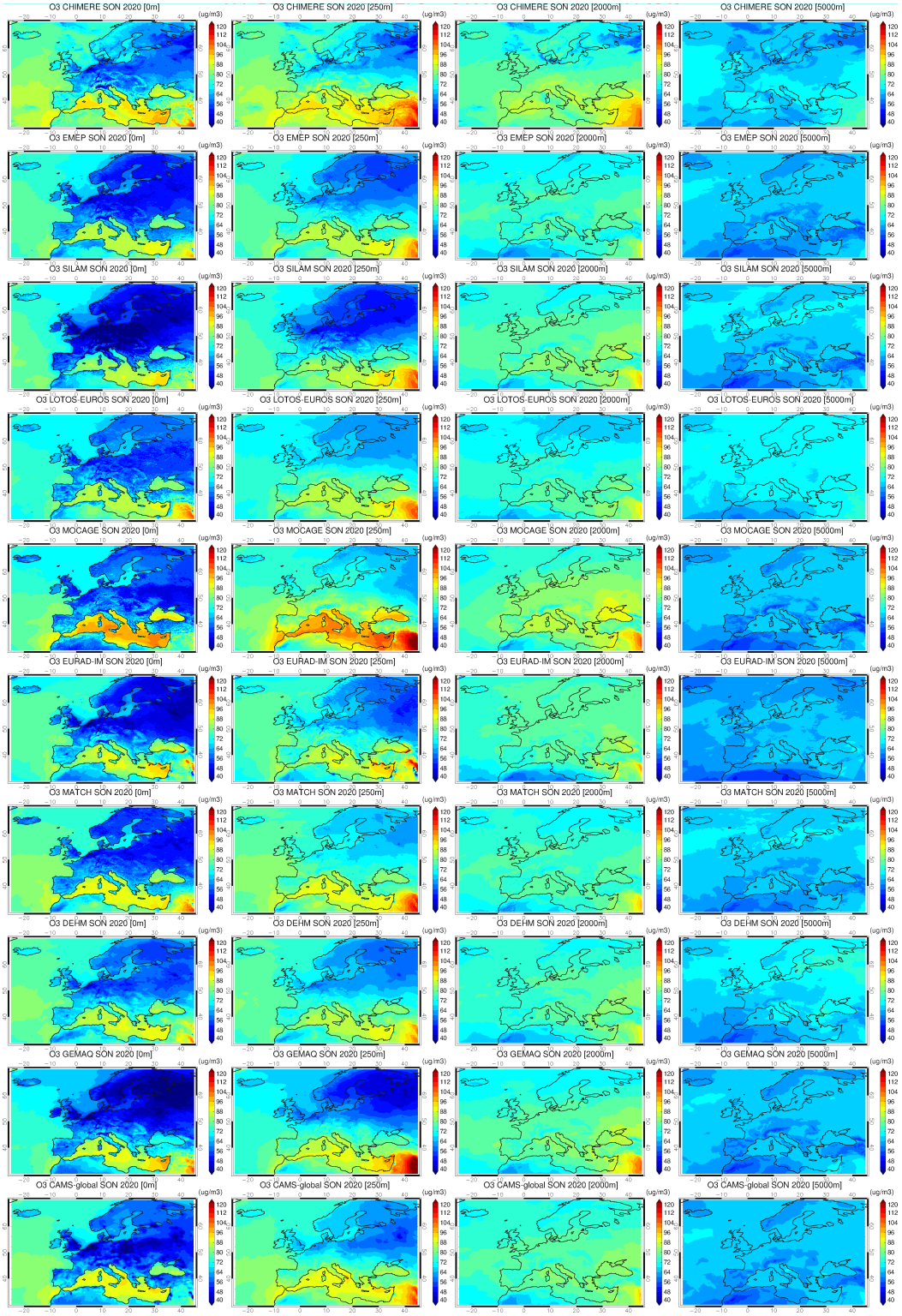


Figure 3.6 Mean regional ozone forecasts for SON2020 for four different vertical layers (0, 250, 2000, 5000 m) from the nine ensemble members and CAMS-global (top to bottom: CHIMERE, EMEP, SILAM, LOTOS-EUROS, MOCAGE, EURAD-IM, MATCH, DEHM, GEM-AQ and CAMS-global).

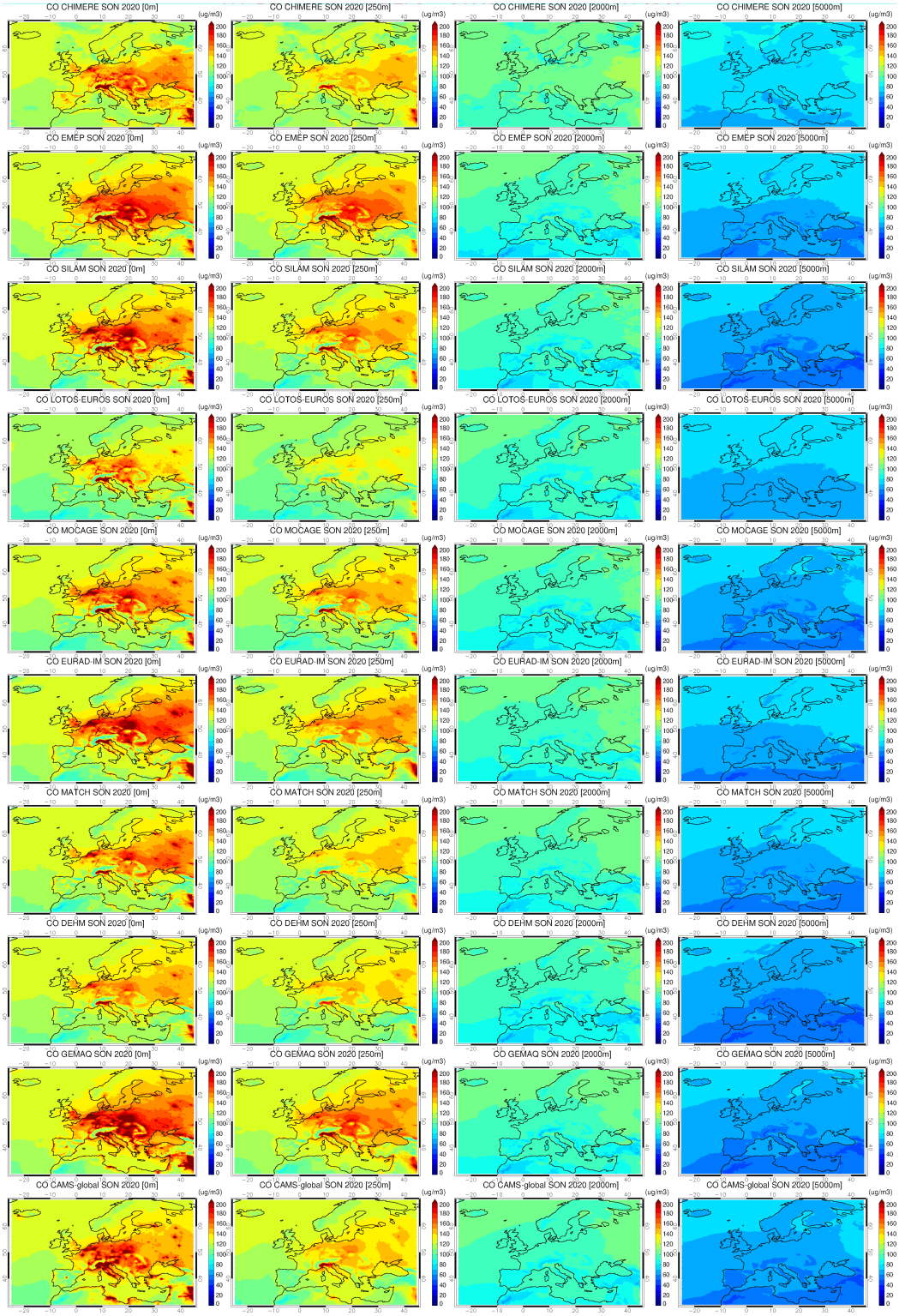


Figure 3.7. Mean regional CO forecasts for SON2020 for four different vertical layers (0, 250, 2000, 5000 m) from the nine ensemble members and CAMS-global (top to bottom: CHIMERE, EMEP, SILAM, LOTOS-EUROS, MOCAGE, EURAD-IM, MATCH, DEHM, GEM-AQ and CAMS-global).

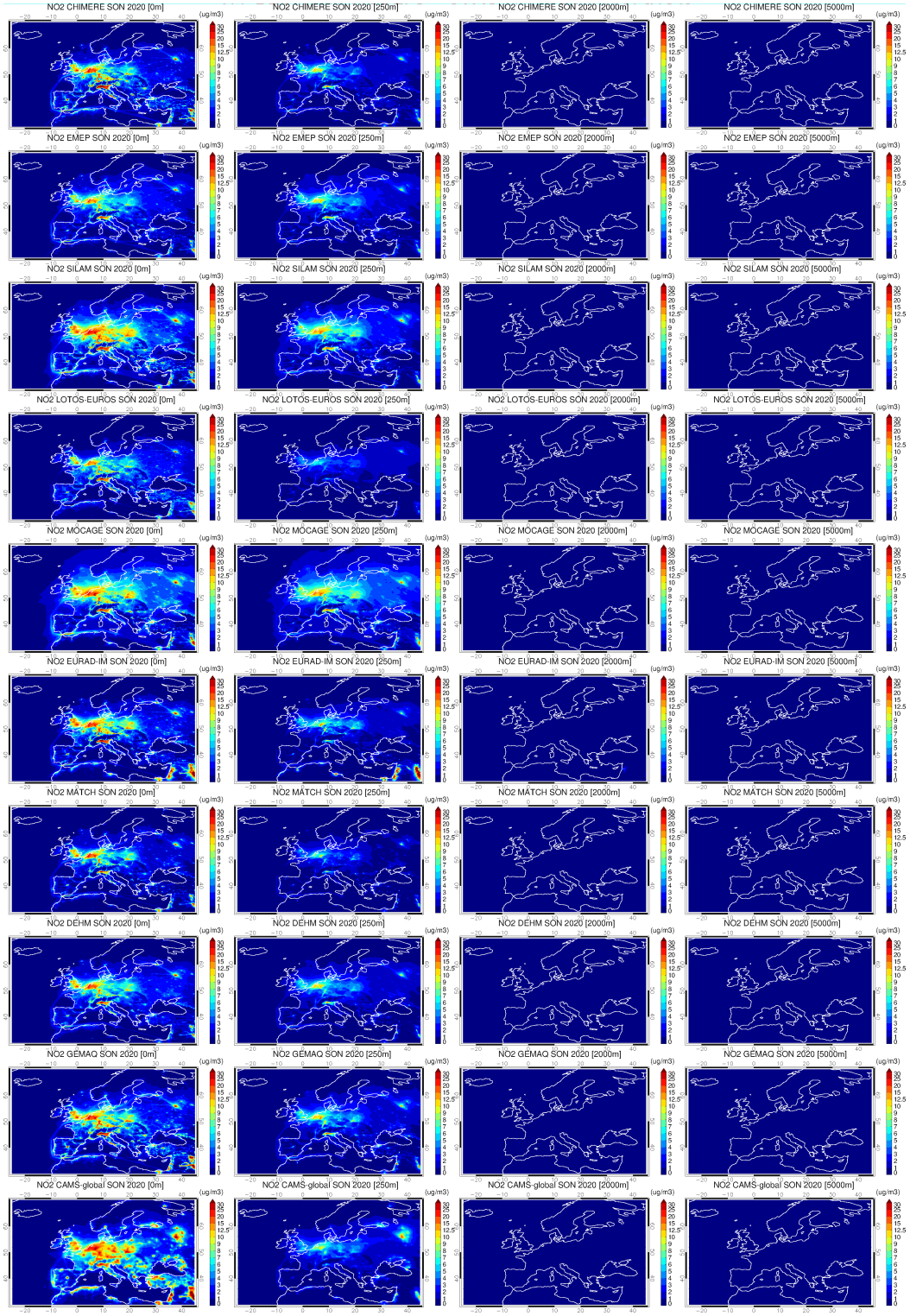


Figure 3.8. Mean regional $NO_2$ forecasts for SON-2020 for four different vertical layers (0, 250, 2000, 5000 m) from the nine ensemble members and CAMS-global (top to bottom: CHIMERE, EMEP, SILAM, LOTOS-EUROS, MOCAGE, EURAD-IM, MATCH, DEHM, GEM-AQ and CAMS-global).

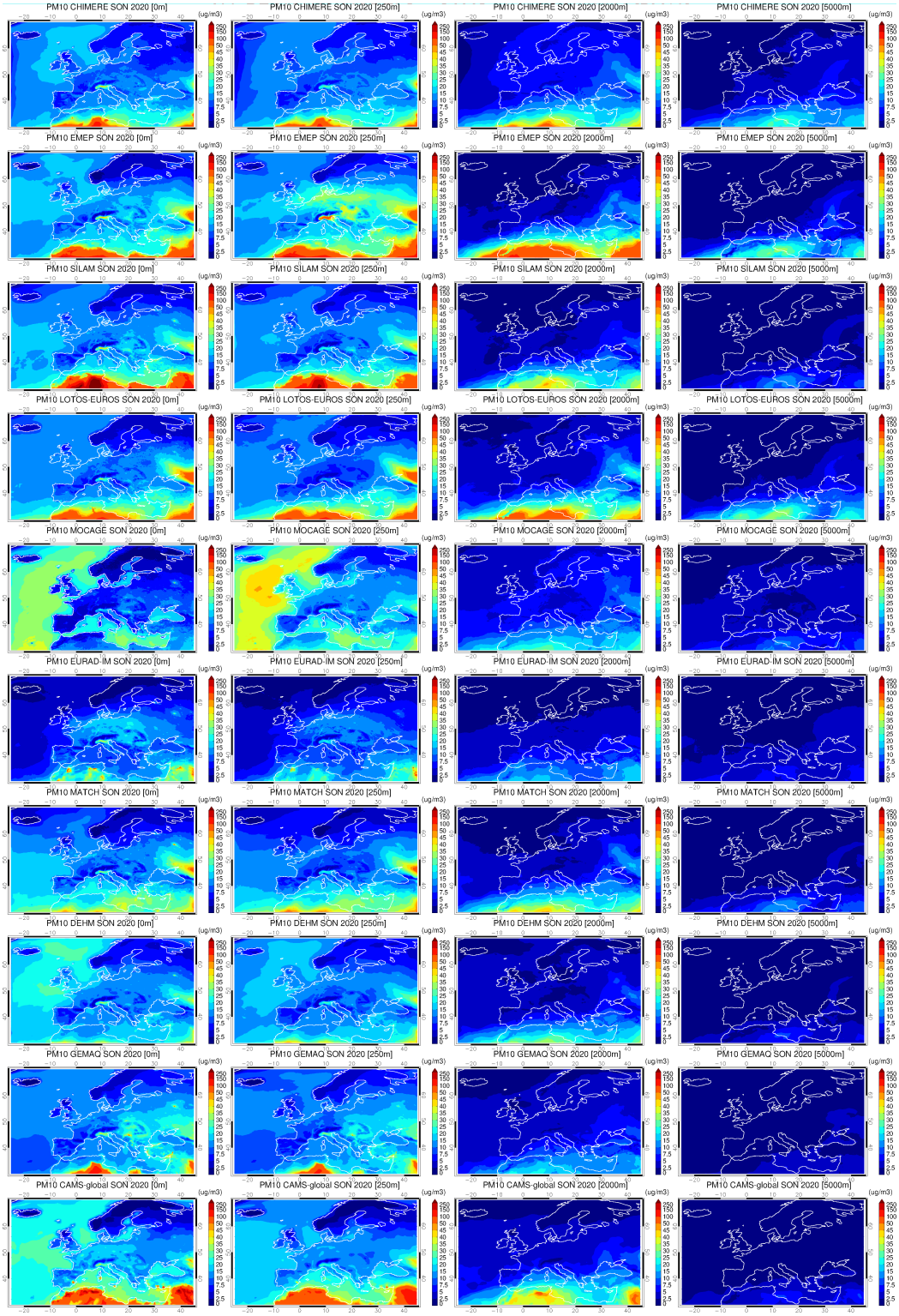


Figure 3.9. Mean regional $PM_{10}$ forecasts for SON-2020 for four different vertical layers (0, 250, 2000, 5000 m) from the nine ensemble members and CAMS-global (top to bottom: CHIMERE, EMEP, SILAM, LOTOS-EUROS, MOCAGE, EURAD-IM, MATCH, DEHM, GEM-AQ and CAMS-global).

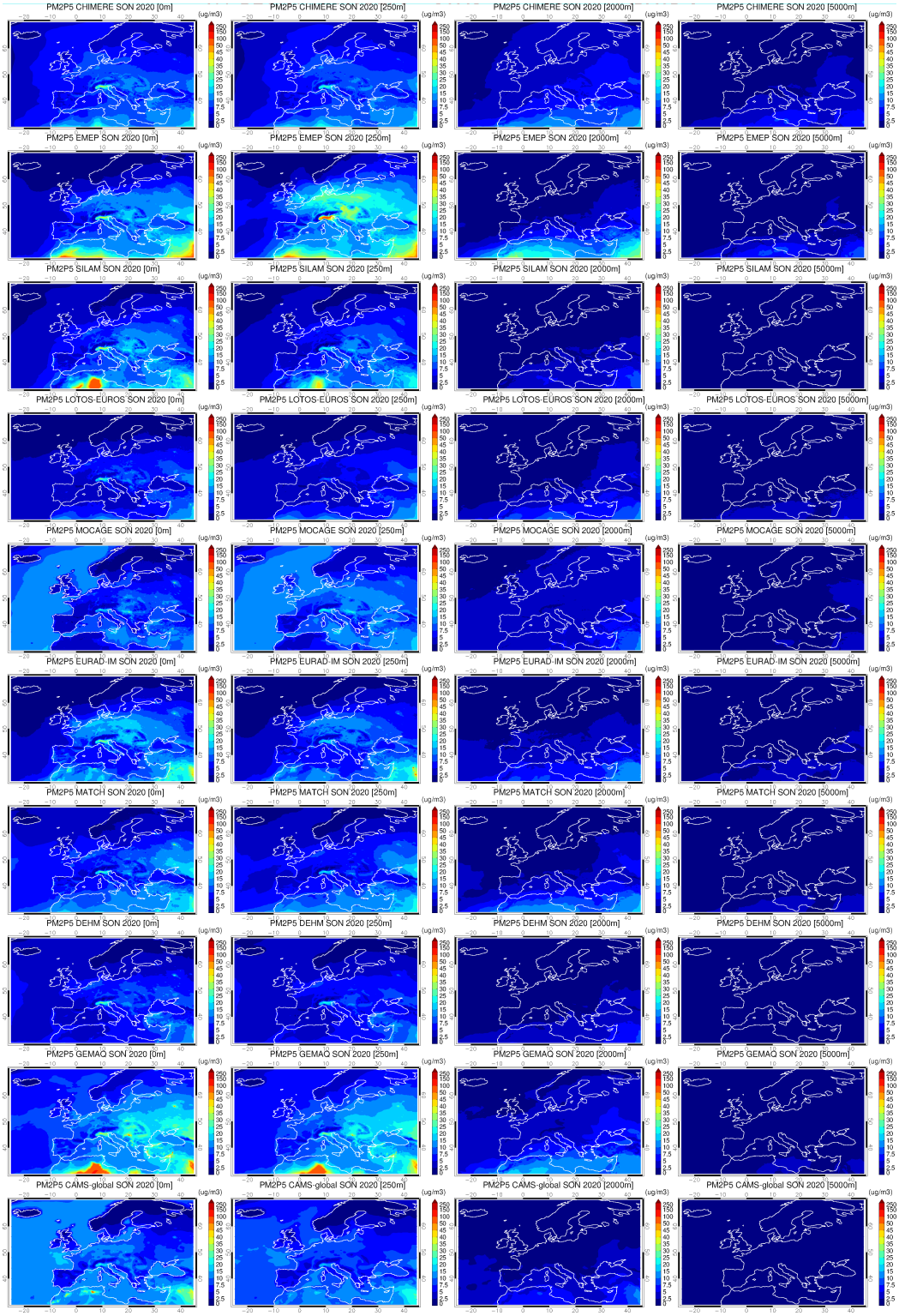


Figure 3.10. Mean regional PM2.5 forecasts for SON2020 for four different vertical layers (0, 250, 2000, 5000 m) from the nine ensemble members and CAMS-global (top to bottom: CHIMERE, EMEP, SILAM, LOTOS-EUROS, MOCAGE, EURAD-IM, MATCH, DEHM, GEM-AQ and CAMS-global).

## 3.5 Time series

Figure 3.11 shows the mean daily time series for SON2020 for the five species, namely $O_3$, CO, $NO_2$, PM10 and PM2.5 (from left to right) for different European sub-regions (from top to bottom): Alps (AL), British Isles (BI), East Europe (EA), France (FR), Iberian Peninsula (IP), Mediterranean (MD), Mid-Europe (ME), Scandinavia (SC).

Each subregion is defined with the following latitude/longitude boundaries:

Name = (BI, IP, FR, ME, SC, AL, MD, EA)

West = (-10, -10, -5, 2, 5, 5, 3, 16)

East = (2, 3, 5, 16, 30, 15, 25, 30)

South = (50, 36, 44, 48, 55, 44, 36, 44)

North = (59, 44, 50, 55, 70, 48, 44, 55)

The letter R denotes the temporal correlation between the two products. Only concentrations over land are used.

For $O_3$ the temporal variability between CAMS-global and ENSEMBLE is in very good agreement (R values of 0.89 to 0.97). LOTOS-EUROS, unlike every other model, exhibits an extreme minimum in November.

The temporal correlation for CO is also very good (0.77 to 0.96), with CAMS-global exhibiting higher levels mostly for the Alps.

For $NO_2$ the temporal variability between CAMS-global and ENSEMBLE is very good (R values of 0.76 to 0.94).

The agreement in the PM10 daily timeseries between the global and regional forecasts ranges is mediocre in the majority of the regions, with the exception of EA (0.16) and SC (0.75). LOTOS-EUROS produces very high PM10 over the Mediterranean at the beginning of October, unlike all other regional ensemble members and CAMS-global. This is a known issue with LOTOS-EUROS, which tends to occasionally overestimated desert dust events.

The magnitude of PM10 in CAMS-global is close to the regional ENSEMBLE, however CAMS-global PM10 is higher over FR, IP, MD.

The temporal agreement in surface PM2.5 is quite good (0.63 to 0.83) except for EA (0.36).

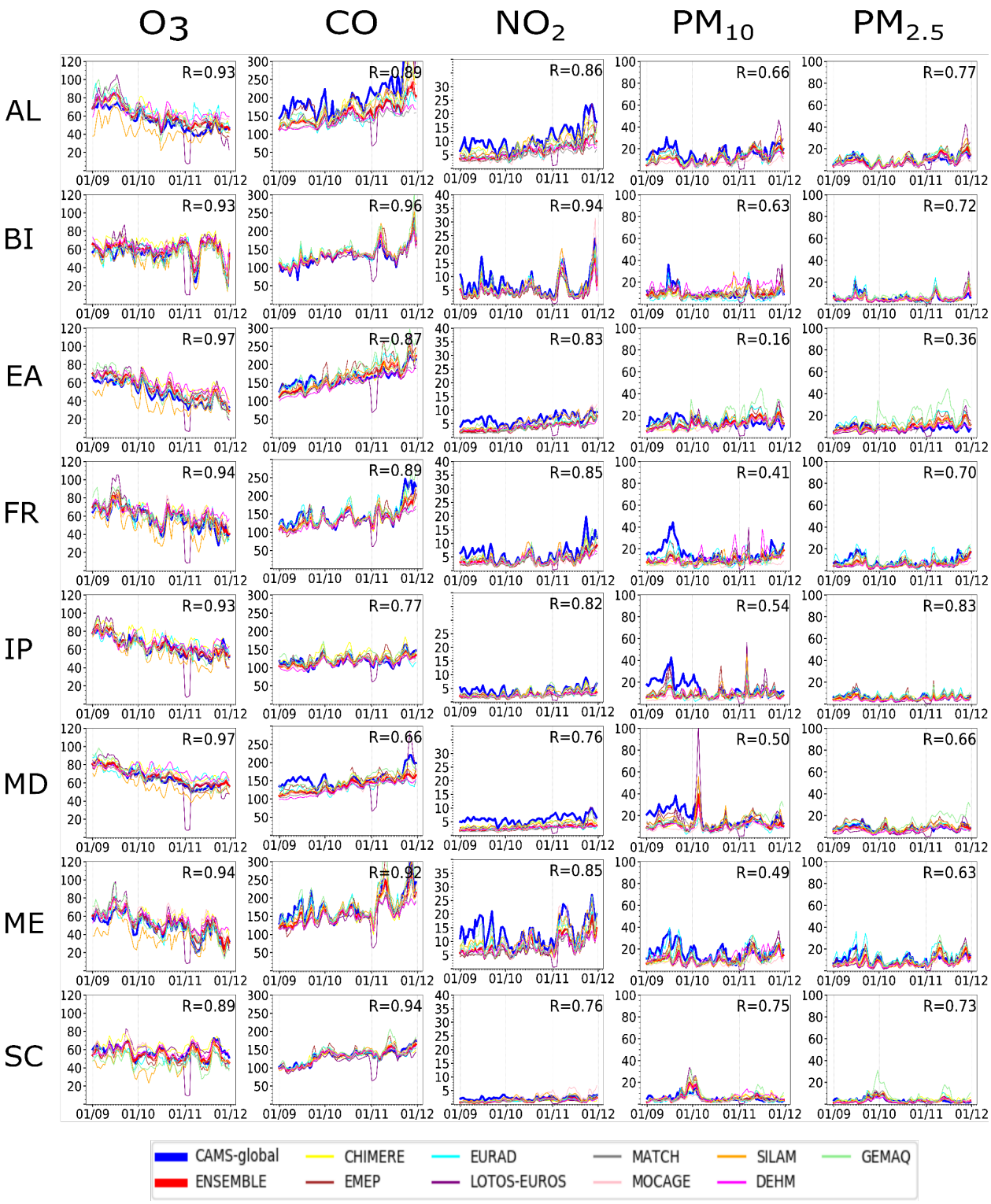


Figure 3.11. Mean daily time series for surface $O_3$, CO, $NO_2$, PM10 and PM2.5 for SON2020 (unit µg/m$^3$). The blue line is CAMS-global and the red line the ENSEMBLE forecasts. Each line in the composite plot denotes a different European subregion.

## 3.6 Diurnal cycles

Figure 3.12 shows the diurnal cycles for surface $O_3$, CO, $NO_2$, PM10 and PM2.5 averaged over the period SON2020 for different European sub-regions (from top to bottom): Alps (AL), British Isles (BI), East Europe (EA), France (FR), Iberian Peninsula (IP), Mediterranean (MD), Mid-Europe (ME), Scandinavia (SC). The red colour is used for the regional ENSEMBLE and the blue for CAMS-global.

There is a good agreement between the $O_3$ CAMS-global and the regional diurnal cycles, both in timing and amplitude of the diurnal cycle.

The diurnal range for surface CO is less pronounced for the regional products over some regions, mostly over the Alps and to a lesser extent over the southern Europe and central Europe.

The diurnal cycle of $NO_2$ at the surface reveals that regional product and the CAMS-global forecasts agree on the shape, yet the diurnal range is higher in CAMS-global over all regions except Scandinavia.

There is a mediocre agreement of the PM10 diurnal cycle between the global and the regional product, while the agreement is better for PM2.5, which generally exhibit less pronounced diurnal cycles than PM10.

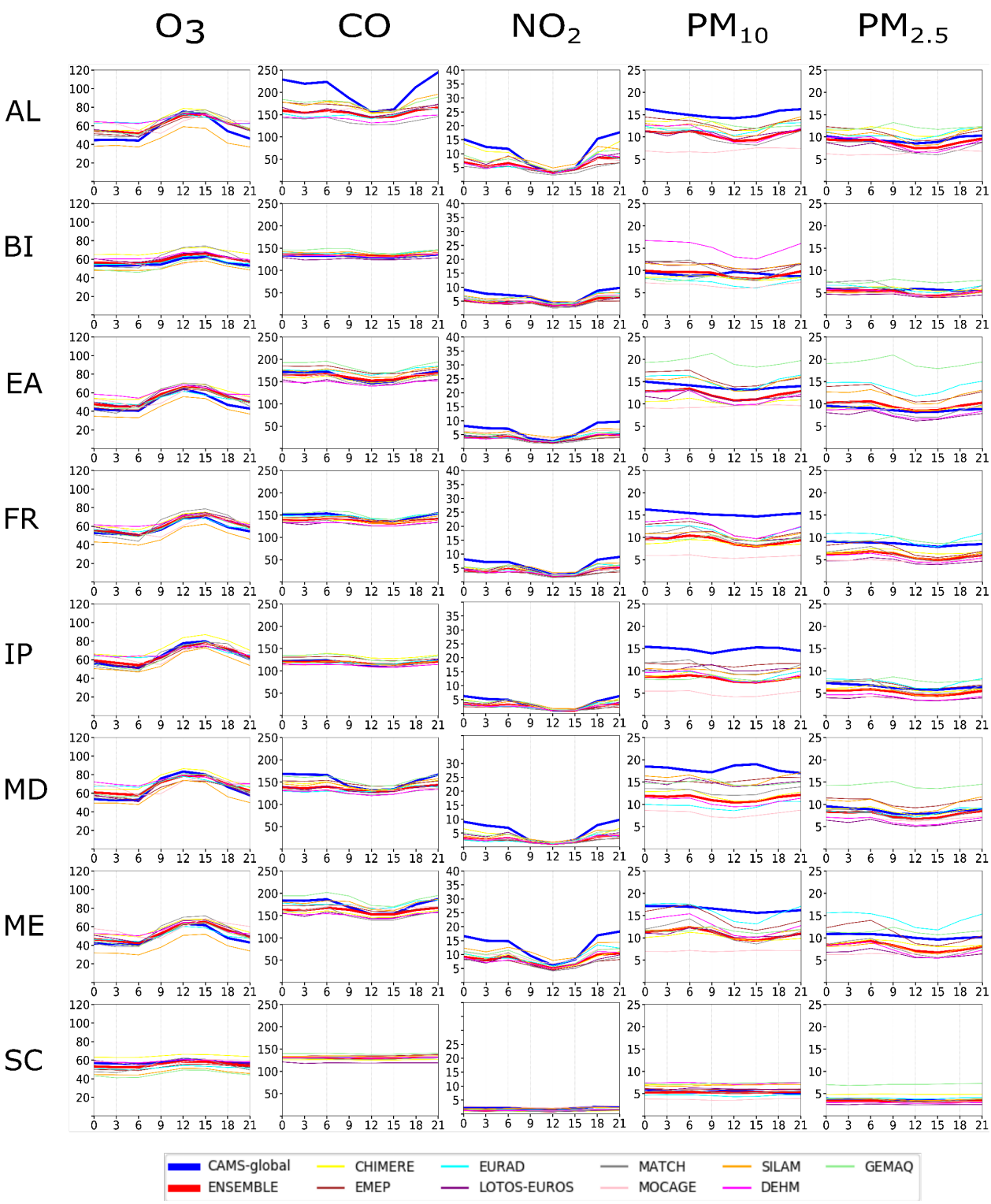


Figure 3.12. Diurnal cycles for surface $O_3$, CO, $NO_2$, PM10 and PM2.5 for the period SON2020 (unit µg/m$^3$). The blue line is CAMS-global and the red line the ENSEMBLE forecast. Each line in the composite plot denotes a different European sub-region.

## 3.7 Regional domain boundary cross sections

*Ozone ($O_3$)*

Figure 3.13 shows the regional variability in the lateral domain boundary cross sections of $O_3$ (from left to right): south, west, north, east and the different ensemble members and CAMS-global (from top to bottom) averaged over the period SON2020. CHIMERE and to a lesser extent EURAD have spurious implementation of $O_3$ boundaries.

*Carbon monoxide (CO)*

Figure 3.14 shows the regional variability in the lateral cross sections of CO (from left to right): south, west, north, east and the different ensemble members and CAMS-global (from top to bottom) averaged over the period SON2020. CHIMERE seems to have problematic boundaries implementation, especially at the eastern.

*Carbon monoxide ($NO_2$)*

Figure 3.15 shows the regional variability in the lateral cross sections of $NO_2$ (from left to right): south, west, north, east and the different ensemble members and CAMS-global (from top to bottom) averaged over the period SON2020. Overall, no particular outlier for $NO_2$ boundaries. LOTOS-EUROS exhibits the lower $NO_2$ levels at the boundaries and MOCAGE the higher, at the southern and eastern boundaries of the domain.

*Aerosols (PM10 and PM2.5)*

Figure 3.16/3.17 shows the regional variability in the lateral cross sections of PM10/PM2.5 respectively (left to right): south, west, north, east and the different ensemble members and CAMS-global (top to bottom). We note the following inconsistencies:

- MOCAGE, EURAD, DEHM and to a lesser extent GEM-AQ exhibit lower PM10 concentrations over the southern boundaries than CAMS-global.
- MOCAGE has concentrations higher than those of CAMS-global for PM10 at the western and northern boundaries, probably due to the sea salt boundaries used.
- MOCAGE, EURAD, DEHM and GEM-AQ have lower PM10 at the eastern boundaries.
- All models except LOTOS-EUROS, MOCAGE and DEHM have higher southern PM2.5 boundaries that CAMS-global.
- EMEP, EURAD and GEM-AQ have higher eastern $PM_{2.5}$ boundaries than CAMS-global.

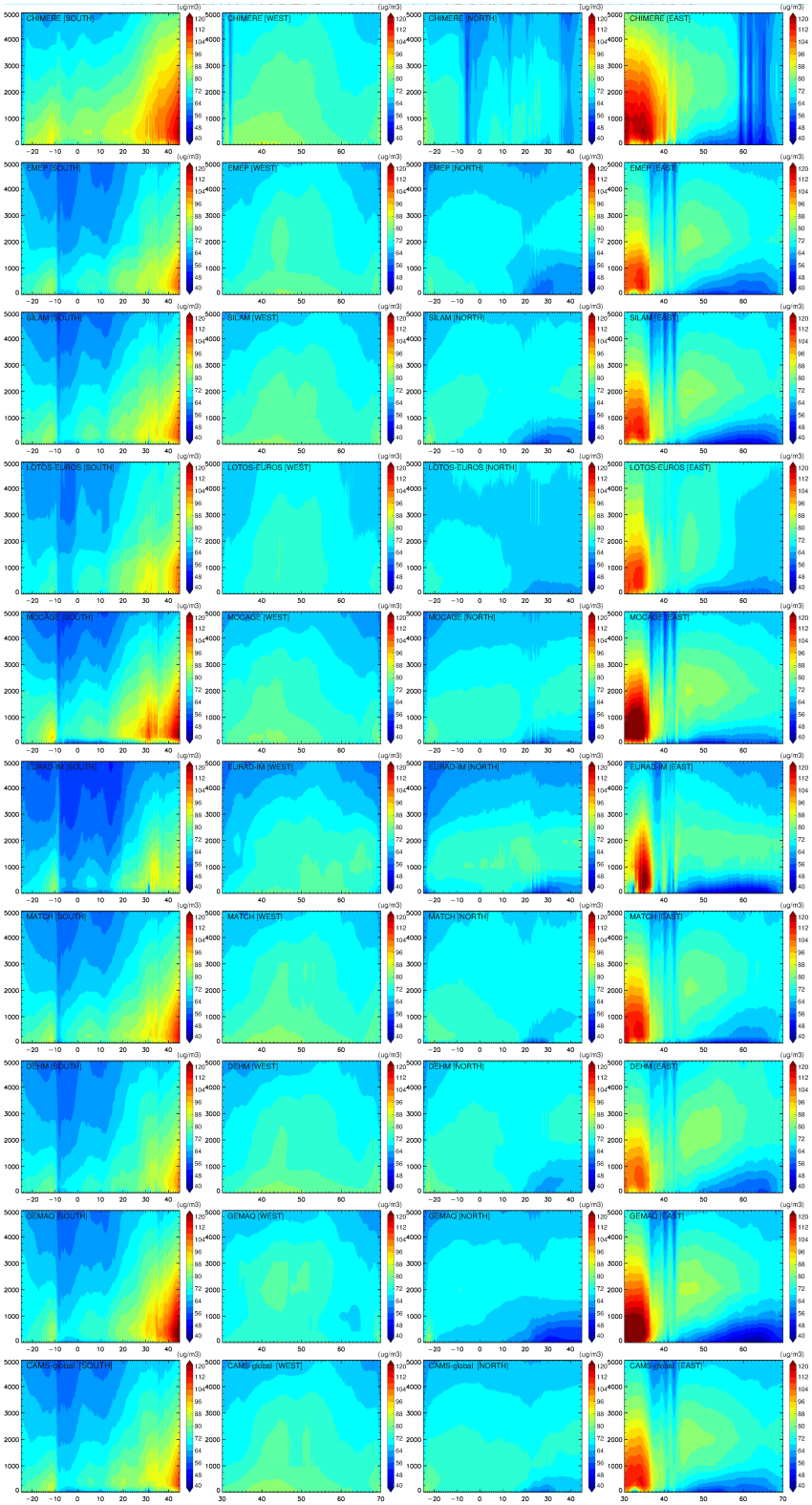


Figure 3.13. Ozone cross sections for SON-2020 for the nine ensemble members and CAMS-global (top to bottom: CHIMERE, EMEP, SILAM, LOTOS-EUROS, MOCAGE, EURAD-IM, MATCH, DEHM, GEM-AQ and CAMS-global) and the lateral boundaries (left to right: south, west, north, east).

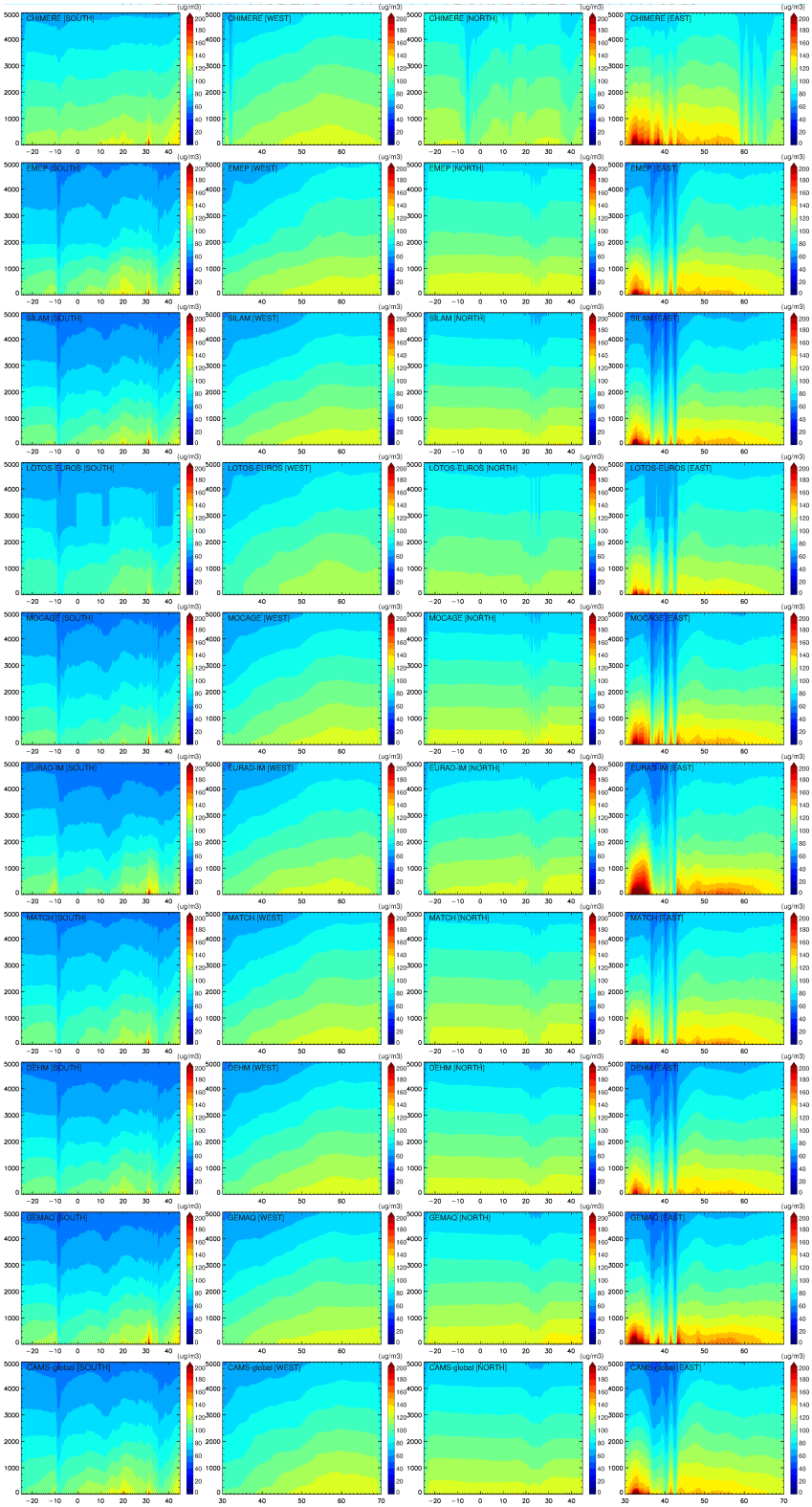


Figure 3.14. Carbon Monoxide cross sections for SON-2020 for the nine ensemble members and CAMS-global (top to bottom: CHIMERE, EMEP, SILAM, LOTOS-EUROS, MOCAGE, EURAD-IM, MATCH, DEHM, GEM-AQ and CAMS-global) and the lateral boundaries (left to right: south, west, north, east).

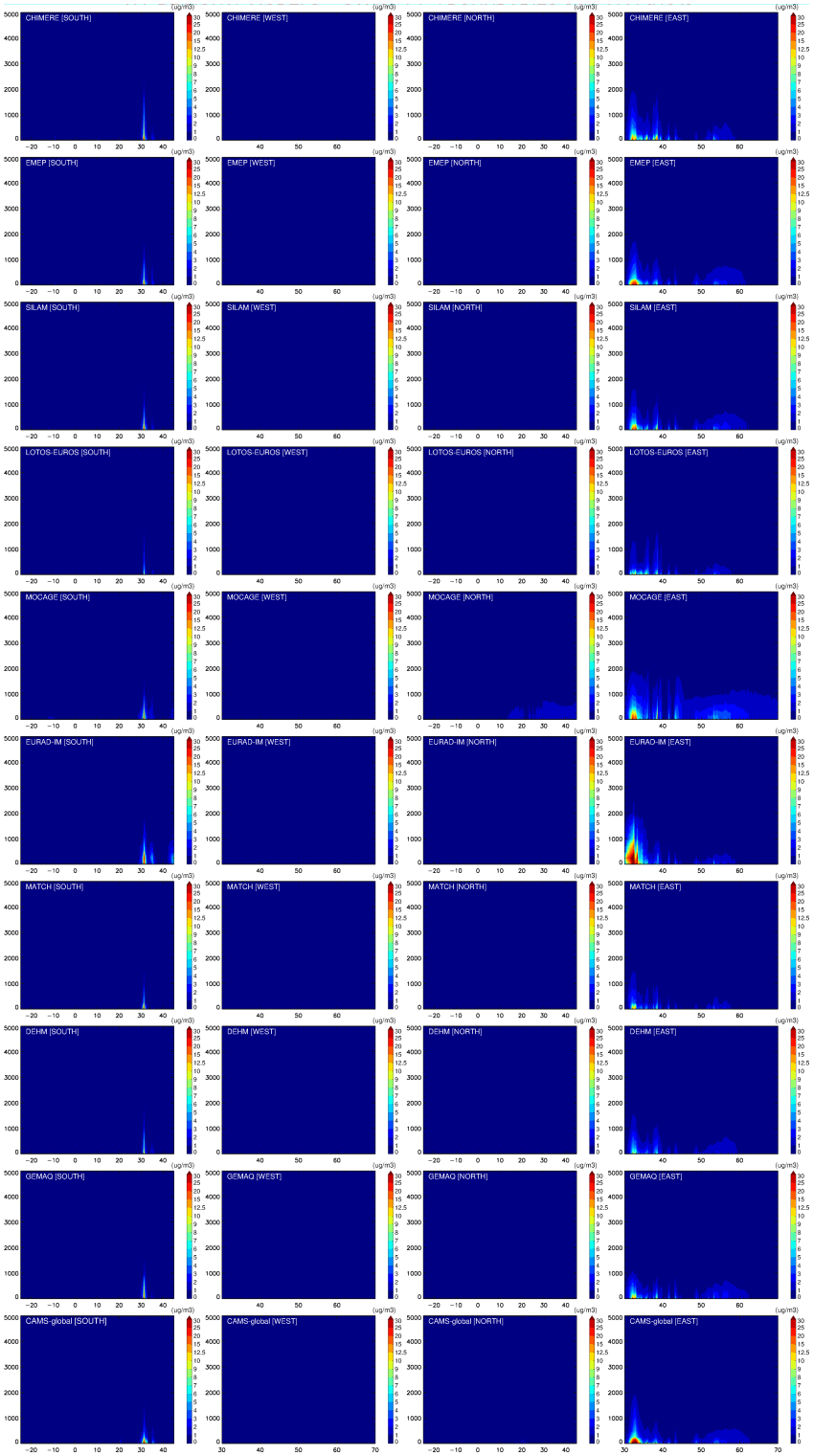


Figure 3.15. Nitrogen dioxide cross sections for SON-2020 for the nine ensemble members and CAMS-global (top to bottom: CHIMERE, EMEP, SILAM, LOTOS-EUROS, MOCAGE, EURAD-IM, MATCH, DEHM, GEM-AQ and CAMS-global) and the lateral boundaries (left to right: south, west, north, east).

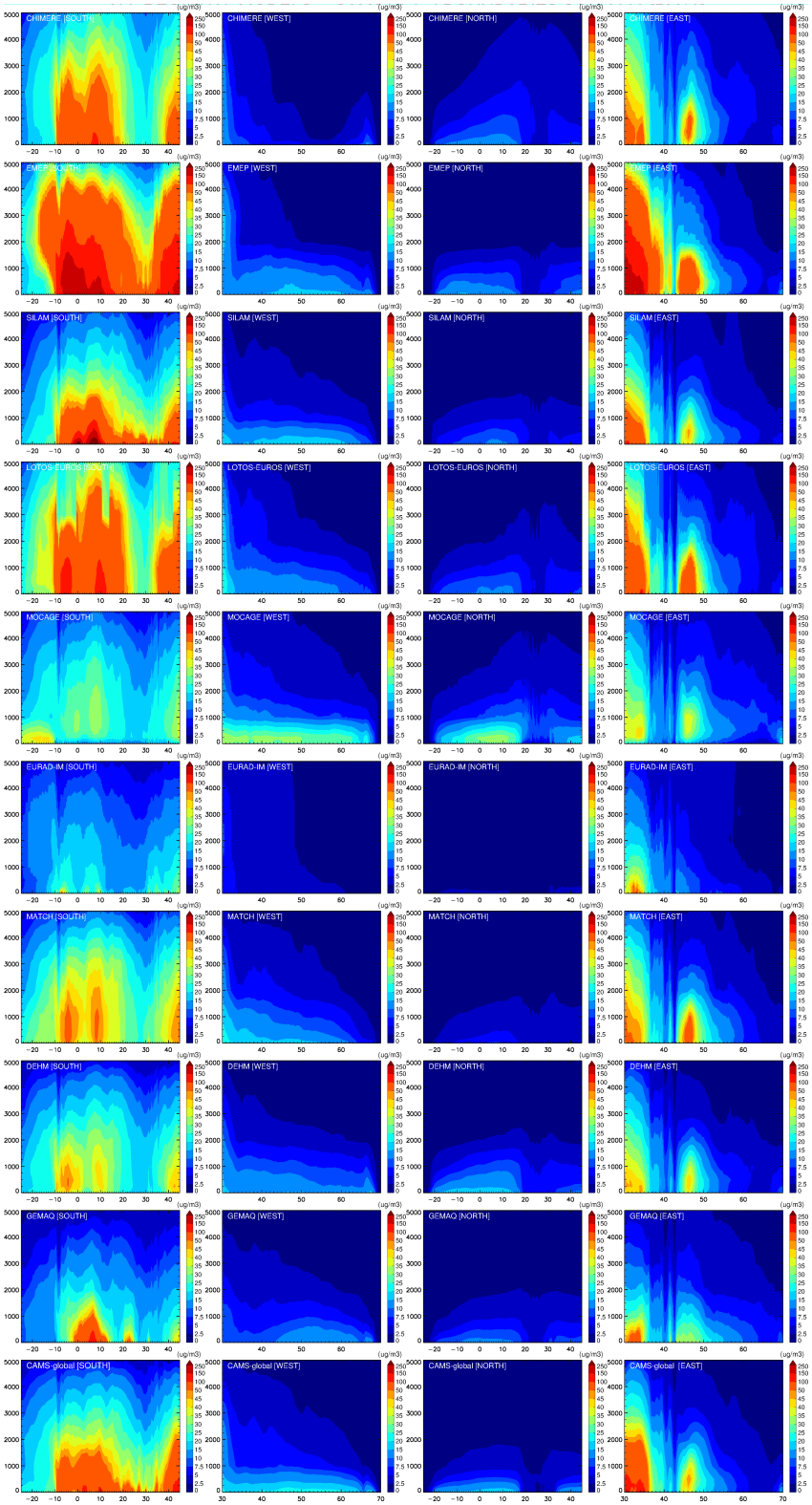


Figure 3.16. Aerosol $PM_{10}$ cross sections for SON-2020 for the nine ensemble members and CAMS-global (top to bottom: CHIMERE, EMEP, SILAM, LOTOS-EUROS, MOCAGE, EURAD-IM, MATCH, DEHM, GEM-AQ and CAMS-global) and the lateral boundaries (left to right: south, west, north, east).

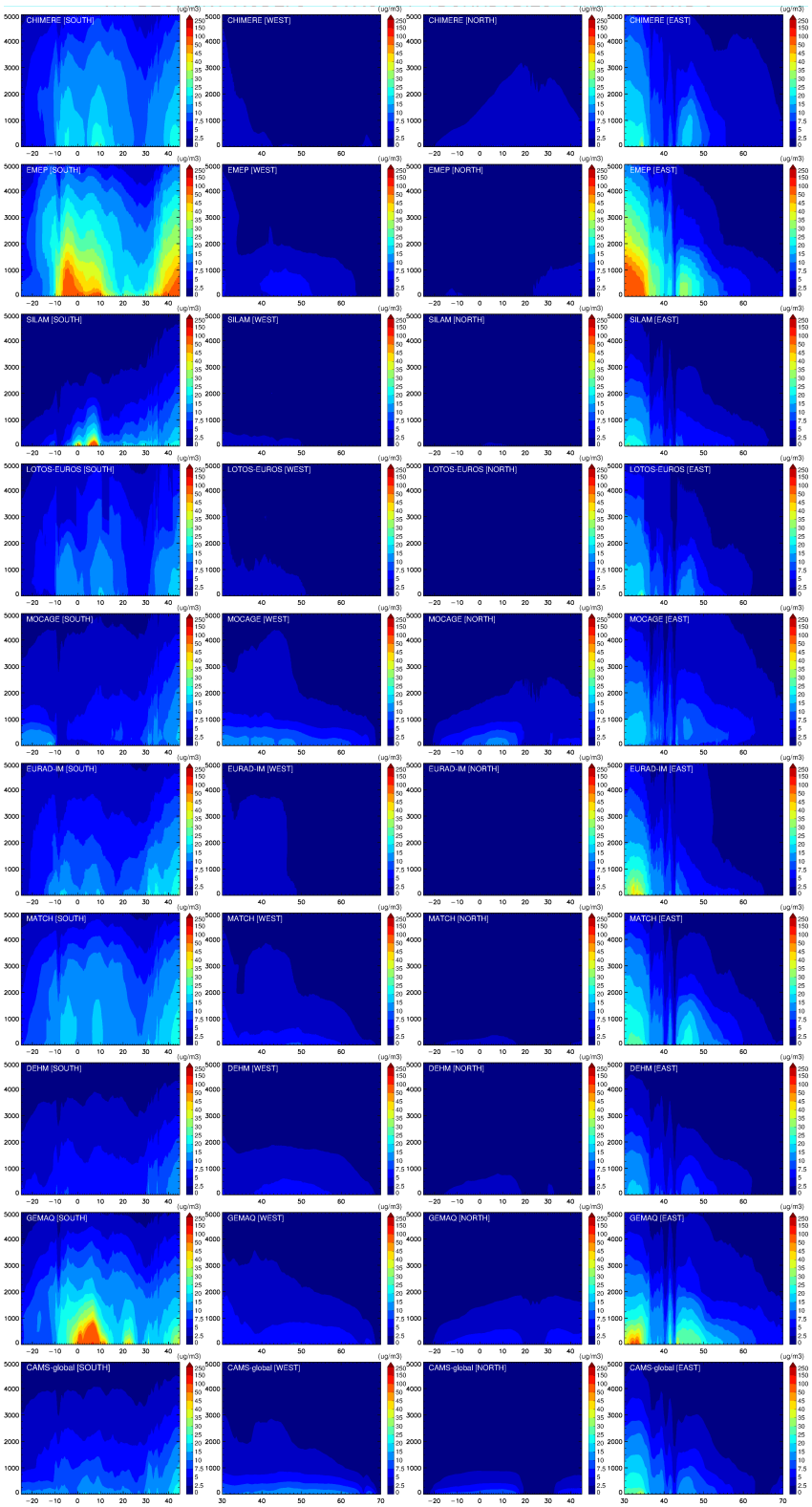


Figure 3.17 Aerosol $PM_{2.5}$ cross sections for SON-2020 for the nine ensemble members and CAMS-global (top to bottom: CHIMERE, EMEP, SILAM, LOTOS-EUROS, MOCAGE, EURAD-IM, MATCH, DEHM, GEM-AQ and CAMS-global) and the lateral boundaries (left to right: south, west, north, east).

## 3.8 Regional analysis vs. regional forecasts

In this section, we compare the regional analysis products with the regional forecasts (1st day). The four following figures (3.18-3.22) show the mean regional differences between analysis and forecasts for the time period SON2020 at four different vertical layers (0, 250, 2000, 5000 m, left to right) including $O_3$, CO, $NO_2$, PM10 and PM2.5, respectively.
Regional models with the largest differences between the analyses and the 1st day forecasts are for:

*Ozone*

- CHIMERE and SILAM in the surface layer.
- EMEP, MOCAGE, DEHM mostly within the PBL (patchy patterns)
- MATCH and to a lesser extend LOTOS-EUROS, at all levels.

*Carbon monoxide*

Differences are seen in:

- MATCH and SILAM exhibit (up to 2000m) much lower CO levels compared to the analysis.
- CHIMERE and GEM-AQ at the surface.
- EMEP in the boundary layer.

*Nitrogen dioxide*

- Lower $NO_2$ forecast compared to analysis at the surface and in the boundary layer for CHIMERE and EMEP, respectively.

*$PM_{10}$ and $PM_{2.5}$*

- Minor differences in some models, most pronounced in MATCH for $PM_{10}$ and $PM_{2.5}$.

It is important to note that the differences observed between the analysis and the forecast do not only reflect the impact of the assimilation but may also result from differences in the model setup between the analysis systems and the forecast systems.

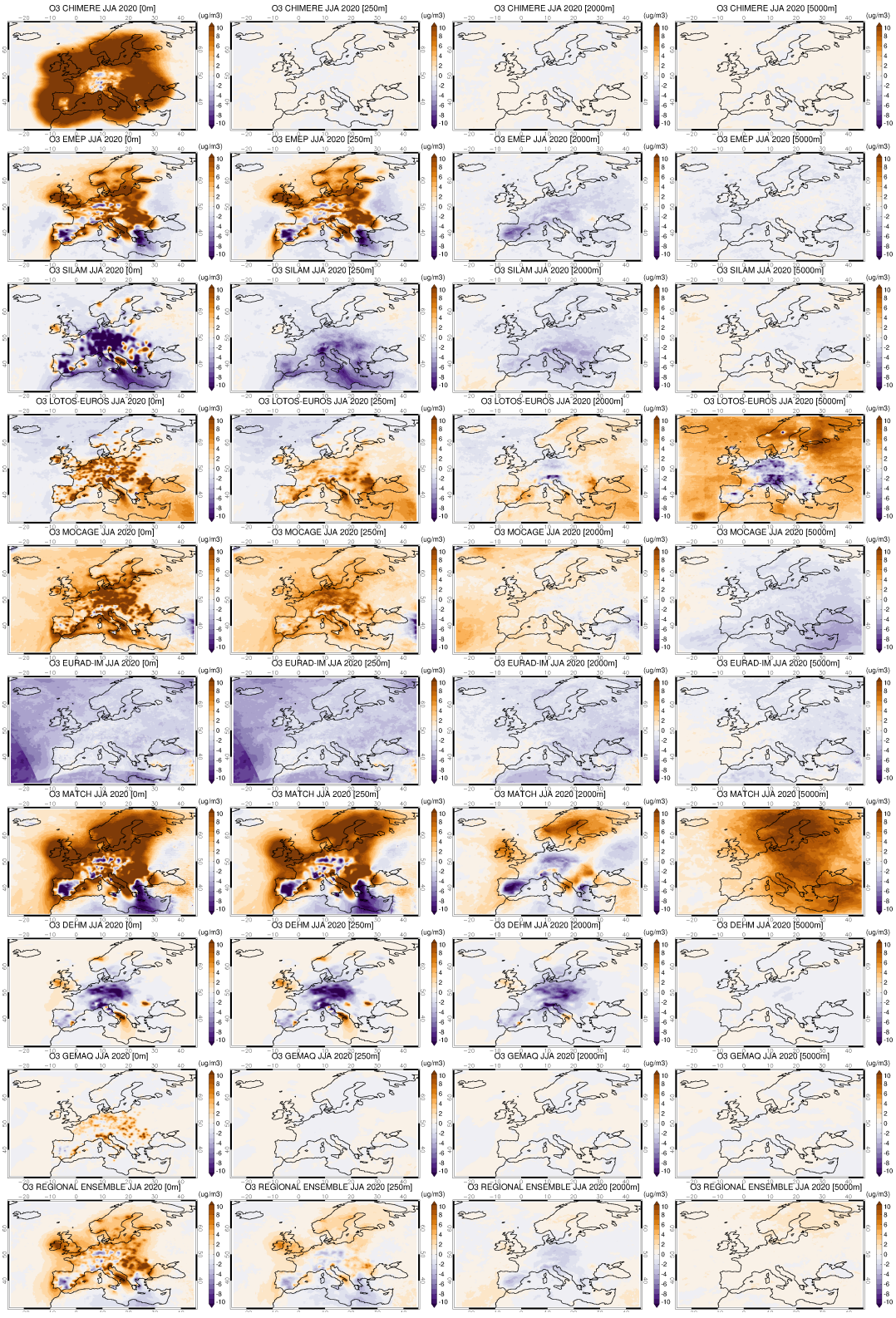


Figure 3.18. Mean regional $O_3$ differences between analysis and forecast for SON-2020 for four different vertical layers (0, 250, 2000, 5000 m) from regional ENSEMBLE and individual ensemble members (top to bottom: CHIMERE, EMEP, SILAM, LOTOS-EUROS, MOCAGE, EURAD-IM, MATCH, DEHM, GEM-AQ and ENSEMBLE).

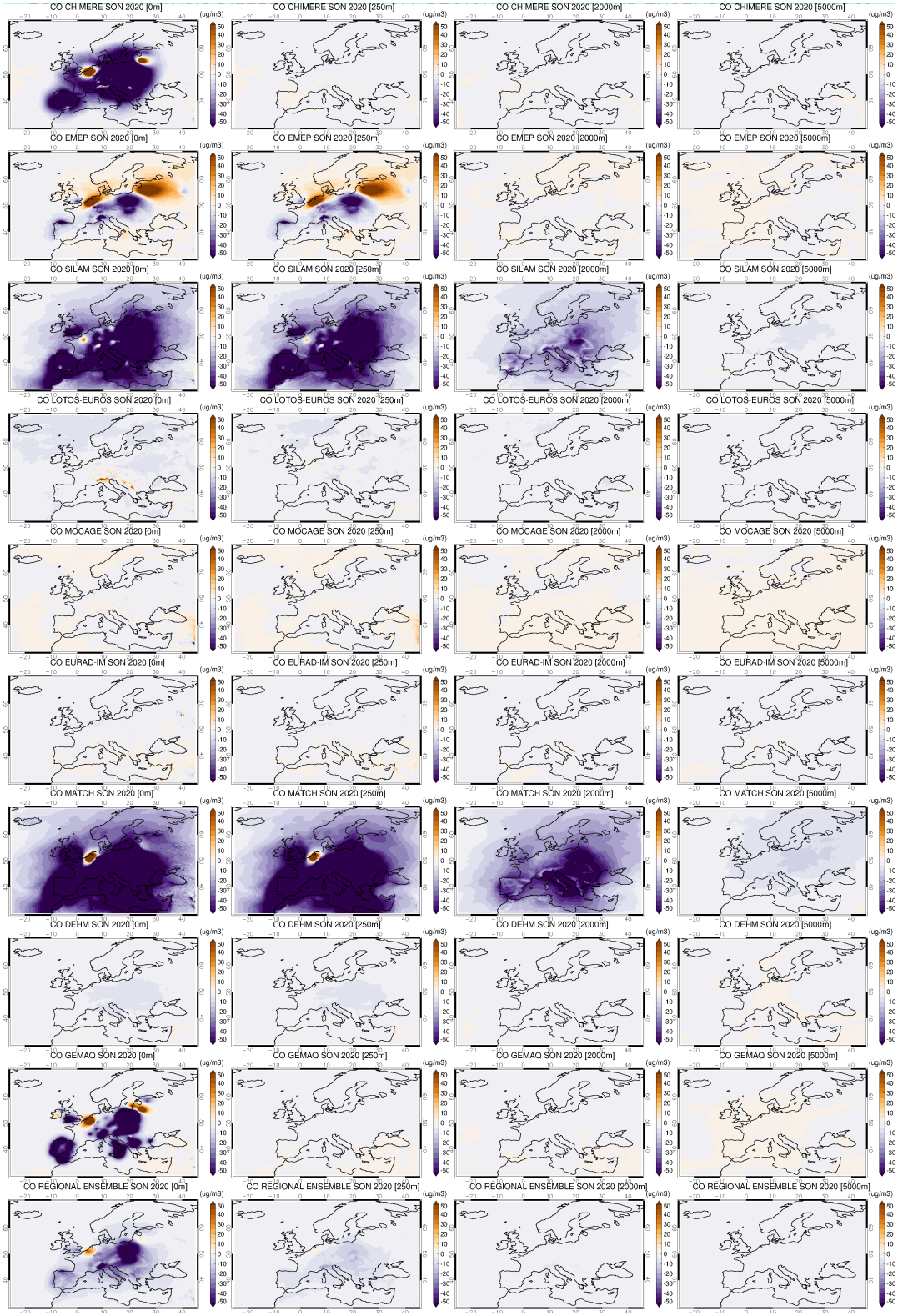


Figure 3.19. Mean regional CO differences between analysis and forecast for SON-2020 for four different vertical layers (0, 250, 2000, 5000 m) from regional ENSEMBLE and individual ensemble members (top to bottom: CHIMERE, EMEP, SILAM, LOTOS-EUROS, MOCAGE, EURAD-IM, MATCH, DEHM, GEM-AQ and ENSEMBLE).

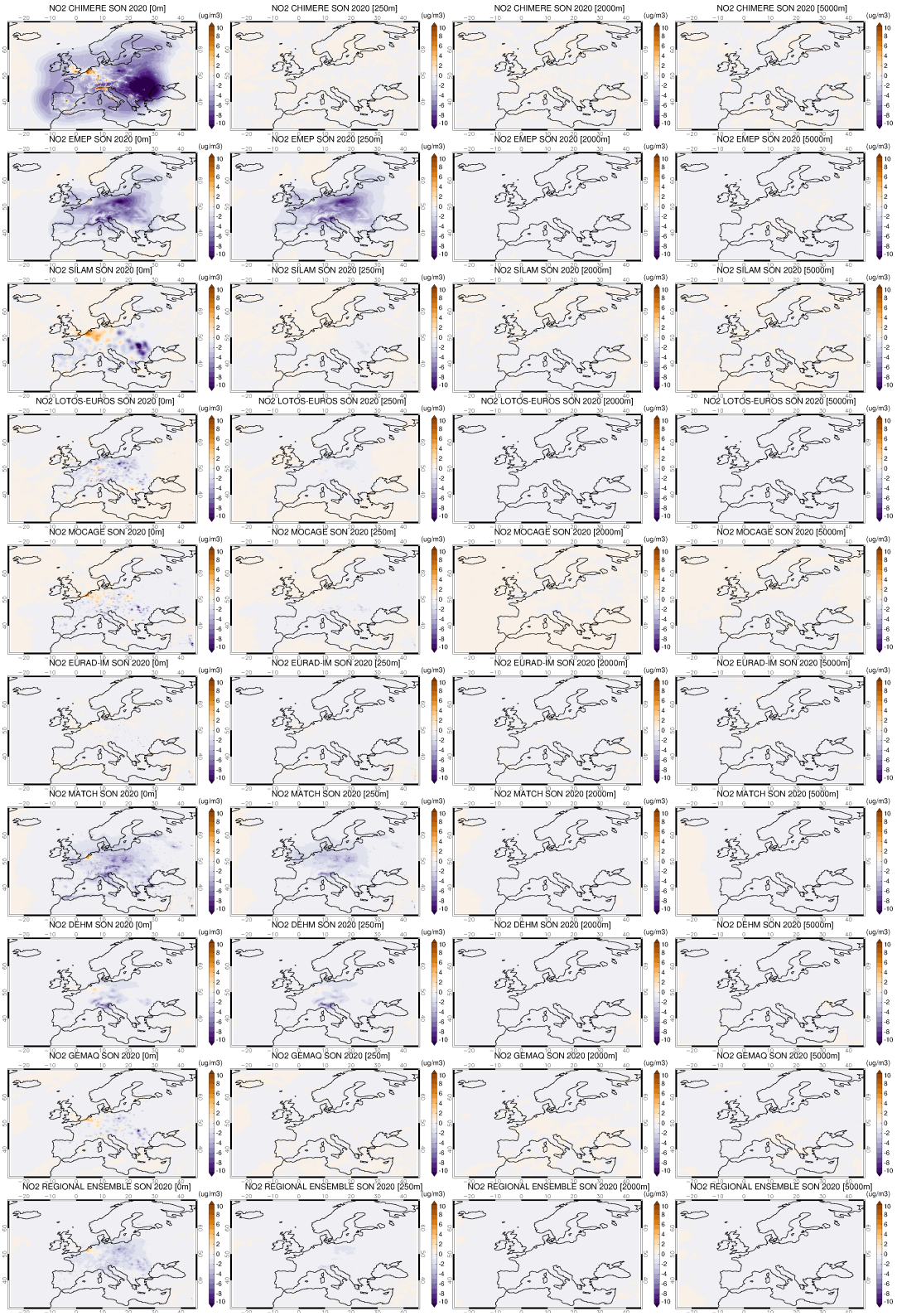


Figure 3.20. Mean regional $NO_2$ differences between analysis and forecast for SON-2020 for four different vertical layers (0, 250, 2000, 5000 m) from regional ENSEMBLE and individual ensemble members (top to bottom: CHIMERE, EMEP, SILAM, LOTOS-EUROS, MOCAGE, EURAD-IM, MATCH, DEHM, GEM-AQ and ENSEMBLE).

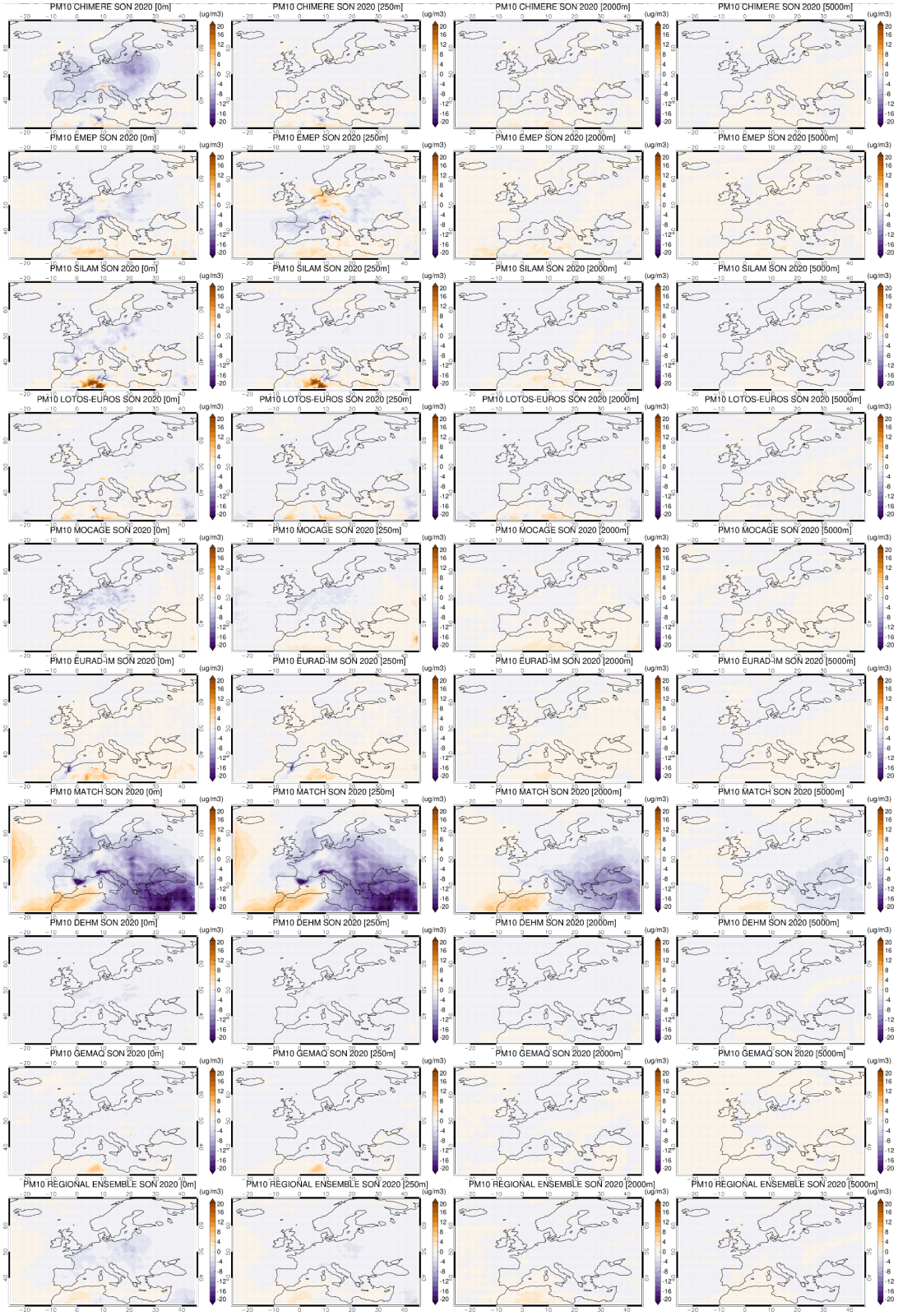


Figure 3.21. Mean regional $PM_{10}$ differences between analysis and forecast for SON-2020 for four different vertical layers (0, 250, 2000, 5000 m) from regional ENSEMBLE and individual ensemble members (top to bottom: CHIMERE, EMEP, SILAM, LOTOS-EUROS, MOCAGE, EURAD-IM, MATCH, DEHM, GEM-AQ and ENSEMBLE).

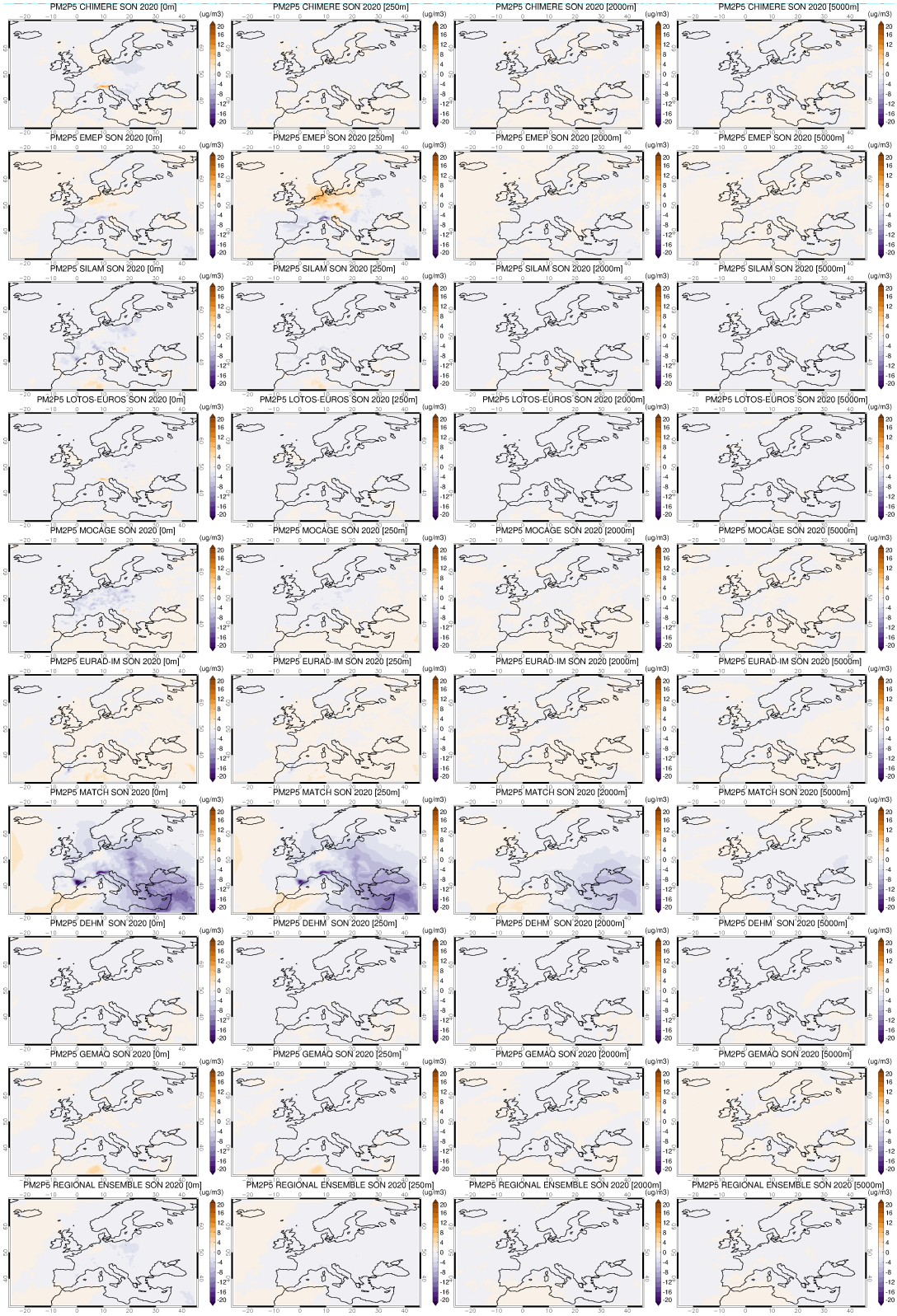


Figure 3.22. Mean regional $PM_{2.5}$ differences between analysis and forecast for SON-2020 for four different vertical layers (0, 250, 2000, 5000 m) from regional ENSEMBLE and individual ensemble members (top to bottom: CHIMERE, EMEP, SILAM, LOTOS-EUROS, MOCAGE, EURAD-IM, MATCH, DEHM, GEM-AQ and ENSEMBLE).

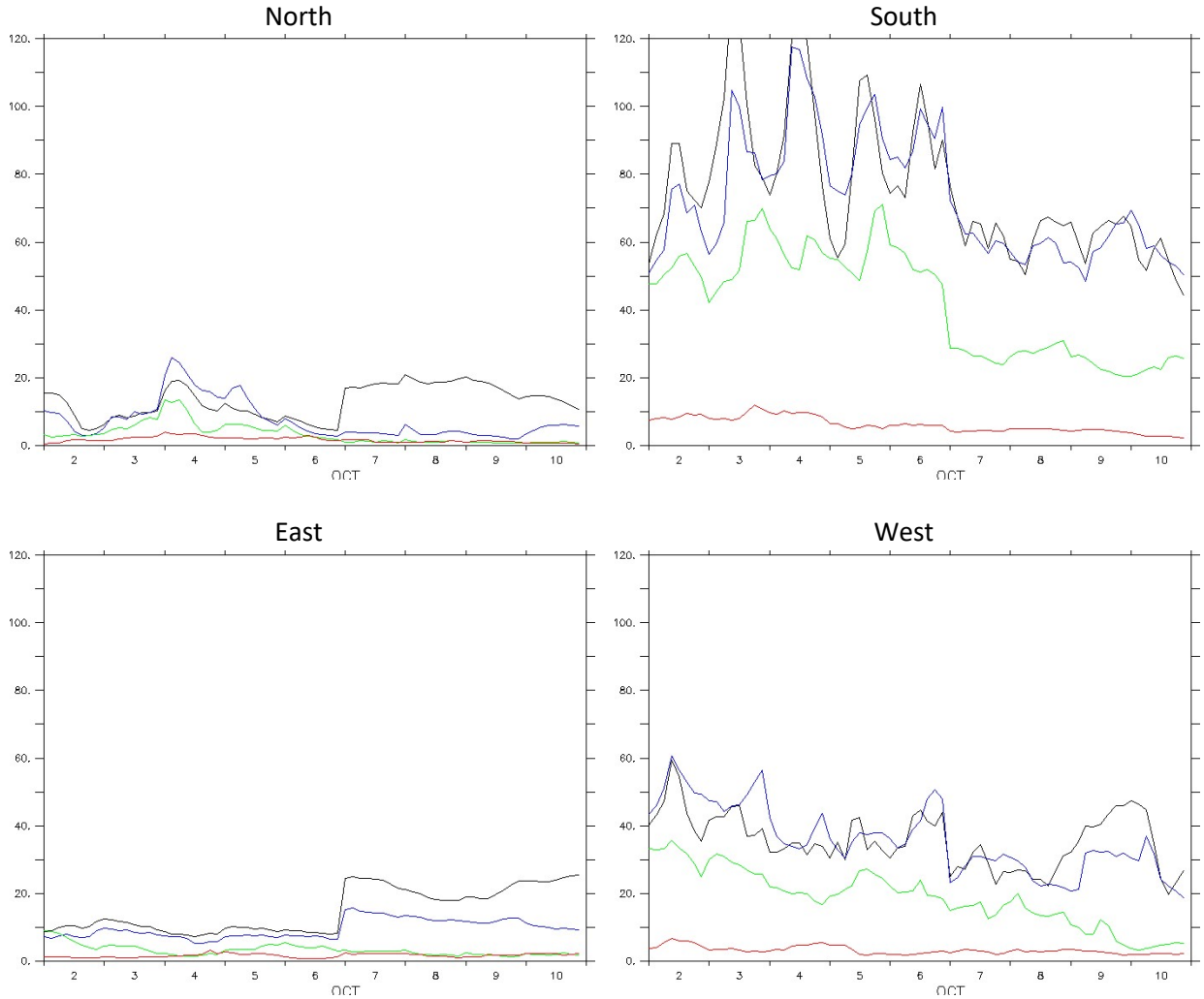


Figure 3.23. CAMS-global hourly time-series (2nd to 10th of October) of PM10 concentrations averaged across the four boundaries of the regional domain at various levels: surface (black), 250m (blue), 2000m (green) and 5000m (red).

## 3.9 CAMS-global upgrade to cycle 47R1 and its impact on the operational regional products.

CAMS-global has been upgraded from cycle 46R1 to cycle 47R1 on the 6th of October 2020. This upgrade involved a number of changes, but the most relevant to the regional products were expected to be those related to sea salt and desert dust. Specifically, the upgrade introduced improved parametrisations for sea salt and desert emissions and because of this, changes in the predicted concentrations of PM10 and PM2.5 were anticipated, especially over the Atlantic as well as Northern Africa and the Mediterranean. Figure 3.23 shows the CAMS-global hourly PM10 concentrations averaged across the four boundaries of the regional domain at various levels indicated with different colors. The upgrade appears to introduce a clear jump in PM10 concentrations, most prominently near the surface, across the Northern and Eastern boundaries, presumably associated with an increased production and transport of sea salt. On the contrary, the Southern and Western boundaries show a sharp drop, indicative of lower dust loads.

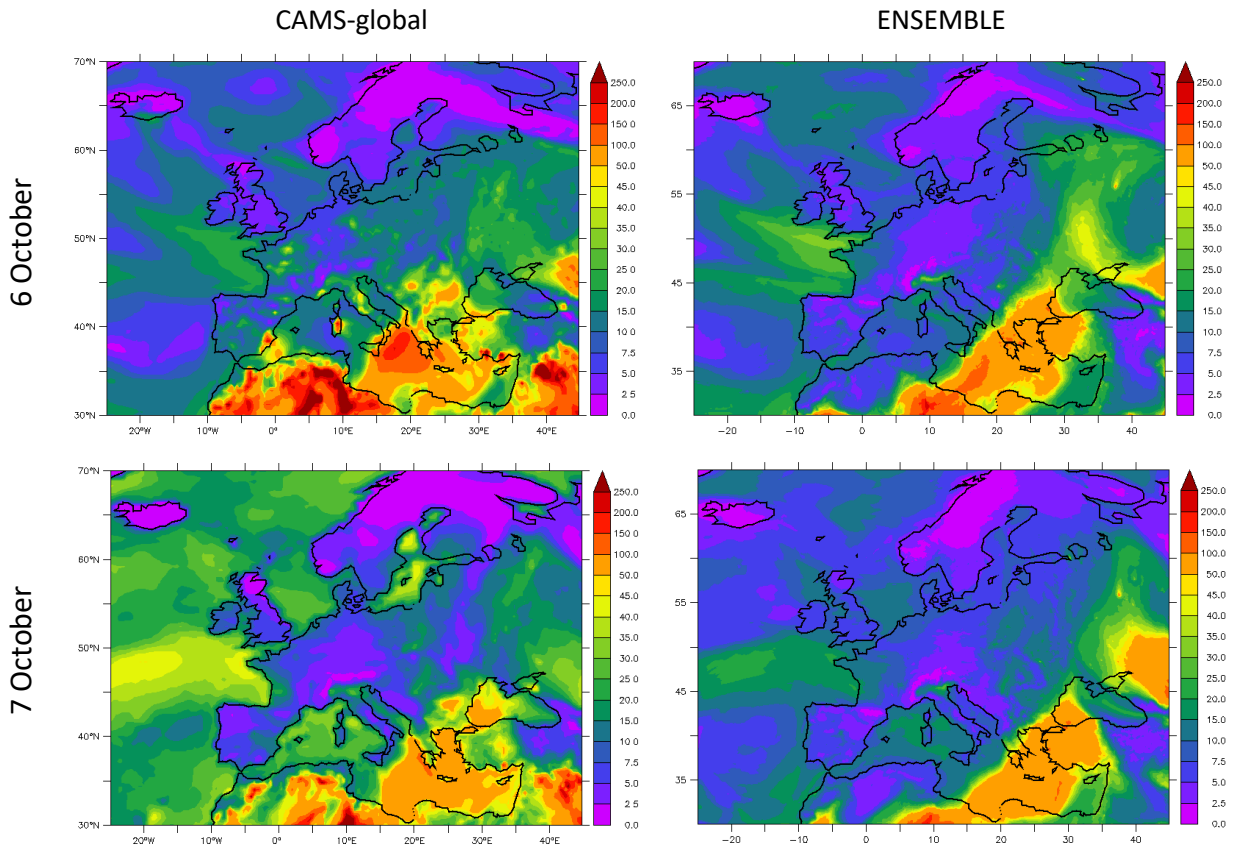


Figure 3.24. Mean daily PM10 surface fields of CAMS-global (left column) and the regional ENSEMBLE (right column) around the upgrade of CAMS-global. First row corresponds to the 6th of October (pre-upgrade) and second row to the 7th of October (post-upgrade)

Figure 3.24 shows daily PM10 surface fields around the time of the CAMS-global upgrade, for both CAMS-global and the regional ENSEMBLE. For CAMS-global, the upgrade seems to lead to generally higher concentrations over the Atlantic, and lower concentrations over North Africa. It also evidently eliminates the spurious hotspots at several Mediterranean coastal locations. Based on this very limited glance, the ENSEMBLE appears to be following the sea salt features of CAMS-global over the Atlantic but the impact near the Southern boundary is not so clear.

# 4 Vertical profile and column aerosol comparisons

## 4.1 Summary for the EARLINET lidar and Aeronet comparisons

The regional models are compared with climatological lidar profiles for each season (EARLINET/ACTRIS data from 2006-2018). Missing information on composition, size and humidity growth of the aerosol in the models introduces considerable uncertainty to the PM derived extinction, which conservatively spans up to a factor 10 for absolute extinction values. Aeronet data are used to calibrate the conversion from modelled mass to optical property aerosol extinction. This way the order of magnitude in extinction is similar between the models and the lidar profiles, but also significant differences appear at some stations in the lowest layers (Granada, Athens). Relative differences in the form of extinction profiles are more certain. We choose the most representative five stations to compare in retrospective the seasonal average aerosol profiles since 2016. The retrospective of the seasonal comparisons since 2016 shows very similar profiles during this season. The respective overestimation or underestimation of the extinction found in 2016 are usually also found in following years with the ENSEMBLE.

## 4.2 Introduction

The vertical distribution of aerosol reflects processes like atmospheric mixing, removal, and aerosol transport from outside of the domain or formation of secondary aerosol. The vertical mixing processes determine ground concentrations in polluted areas. Long-range transported aerosol, often carried aloft, may contribute to pollution in clean regions. Evaluation of the simulated aerosol column and vertical profiles are thus valuable for the performance characterisation of air quality models.

The 9 regional models provide mass concentration vertical profiles (PM2.5 and PM10) over Europe and may thus be evaluated for their aerosol vertical distribution. However, only very few aircraft campaigns and mountain sites are available to validate aerosol mass at altitude. In contrast frequent measurements of vertical profiles of aerosol backscatter, extinction or its integral, aerosol optical depth, exist. Deriving aerosol optical properties from the mass concentrations is thus needed, assuming lidar ratios and mass extinction coefficients, at least until the models provide more specific output on aerosol composition and optical properties.

In order to assess mass extinction coefficients chosen, the aerosol optical depth derived from the model mass profiles is first compared to AERONET AOD measurements. Secondly, we document a comparison of the extinction profiles derived from modelled mass concentration with climatological extinction profiles derived from European EARLINET/ACTRIS lidars.

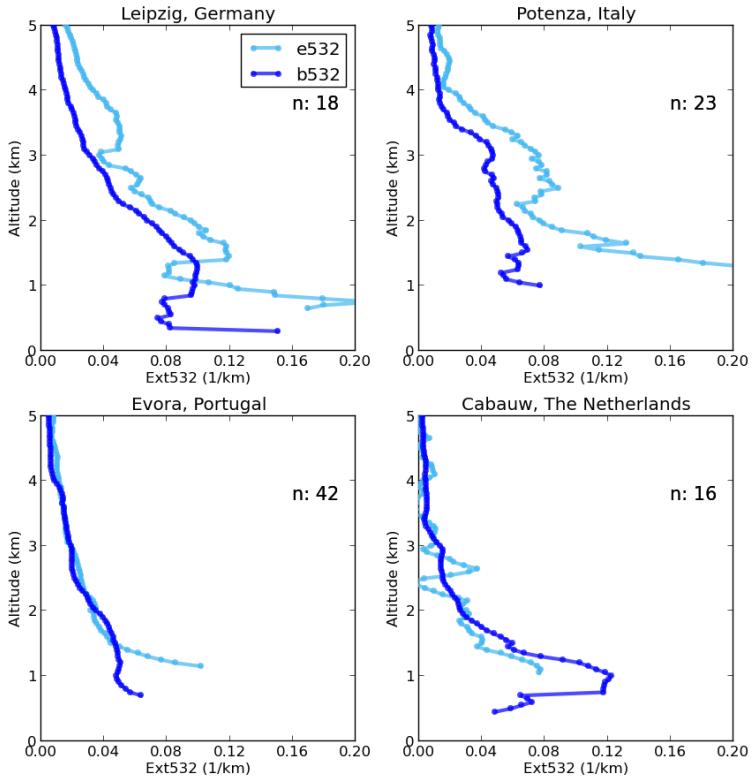


Figure 4.1. Comparison of mean profiles of two aerosol optical properties derived from the same Earlinet Raman lidar at the same time: a) aerosol extinction @532nm (light blue line) and b) extinction @532nm derived from the aerosol backscatter coefficient (dark blue) using a lidar ratio of 50 sr. The profiles use data taken at simultaneous times at each station; number of profiles given as n: x.

## 4.3 Methodology

*AERONET data*

The AERONET sun-photometers measure in non-cloudy conditions the aerosol optical depth at several wavelength and in near real time. The spatial distribution of the instruments allows a good coverage of aerosol observation over Europe. The version 3 level 1.5 data has been used in the reporting period presented here. This version and quality level ensures an efficient filtering of the residual clouds (mainly cirrus) for data in near real time. Daily AERONET aerosol optical depth, measured at 550 nm, has been averaged over summer for the European sites available in CAMS model output.

*Lidar data*

The EARLINET/ACTRIS Lidars are distributed over several locations in Europe and allow comparison across different climates in Europe (Pappalardo et al., 2014). Yet, up to now, there are no near-real-time data available. Regular measurements in EARLINET are sparse and often acquired once per week, with gaps due to maintenance or funding restrictions. A climatology has been computed per station and per season with all measurements available between 2006 and 2018.

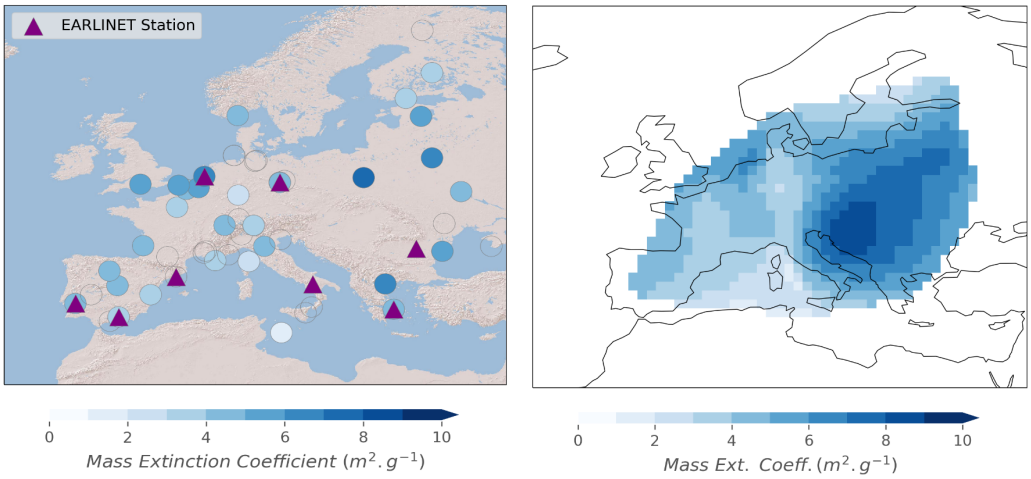


Figure 4.2. Mass extinction coefficient estimated at AERONET location sites (blue dots) and EARLINET stations (triangles) for SON2020 (left). A European map of the Mass Extinction Coefficient has been constructed with cubic interpolation in the inner part of the region covered by AERONET on the model grid (right), and with the nearest neighbours in the outer part of this region (not shown).

The backscatter coefficient and extinction profiles at 532 nm have been extracted from the EARLINET database. The more frequently measured backscatter profiles are considered here with priority. An aerosol extinction coefficient profile is computed from the backscatter coefficient using a range of plausible lidar ratios. This latter parameter depends on the aerosol type and is more likely decreasing with the size of the aerosol. Minimum values are observed for sea salt aerosol (below 30 sr at 550 nm, [Ackermann et al., 1998, Omar et al., 2009]), while larger values are related to urban particles (55 sr in [Muller et al., 2007], 70 sr in [Cattrall et al., 2005]). Desert dust is associated with intermediate lidar ratios, ranging from 30 sr to 60 sr depending on the sources and the transport regime. A climatology of aerosols in West Africa published in Mortier et al. [2016] revealed an average lidar ratio (over 9 years) of about 30±15 sr. Due to the location of the stations involved in this study, both dust and urban aerosols and any a mix of them might occur. In order to represent the uncertainty on the nature of aerosols, we show the range in likely mean extinction using a lidar ratio extending from 30 to 70 sr.

As a test, the conversion of lidar backscatter to extinction coefficient is performed assuming a constant average lidar ratio of 50 sr at locations where both backscatter and extinction coefficients are measured in EARLINET. This allows consistent comparison and visualization of some of the error associated to our simplified constant lidar ratio assumption. We have excluded from this comparison cases where local extinction coefficient was above 0.5 $km^{-1}$ in order to avoid outliers. The profiles shown in figure 4.1 from 4 stations reveal an error in the mean profile of 0-30% in extinction, which is small compared to the model spread documented below. The extinction profiles derived from the backscatter coefficients look vertically smoother. We have excluded from this comparison cases where local extinction coefficient was above 0.5 $km^{-1}$ in order to avoid outliers.

In addition to this aerosol typing uncertainty, a sampling error should be accounted for. The observations are sporadic, while the models predict the aerosol concentration continuously. Therefore, seasonal averages are not computed with the same coverage in model and

observation. Our earlier model-based bootstrap studies revealed, that, depending on the station, a set of ca. 30 daily observations allows reproducing the seasonal average with an error of about 10% [ACTRIS Deliverable WP6/D6.21]. In our case, this error might be larger since the synoptic situation is very different between our EARLINET climatological dataset, covering 2006-2018, and the season covered in this report. An overall uncertainty of about 20% has been chosen to represent the sampling error.

*Model data*

The ensemble and the underlying 9 regional CAMS models are investigated. For each of these models, the hourly PM10 and PM2.5 vertical profiles are extracted at the EARLINET station locations from the first day of each daily forecast at levels 0, 50, 250, 500, 1000, 2000, 3000, 5000 m.

The conversion of PM10 mass concentration to extinction requires a mass extinction coefficient (MEC). MEC depends on the size distribution, refractive index and density of the particles. This information is not yet available from the models. For different kind of aerosols, MEC values can vary from about 0.5 $m^2g^{-1}$ in the case of desert dust aerosols up to 8 $m^2g^{-1}$ for urban particles [Chin et al., 2002]. No variation with height or aerosol type is taken into account, mainly because the models provide no further info on aerosol speciation. We derive the MEC value to convert the model profile data to extinction profiles from a combination of the modelled mass column load and consistent Aeronet AOD data.

For the Aeronet based computation of the MEC, the model data are picked at the location and on the day when sun photometer observations were available. The CAMS-regional mass concentrations have been averaged for coincident days (with the measurements) and averages are converted, with a seasonal and site dependent mass extinction coefficient estimated with AERONET retrievals, into extinction profiles. A seasonal and site dependent mass extinction coefficient is obtained when combining it with AERONET AOD retrievals. Values of MEC are ranging from 1 $m^2g^{-1}$ in South-West of Europe to more than 10 $m^2g^{-1}$ in the North-East. Since some of the EARLINET stations are not co-located with Sun photometers, a European map of MEC has been constructed, for each season, by interpolating (cubic interpolation) and extrapolating (nearest neighbour) the available AERONET based MEC calculations on the grid of the model (figure 4.2). One can notice a gradient with the longitude with lower values found in the Western part while the highest values are observed in the Eastern part of Europe. Also, the values are generally lower as compared to last year, which might reveal a higher concentration in coarse particles (dust). The seasonal AERONET-based MEC is then used at each EARLINET station to calculate the model extinction from concentration profiles. The uncertainty on the MEC being removed allows more accurate comparisons with the observed vertical profiles than using an average MEC over whole Europe.

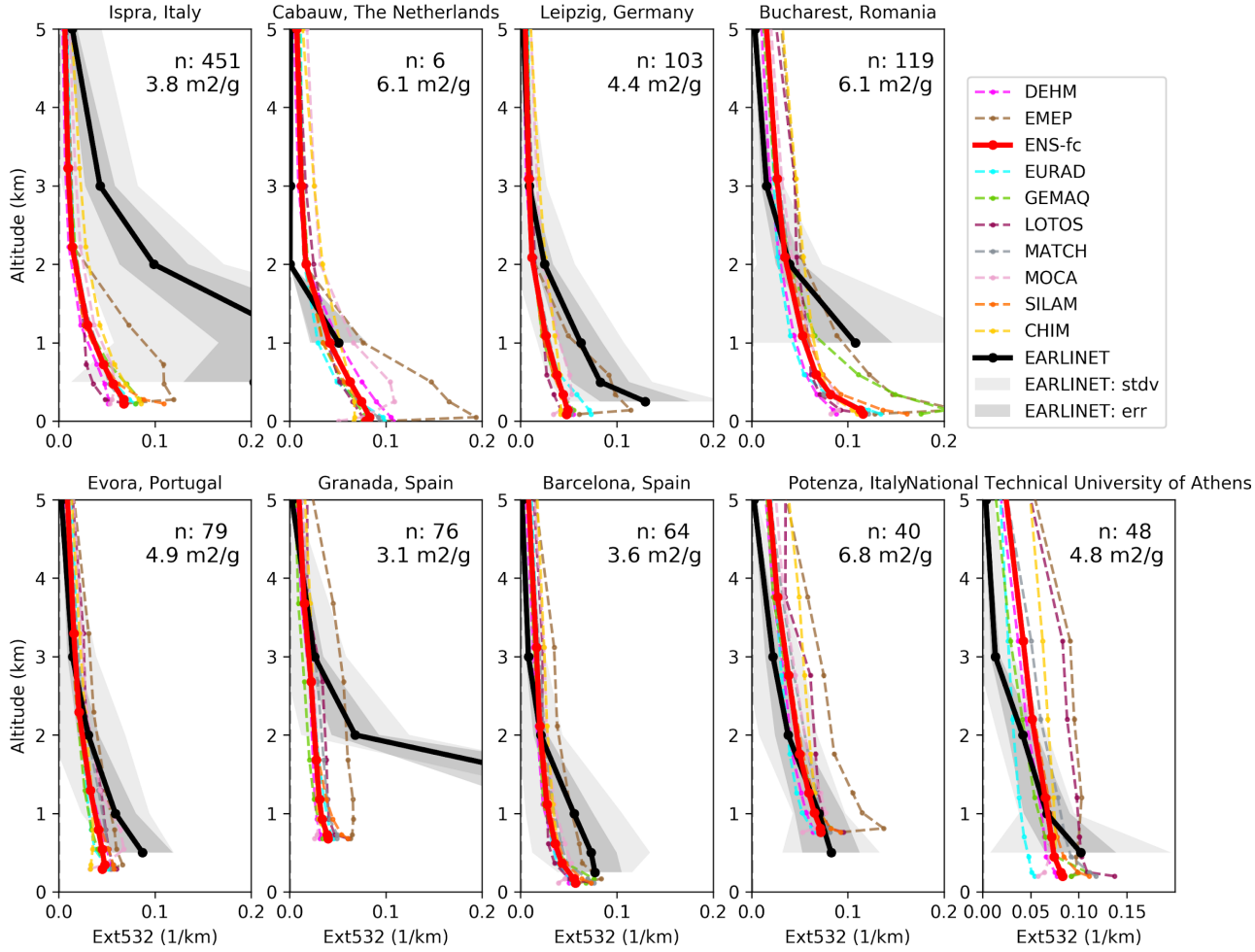


Fig 4.3. Extinction profiles September - November 2020 derived from the ENSEMBLE forecast mass concentration profiles (red envelope) and from EARLINET (climatology) backscatter profiles (grey envelope: lidar ratio uncertainty, light grey: including sampling error). "n: XX means number of individual EARLINET profiles assembled (September - November 2006-2018). The EMC used for the calculation of the extinction from the concentration profiles is indicated for each station below the number of EARLINET profiles "n" used for the calculation of the climatology.

## 4.4 Results

### 4.4.1 Comparison of extinction profiles

The extinction profiles estimated from the 9 CAMS models and the ENSEMBLE and EARLINET measurements are compared for SON 2020 (figure 4.3).

One observes generally a good agreement between the two datasets at the exception of Ispra and Granada while Ispra is associated with the highest number of measurements. In Cabauw, and Potenza, the models are in perfect agreement with the observed climatology. As noticed in the previous seasons, in Leipzig, where the observations are also available close to the ground, the ENSEMBLE underestimates the extinction, while one of the models (EMEP) shows a similar pattern than in the observation dataset. The same pattern is found in Bucharest. In Athens, all of the models overestimate the extinction above 2 km of altitude.

### 4.4.2 Seasonal variability

In order to investigate the performance of the model in reproducing the vertical profiles, it is interesting to observe the inter-annual variability for the different seasons. This will be of use for the development of a score providing an assessment of the model skill and is also useful to investigate the models synoptic variability. The seasonal profiles have been reported since 2016 at 5 stations (Leipzig, Barcelona, Potenza, Evora and Bucharest) in Figure 4.4, using the new EARLINET climatology. Performances of the models in 2020 look similar to the performances observed in autumn 2019. However, in Leipzig, the underestimation of the extinction in the lowest layers has increased, as well as the overestimation of the extinction above 2 km of altitude in Potenza, where the profile appears to be too flat vertically.

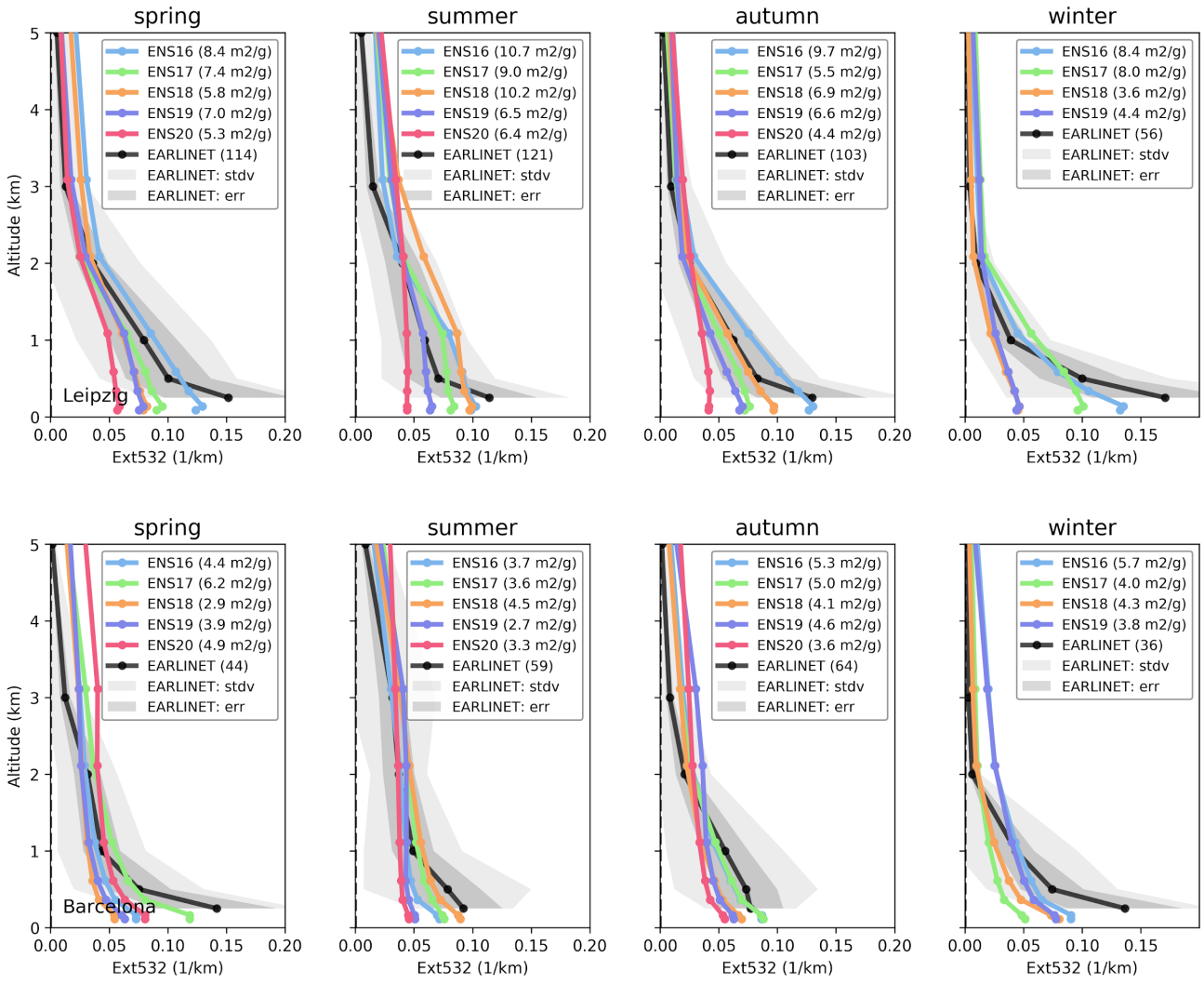

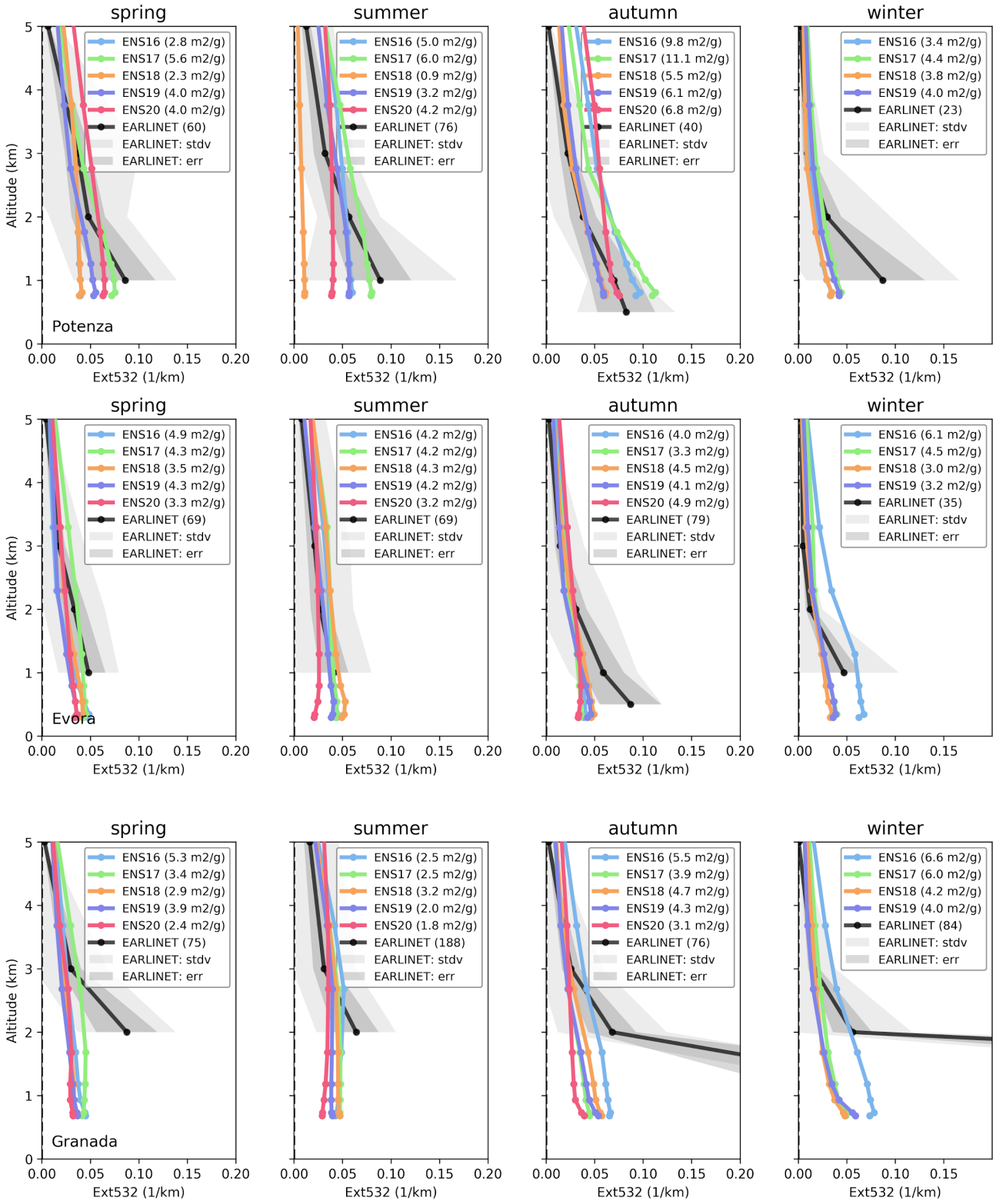


Fig 4.4: Seasonal extinction profiles derived from ENSEMBLE forecast mass concentration profiles for 2016 (ENS16), 2017 (ENS17), 2018 (ENS18), 2019 (ENS19), 2020 (ENS20) and EARLINET climatology. The parenthesis indicates for the CAMS profiles, the MEC used for the extinction estimation, and for the EARLINET, the number of profiles used for constructing the climatology.

# 5 IAGOS aircraft CO and $O_3$ profile comparisons

## 5.1 Summary

Routine observations of ozone and CO over European airports are available from the IAGOS fleet. Unfortunately, due the COVID-19 crisis and its impact on the airline operations, only one IAGOS flight has been recorded during this reporting period. It is worth mentioning that this is the first time since the beginning of IAGOS that almost no data are available.

Take-off and landing profiles were sampled from the hourly model 3D forecasts along the flight tracks.

For the single available profile, ozone from the regional ENSEMBLE and CAMS-global in the lowest layer is represented well but is slightly underestimated above 1km altitude. Carbon monoxide is mostly underestimated.

IAGOS Validation Method

Validation is possible at the European airports visited by the IAGOS fleet. For the European-based carriers, there are regular profiles at the home airports. There are two aircraft operated by Lufthansa, one operated by Air France. Thus, when the fleet is fully operational, there are daily profiles Frankfurt and Paris (CDG). IAGOS is also installed on two aircraft operated by the Asian-based carrier China Airlines. Aircraft fly regularly from Taipei to Amsterdam or Vienna and sometimes to Rome. Other airports may be visited depending on the operational schedules of the airlines

We download the daily latitude-longitude datasets for the 9 regional models and the ENSEMBLE for two species (carbon monoxide and ozone) on 8 vertical levels (surface, 50m, 250m, 500m, 1000m, 2000m, 3000m, 5000m). The aircraft takes about 10 minutes to climb or descend the 5000m vertical extent covered by the regional models. During this time and travelling at up to 166 m $s^{-1}$, it covers about 120km and therefore traverses many grid-boxes of resolution 10km. We perform a spatial interpolation from the grid of the regional models to the aircraft's trajectory. The IAGOS measurements in ppbv are converted to µg $m^{-3}$ using the temperatures measured by IAGOS. The data are validated by the PI but are not yet calibrated. Calibration takes place after an operational period of about 6 months.

## 5.2 IAGOS Ozone

Figure 5.1 shows the IAGOS ozone profile recorded at 8:36 am local time and the ENSEMBLE is shown at 4 forecast times. This IAGOS profile highlights relatively normal conditions, close to the seasonal average. Figure 5.2 shows the IAGOS profile together with the profiles of the 9 CAMS regional models. Especially in the first km, ozone is quite well reproduced by all 9 models but is slightly overestimated above that.

## 5.3 IAGOS Carbon Monoxide

Figures 5.3 and 5.4 indicate that in the morning of the 17$^{th}$ of November, CO was underestimated by the models throughout the atmosphere. This is a quite typical behavior that has been featured in the past.

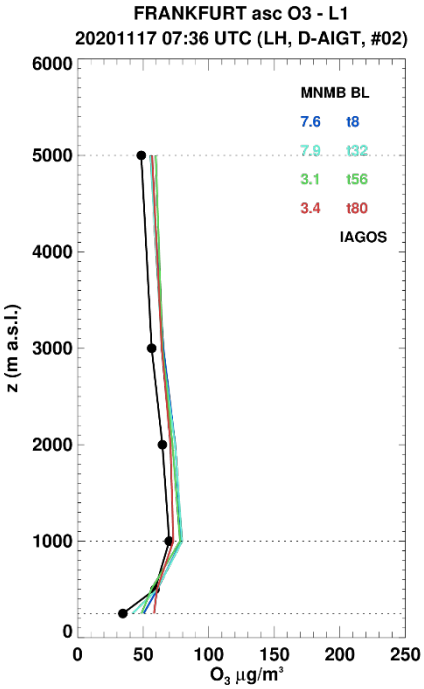


Figure 5.1. Ozone profile on the 16th of November 2020. IAGOS is shown in black and the ENSEMBLE is shown at 4 forecast times (blue: 1-day; cyan: 2-day; green: 3-day; red: 4-day). (Units: µg $m^{-3}$).

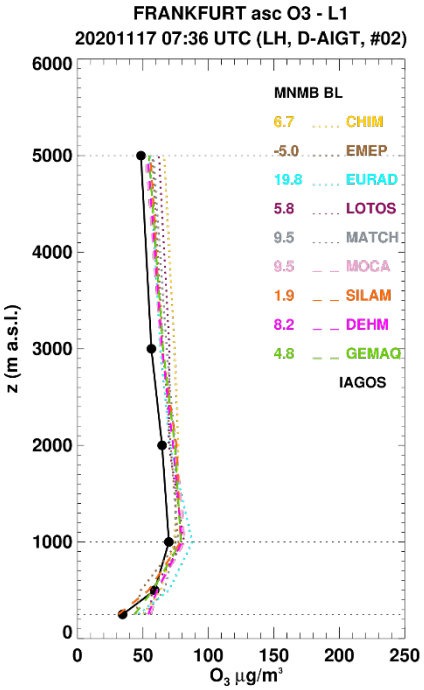


Figure 5.2: Ozone profile at Frankfurton the 17th of November 2020. IAGOS is shown in black and each colour/ line style corresponds to one of the 9 models for the ENSEMBLE. In the legend, the models are CHIM=CHIMERE, EMEP=EMEP, SILAM=SILAM, LOTOS=LOTOS-EUROS, MOCA=MOCAGE, EURAD=EURAD, MATCH=MATCH, DEHM=DEHM, GEMAQ=GEM-AQ. (Units: µg.$m^3$).

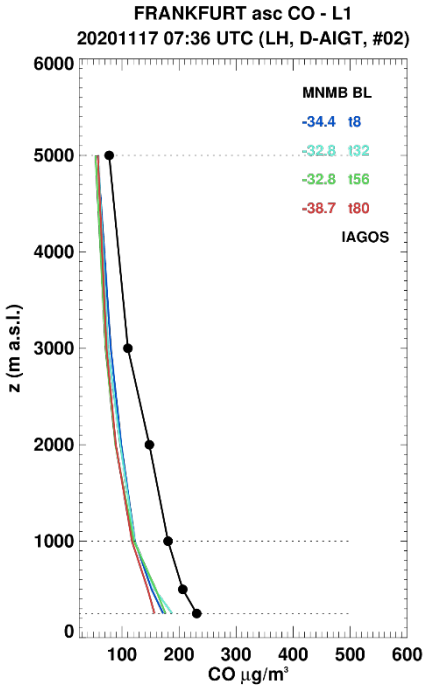


Figure 5.3: CO profile at Frankfurt, on the 17th of November 2020. IAGOS is shown in black and the ENSEMBLE is shown at 4 forecast times (blue: 1-day; cyan: 2-day; green: 3-day; red: 4-day). (Units: µg.m$^3$).

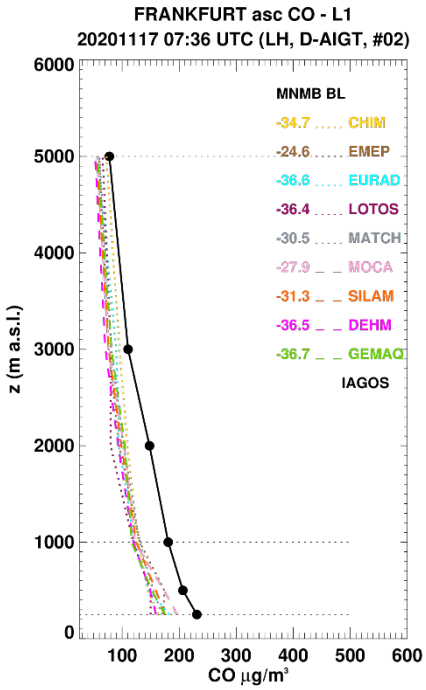


Figure 5.4: CO profile at Frankfurt on the 17th of November 2020. IAGOS is shown in black and each colour/ line style corresponds to one of the 9 models for the ENSEMBLE. In the legend, the models are CHIM=CHIMERE, EMEP=EMEP, SILAM=SILAM, LOTOS=LOTOS-EUROS, MOCA=MOCAGE, EURAD=EURAD, MATCH=MATCH, DEHM=DEHM, GEMAQ=GEM-AQ. (Units: µg.m$^3$).

# 6 Validation of regional model tropospheric $NO_2$ using MAX-DOAS

## 6.1 Summary

MAX-DOAS surface remote sensing observations provide tropospheric columns of $NO_2$, with the largest sensitivity in the boundary layer. While the magnitude of VCDs derived from the measurements for the urban stations De Bilt and Bremen are reproduced well by the model ENSEMBLE, the ENSEMBLE underestimates the values in Athens (bias ~-2 x $10^{15}$ molec. $cm^{-2}$). Large differences can be found between individual models depending on the station. Although many of the model simulated values probably fall within the uncertainty range of MAX-DOAS retrievals, the latter alone cannot explain differences between retrievals and simulations, especially those found for variations in time. For the regional ENSEMBLE, moderate correlations on the order of 30-65 % are found for each station. The regional ENSEMBLE performs significantly better than the global model in terms of correlation at all stations except for De Bilt. However, some of the larger $NO_2$ values inside individual pollution plumes are underestimated by the models.

## 6.2 Introduction

MAX-DOAS observations of atmospheric composition are performed by taking measurements of the scattered sunlight at different elevation (and sometimes also azimuthal) angles. Depending on the viewing angle and solar position, the light path through the atmosphere is different, with the observation in the zenith direction usually providing the shortest light path through the lower troposphere. Therefore, using the zenith measurement as intensity of incident radiation and the observations in other angles as intensity of transmitted radiation, the total amount of molecules of a certain species along the light path difference, the so-called slant column densities, can be determined using Lambert Beer's law. Using radiative transfer modelling and Optimal Estimation techniques, this can be inverted to tropospheric columns and even lower altitude tropospheric profiles.

The advantage of MAX-DOAS measurements is their ability to observe several pollution related species at the same time (e.g., $NO_2$, HCHO, CHOCHO, $SO_2$, aerosols, potentially also $O_3$) and to provide data which is virtually free of interferences from other species such as PAN or $NO_y$ for $NO_2$. Also, the fact that the observations integrate over a comparatively large volume can be an advantage for satellite and model validation as the observed quantity is relatively close to the modelled one. On the other hand, the uncertainty of the retrievals is considerable (on the order of 30% for $NO_2$ tropospheric columns and larger for individual layers) and depends on cloud occurrence and aerosol loading.

In this report, regional air quality model forecasts of tropospheric $NO_2$ columns are compared to MAX-DOAS retrievals from 3 urban stations (De Bilt– KNMI, Bremen – IUP-UB, Athens – IUP-UB). The reader is referred to previous reports for comparisons from the rural station OHP (BIRA-IASB) (which showed in general an underestimation by the model ENSEMBLE and an overall better performance for CAMS-global here) as the instrument at this site stopped working in March 2017. The MAX-DOAS instrument for the urban site in Uccle (BIRA-IASB) was dismantled in March 2020, and comparisons for this station are therefore not continued since this time. Since the MAM 2020 report, the MAX-DOAS data used in the comparisons is based on tropospheric column retrievals, meaning that no profile information is

incorporated in the comparisons since this time. A simple block profile is assumed in the MAX-DOAS retrievals and column averaging kernels are estimated based on the box air mass factor for each observation layer. An overview of the station data is given by Table 6.1. The MAX-DOAS instrument in Athens was not working correctly in August and September 2020 leading to gaps in the measurements during these months.

Note that the time period investigated starts in June 2020 for consistency, as two new models were recently introduced to the ENSEMBLE.

## 6.3 Inter-comparison method

Model VCDs (vertical column densities) have been calculated based on regional model data interpolated to MAX-DOAS output altitudes. Column averaging kernels (AVKs) from the measurements were applied to model $NO_2$ partial columns before summing up $NO_2$ values in the vertical:

$$VCD_{method2}^{model} = \sum_{i=1}^{Nobs} AVK_i \cdot VCD_i^{model}$$

The averaging kernels are part of the profiling output and represent the sensitivity of the retrieved column to the $NO_2$ amount at different altitudes. As the sensitivity of MAX-DOAS retrievals is largest in the boundary layer, the application of averaging kernels from the measurements to model simulations can have a crucial influence on validation results.

Only those model values closest to the measurement time are used below. As the model output is given in hourly time steps, the maximum possible time difference between measurements and simulations shown here is 30 minutes.

## 6.4 Results

Figure 6.1 shows time series of tropospheric $NO_2$ VCDs derived from MAX-DOAS for the model ENSEMBLE. The magnitude of VCDs from the measurements for De Bilt and Bremen is reproduced by the models, an underestimation is found for Athens. The underestimation for Athens may be related to problems in simulating vertical transport of pollution within the boundary layer, as the instrument is placed on a small hillside above the city centre and the comparisons for Athens are therefore representative for altitudes larger than approximately 500 m absl. The retrievals show a larger variability of values compared to the models. Measurements and simulations don't agree very well for some of the time steps investigated. The models underestimate some of the larger $NO_2$ values inside individual pollution plumes. Models may fail to reproduce these peaks due to errors in NOx emissions, transport of $NO_2$ towards the stations and chemistry.

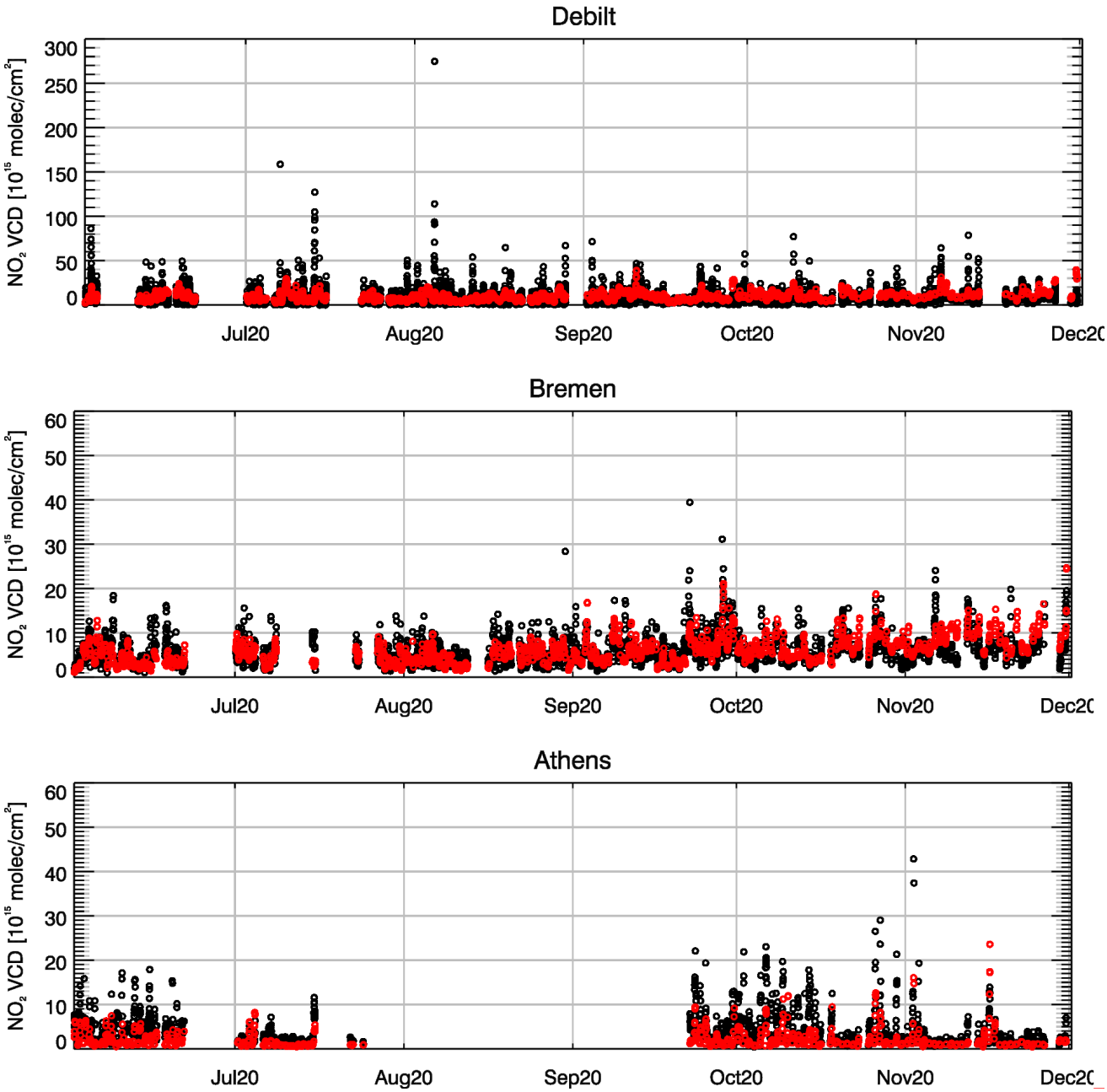


Figure 6.1. Time series of tropospheric $NO_2$ VCDs [$10^{15}$ molec. $cm^{-2}$] from (black circles) MAX-DOAS and (red circles) the ENSEMBLE forecasts for (from top to bottom) De Bilt, Bremen, Athens.). Model results were calculated by multiplying $NO_2$ partial columns with averaging kernels for each observation layer followed by summing up resulting values in the vertical. Model data was interpolated to the averaging kernel layer altitudes prior to calculation of VCDs. Time period: June - November 2020. The MAX-DOAS instrument in Athens was not working correctly for a time period in August and September 2020 leading to gaps in the time series.

Table 6.1. Overview of MAX-DOAS station data used for validation of regional air quality model simulations. The time period covered in this report is June 2020 to November 2020.

| Station | Latitude, longitude | Altitude above sea level | Institution | Quantity | Character |
|---|---|---|---|---|---|
| Bremen (Germany) | 53.106°N, 8.86°E | 21 m | IUP-UB | column | urban |
| De Bilt (Netherlands) | 52.1° N, 5.18° E | 23 m | KNMI | column | urban |
| Athens (Greece) | 38° N, 23.7° E | 527 m | IUP-UB | column | urban |

Figure 6.2 shows comparisons of diurnal cycles. Again, the mean column amounts of the ENSEMBLE are comparable for De Bilt and Uccle, but values are generally underestimated in Athens. Although larger differences are found depending on the regional model, the model ENSEMBLE performs much better than CAMS-global for all stations, CAMS-global is negatively biased. Some regional models show different variations from one hour to another. The afternoon peak observed by MAX-DOAS for De Bilt is not reproduced by all models. This may be related to inadequate photochemistry, scaling of emissions in time or vertical distribution of $NO_2$ and errors in simulating pollution transport towards the station.

Comparisons of weekly cycles are shown in Figure 6.3. Weekly cycles are underestimated by all regional models, with a stronger decrease of $NO_2$ columns from workdays towards the weekend retrieved by MAX-DOAS for all urban stations. CAMS-global mainly fails to reproduce weekly cycles. Note that some variations of values from one day to another may just be coincidence due to data sampling. Large variability is found between the Monday averages by the individual regional models especially for Athens.

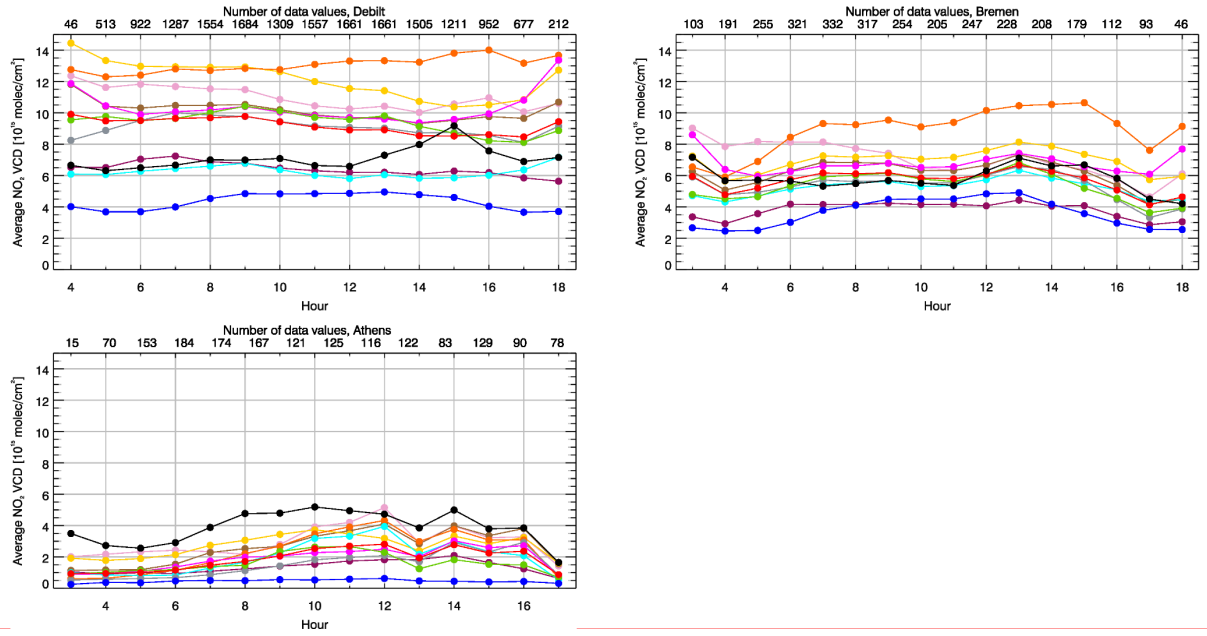


Figure 6.2. Diurnal cycles (averages over hourly bins) of tropospheric $NO_2$ VCDs [$10^{15}$ molec. $cm^{-2}$] for (top left) De Bilt, (top right) Bremen and (lower left) Athens. The black lines show the MAX-DOAS retrievals. All other lines refer to model data: (red) ENSEMBLE, (yellow) CHIMERE, (brown) EMEP, (orange) SILAM, (purple-blue) LOTOS-EUROS, (cyan) EURAD-IM, (pink) MOCAGE, (grey) MATCH, (fuchsia) DEHM, (light green) GEM-AQ and (blue) CAMS-global. Time period: June – November 2020.

Scatter density plots or heat maps of tropospheric $NO_2$ VCDs from MAX-DOAS against model ENSEMBLE values corresponding to the time series displayed in Figure 6.1 as well as statistical values (root mean squared error, bias, correlation) are given in Figure 6.4. Corresponding statistical values for all individual models are given in Table 6.2. Correlations on the order of 20-70 % are found for each station for all models. The ENSEMBLE reaches the highest correlation of about 65 % at Athens. Models tend to overestimate lower and underestimate higher $NO_2$ VCDs for the three urban stations. While the spread of values is quite large for individual data points, there is a fair agreement between models and retrievals for the majority of measurements for urban stations (as shown by the high percentage of values close to the reference line). The ENSEMBLE performs significantly better than CAMS-global in terms of correlation for all stations except for De Bilt. CAMS-global has a rather strong negative bias at all stations and that the correlation is nearly zero for Athens. All regional models are negatively biased in Athens.

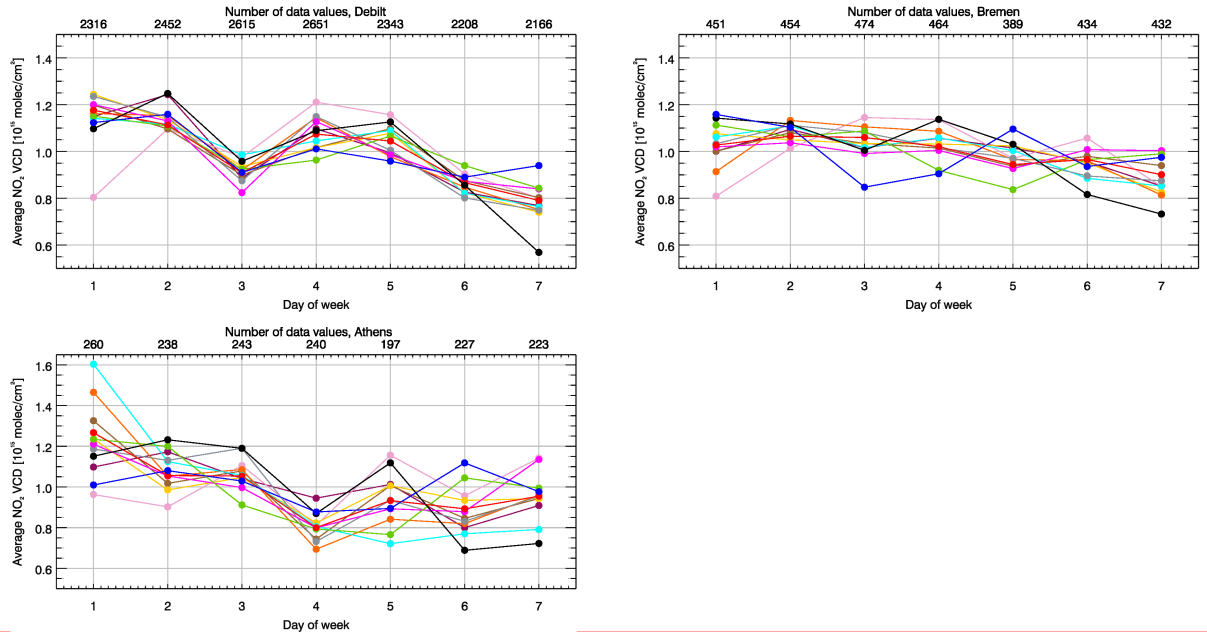


Figure 6.3. Weekly cycles (averages over daily bins divided by mean over whole week) of tropospheric $NO_2$ VCDs [$10^{15}$ molec $cm^{-2}$] for (top left) De Bilt, (top right) Bremen and (lower left) Athens. The black lines show the MAX-DOAS retrievals. All other lines refer to model data: (red) ENSEMBLE, (yellow) CHIMERE, (brown) EMEP, (orange) SILAM, (purple) LOTOS-EUROS, (cyan) EURAD-IM, (pink) MOCAGE, (grey) MATCH, (fuchsia) DEHM, (light green) GEM-AQ and (blue) CAMS-global. Time period: September-November 2020.

| | De Bilt | Bremen | Athens |
|---|---|---|---|
| **ENS** | 6.781/2.004/0.331 | 2.864/0.050/0.540 | 3.730/-2.157/0.651 |
| **CHIMERE** | 8.918/4.800/0.303 | 3.408/1.297/0.543 | 3.111/-1.223/0.687 |
| **EMEP** | 7.225/2.854/0.354 | 3.180/0.582/0.519 | 3.403/-1.370/0.643 |
| **SILAM** | 11.091/5.946/0.270 | 5.927/3.421/0.478 | 3.745/-1.588/0.584 |
| **LOTOS-EUROS** | 6.479/-0.680/0.245 | 3.465/-1.811/0.455 | 4.563/-2.687/0.342 |
| **EURAD-IM** | 8.305/3.714/0.296 | 4.385/1.351/0.443 | 4.291/-1.003/0.417 |
| **MOCAGE** | 6.097/-0.937/0.311 | 3.133/-0.417/0.501 | 3.914/-2.025/0.593 |
| **MATCH** | 7.667/2.071/0.300 | 3.250/-0.270/0.474 | 4.148/-2.570/0.566 |
| **DEHM** | 7.970/2.835/0.253 | 3.483/0.843/0.426 | 3.787/-2.082/0.627 |
| **GEMAQ** | 8.003/2.398/0.212 | 3.536/-0.168/0.410 | 4.277/-2.376/0.422 |
| **OSUITE** | 6.383/-2.614/0.329 | 3.881/-1.913/0.293 | 5.328/-3.592/-0.010 |

Table 6.2: Statistics on how tropospheric $NO_2$ VCDs [$10^{15}$ molec. $cm^{-2}$] from models compare to MAX-DOAS retrievals at the three stations. Each column entry shows from left to right: root mean squared error [$10^{15}$ molec. $cm^{-2}$], bias [$10^{15}$ molec. $cm^{-2}$] and correlation coefficient (cor). Time period: June-November 2020.

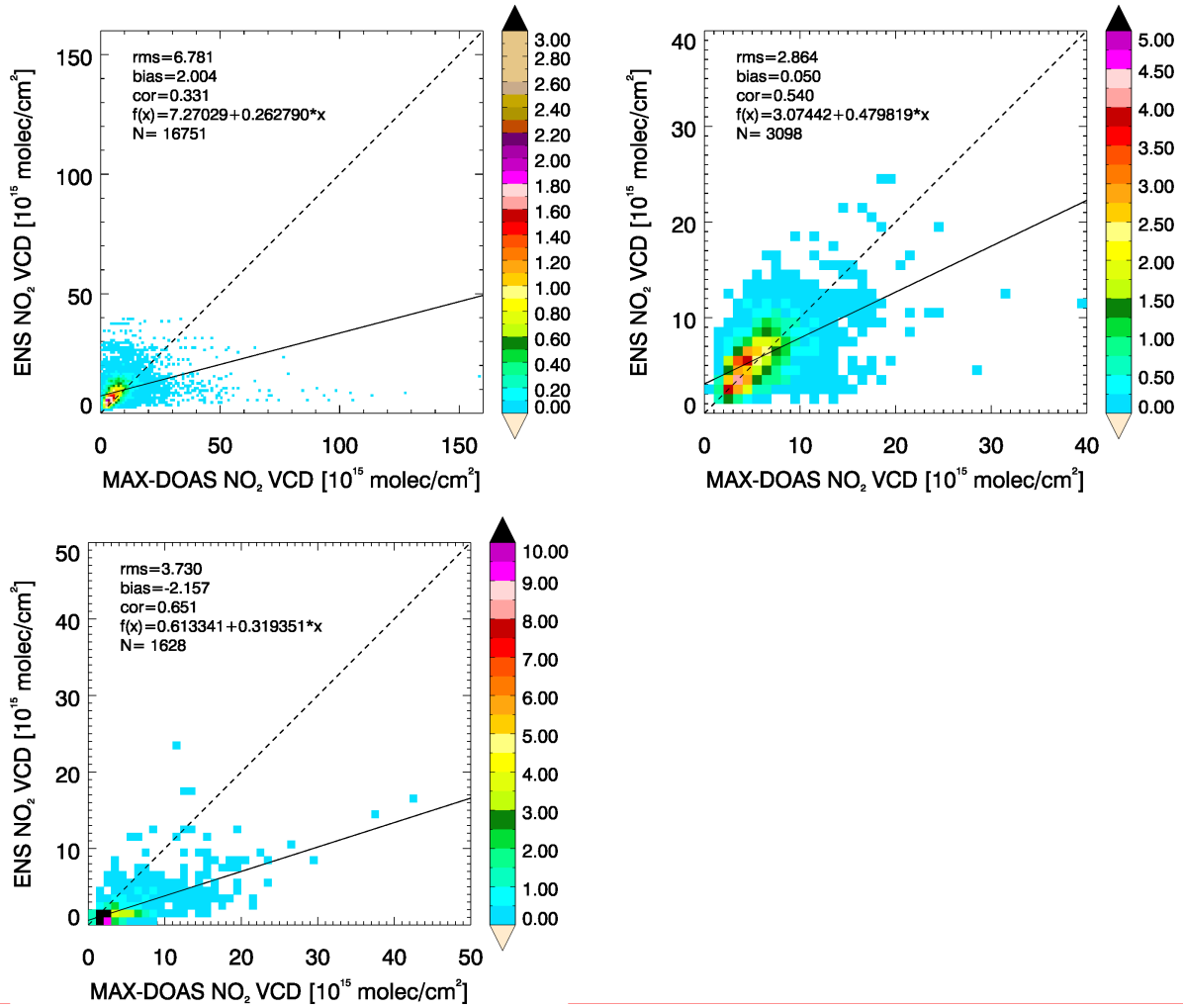


Figure 6.4. Scatter density plots of tropospheric $NO_2$ VCDs [1015 molec. cm−2] from MAX-DOAS against model ENSEMBLE hourly data for (top left) De Bilt, (top right) Bremen and (lower left) Athens. The data is shown with a bin size of 1 x $10^{15}$ molec. $cm^{-2}$ and colour according to the number of data points per bin [%]. The dashed line is the reference line (f (x)=x). The solid line is the regression line (see top left of each plot for f(x) of this line). The root mean squared error (rms) [$10^{15}$ molec. $cm^{-2}$], bias [$10^{15}$ molec. $cm^{-2}$], pearson correlation coefficient (cor) as well as the number of data points N are given at the top left of each plot. Time period: June - November 2020.

# 7 Validation of tropospheric $NO_2$ columns against satellite retrievals

## 7.1 Summary

Regional air quality model columns of tropospheric $NO_2$, derived from the output provided on 8 levels with a top at 5km, are compared to 9:30 local time GOME-2/MetOp-A $NO_2$ satellite retrievals (IUP-UB v1.0 product). The overall spatial distribution of tropospheric $NO_2$ is reproduced by the ENSEMBLE, but values over central European emission hotspots are significantly underestimated by the majority of the models during winter, which results in a strong underestimation over these regions and of the seasonal cycle for the ENSEMBLE. There are stronger shipping signals compared to the satellite data. As a result of a major regional model upgrade in June (2019), which includes the use of an updated European emissions inventory with improved estimates for North African and Middle Eastern anthropogenic emissions, enhanced tropospheric columns of $NO_2$ are reproduced over these regions by all models. Differences between models and satellite observations may result from errors in anthropogenic emissions, photochemistry during winter months and from chemical processing inside ship plumes. In contrast to the analysis, the regional ENSEMBLE forecast shows a negative bias compared to the retrievals which is most pronounced for winter (~2-3 x $10^{15}$ molec/$cm^2$) but smaller during the rest of the year (overall ~0.5 x $10^{15}$ molec/$cm^2$). The negative bias is even larger for CAMS-global, which is in agreement with the stronger underestimation of values for European emission hotspots compared to regional models, demonstrating the benefit of running models at higher horizontal resolution. A systematic negative bias is however not present in the analysis for seasons other than winter.

## 7.2 Comparison with GOME-2 $NO_2$

In this section, regional air quality model columns of tropospheric $NO_2$ are compared to GOME-2/MetOp-A $NO_2$ satellite retrievals (IUP-UB v1.0) [Richter et al., 2011]. This satellite data provides excellent coverage in space and time and very good statistics. However, only integrated tropospheric columns are available, and the satellite data is always taken at 09:30 LT for GOME-2A and at clear sky only. Therefore, model data are vertically integrated, interpolated in time and then sampled to match the satellite data. Uncertainties in $NO_2$ satellite retrievals are large and depend on the region and season. Winter values in mid and high latitudes are usually associated with larger error margins. As a rough estimate, systematic uncertainties in regions with significant pollution are on the order of 20% – 30%. Conclusions may differ for comparisons to other satellite $NO_2$ products (e.g., TEMIS GOME-2A, http://www.temis.nl shows lower retrieved $NO_2$ values for January). It should be noted here that model data is only available for altitudes up to 5000 m, meaning that (depending on tropopause height) tropospheric model columns may not be representative of the total amount of $NO_2$ in the troposphere. Note that since the CAMS-global upgrade of 26 June 2018, GOME-2A observations are assimilated by the global system. This is, however, a different retrieval product than what is used in the validation reported here (University of Bremen retrieval).

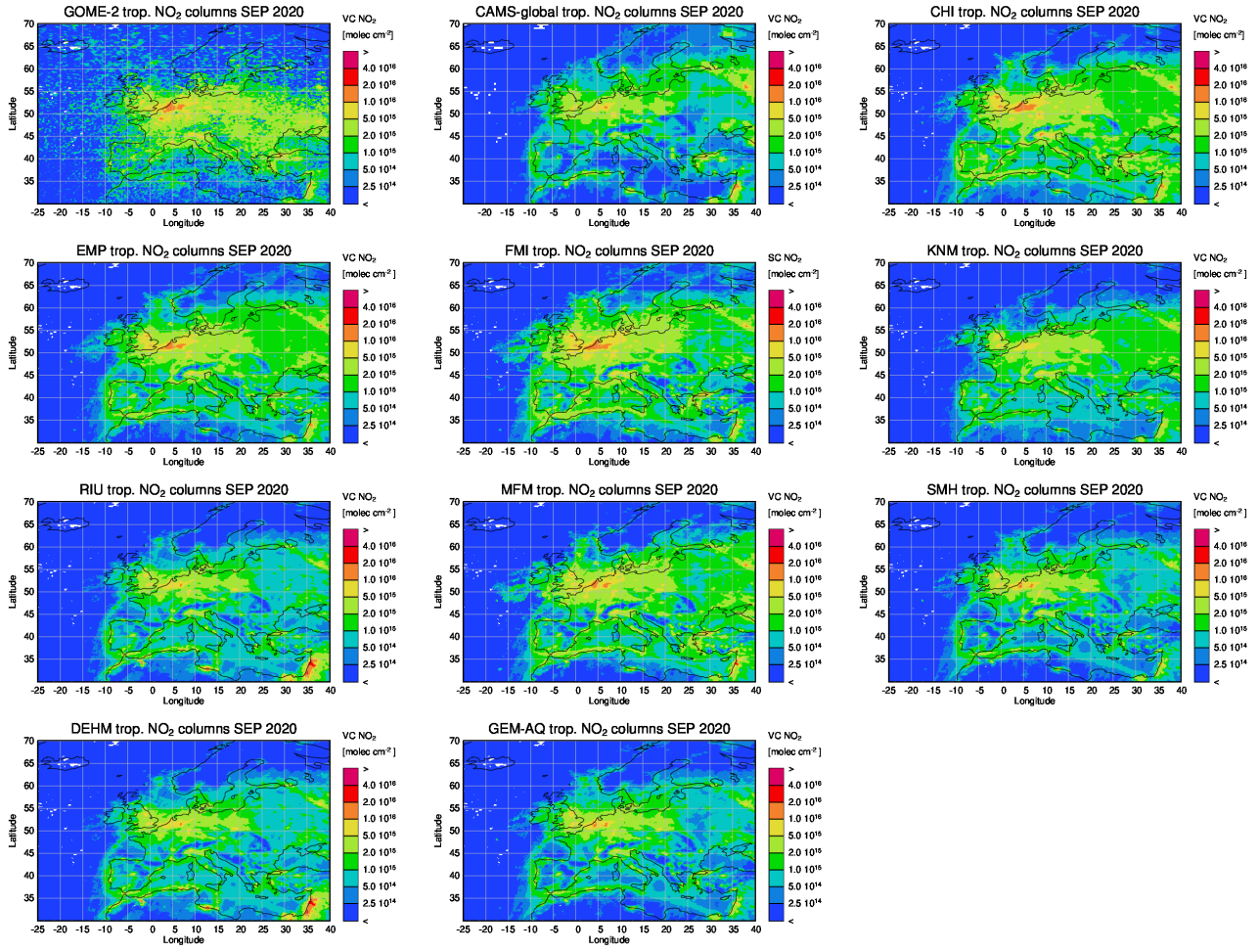


Figure 7.1. Maps of satellite-retrieved and model-simulated tropospheric $NO_2$ columns [molec $cm^{-2}$] for September 2020. From left to right: (first row) GOME-2A, CAMS-global and CHIMERE; (second row) EMEP, SILAM and LOTOS-EUROS; (third row) EURAD-IM, MOCAGE and MATCH; (fourth row) DEHM and GEM-AQ. GOME-2A data were gridded to regional model resolution (i.e. 0.1° x 0.1°). Model data were treated with the same reference sector (25°W - 20°E) subtraction approach as the satellite data and linearly interpolated to the satellite overpass time (9:30 LT).

Figure 7.1 shows maps of monthly mean tropospheric $NO_2$ columns from GOME-2A, regional models and CAMS-global for September 2020. The overall spatial distribution and magnitude of tropospheric $NO_2$ is reproduced by the regional models in principle. There are generally stronger shipping signals in the models compared to the satellite data, which may result from errors in anthropogenic emissions or from chemical processing inside the ship exhaust plumes (see e.g., Vinken et al., 2014).

Compared to CAMS-global, most regional models perform better for Central European emission hotspots, showing the benefit of higher horizontal resolution runs. As a result of a major regional model upgrade in June 2019, which includes the use of an updated European emissions inventory with improved estimates for North African and Middle Eastern anthropogenic emissions, enhanced tropospheric columns of $NO_2$ are now reproduced over these regions (e.g., Lebanon, Israel) by all models.

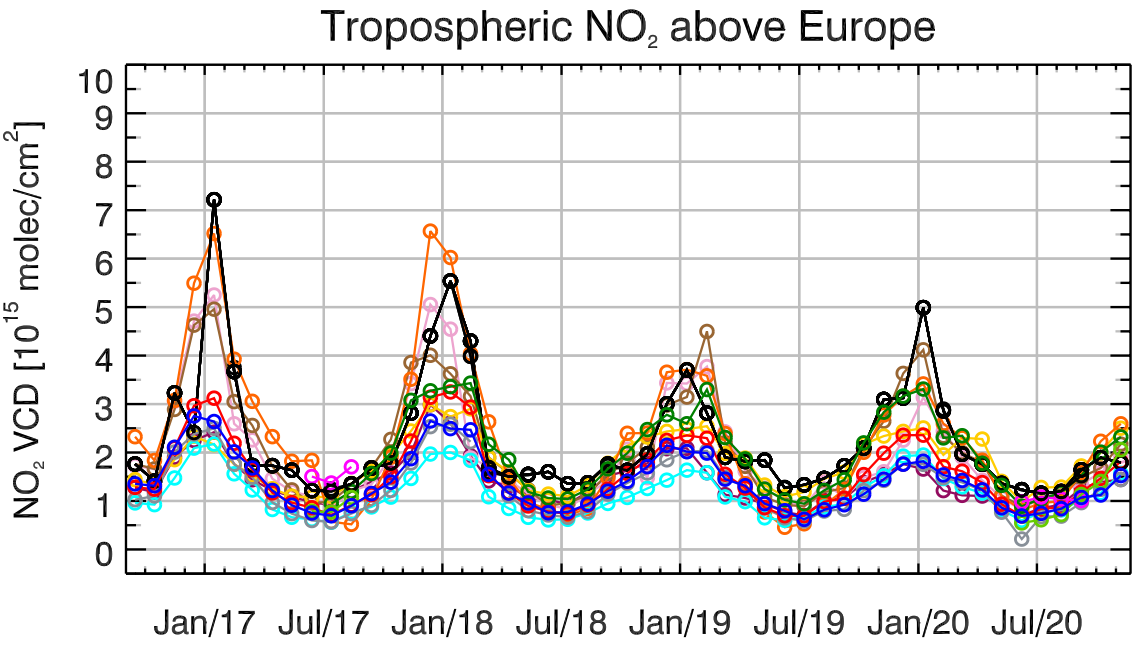


Figure 7.2. Time series of monthly averaged tropospheric $NO_2$ columns [$10^{15}$ molec $cm^{-2}$] retrieved by (black) GOME-2A and simulated by (red) ENSEMBLE forecast, (green) ENSEMBLE analyses, (yellow) CHIMERE, (brown) EMEP, (orange) SILAM, (purple) LOTOS-EUROS, (cyan) EURAD-IM, (pink) MOCAGE, (grey) MATCH, (fuchsia) DEHM, (light green) GEM-AQ and (blue) CAMS-global. GOME-2A data were gridded to regional model resolution (i.e. 0.1° x 0.1°). Model data were treated with the same reference sector (25°W - 20°E) subtraction approach as the satellite data and linearly interpolated to the satellite overpass time (9:30 LT). Time period: September 2016 – November 2020.

Figure 7.2 shows time series of monthly mean tropospheric $NO_2$ columns for GOME-2A and the models. The seasonal variation is better reproduced by SILAM, MOCAGE and EMEP than by the other models. The latter clearly underestimate the seasonal cycle over Europe due to the strong underestimation of values in winter described above. The regional ENSEMBLE forecast shows a negative bias compared to the retrievals which is most pronounced during winter (~2-3 x $10^{15}$ molec/$cm^2$) but smaller during the rest of the year (overall ~0.5 x $10^{15}$ molec/$cm^2$). One of the reasons for this may be that the regional model output is limited to 5 km altitude. Compared to the ENSEMBLE forecast, the negative bias of CAMS-global is a bit larger, which is in agreement with the stronger underestimation over European emission hotspots for CAMS-global especially during winter. A systematic negative bias is not present in the regional model ENSEMBLE analysis for seasons other than winter. The decrease in the retrieved wintertime maxima from 2017 to 2019, and the increase in 2020 is not reproduced by the majority of regional models and CAMS-global.

# 8 Comparison with high-altitude EEA Air Quality e-reporting surface stations

## 8.1 Summary

European ozone EA Air Quality e-reporting measurements from high-altitude stations (above 1km) have been used to evaluate the regional models. Differences between the regional model orography and the true altitude of the station were used to select the model altitude level to compare with. The ensemble median mostly overestimates ozone levels during the period September 2020 – November 2020. More specific, depending on the station the observed ozone levels are reproduced to within 0% and 35% by the ensemble median D+0 forecast (1h-24h). Correlations observed were between 0.51 and 0.89 and the ensemble median D+0 forecast has a performance better than any of the individual nine models. CHIMERE and MOCAGE are deviating significantly from the ensemble median in terms of MNMBs and the EURAD model is deviating significantly from the ensemble median in terms of correlations with observations. Validation metrics are also given for the ENS analysis. The ENS analysis has almost equivalent performance with ENS D+0 forecast in terms of MNMBs but performs better than ENS D+0 forecast in terms of correlations (significantly higher correlations).

## 8.2 Introduction

The nine models and their ENSEMBLE median (D+0 forecast as well as the analysis) have been compared against Background-Rural EA Air Quality e-reporting measurements for surface stations at elevation greater than 1000 m above mean sea level (http://www.eea.europa.eu/data-and-maps/data/airbase-the-european-air-quality-database-7). Elevated stations were selected to fall within classes 1-2 in the $O_3$ Joly-Peuch (2012) classification for EEA Air Quality e-reporting NRT stations. Table 8.1 shows the stations altitude above mean sea level together with the LOTOS-EUROS model altitude (i.e., from model's topography) pertaining to the nearest to the station grid point. Modelled gas mixing ratios were extracted at the model level, which is closest to the stations altitude as defined from the orography (see column 7 in Table 8.1).

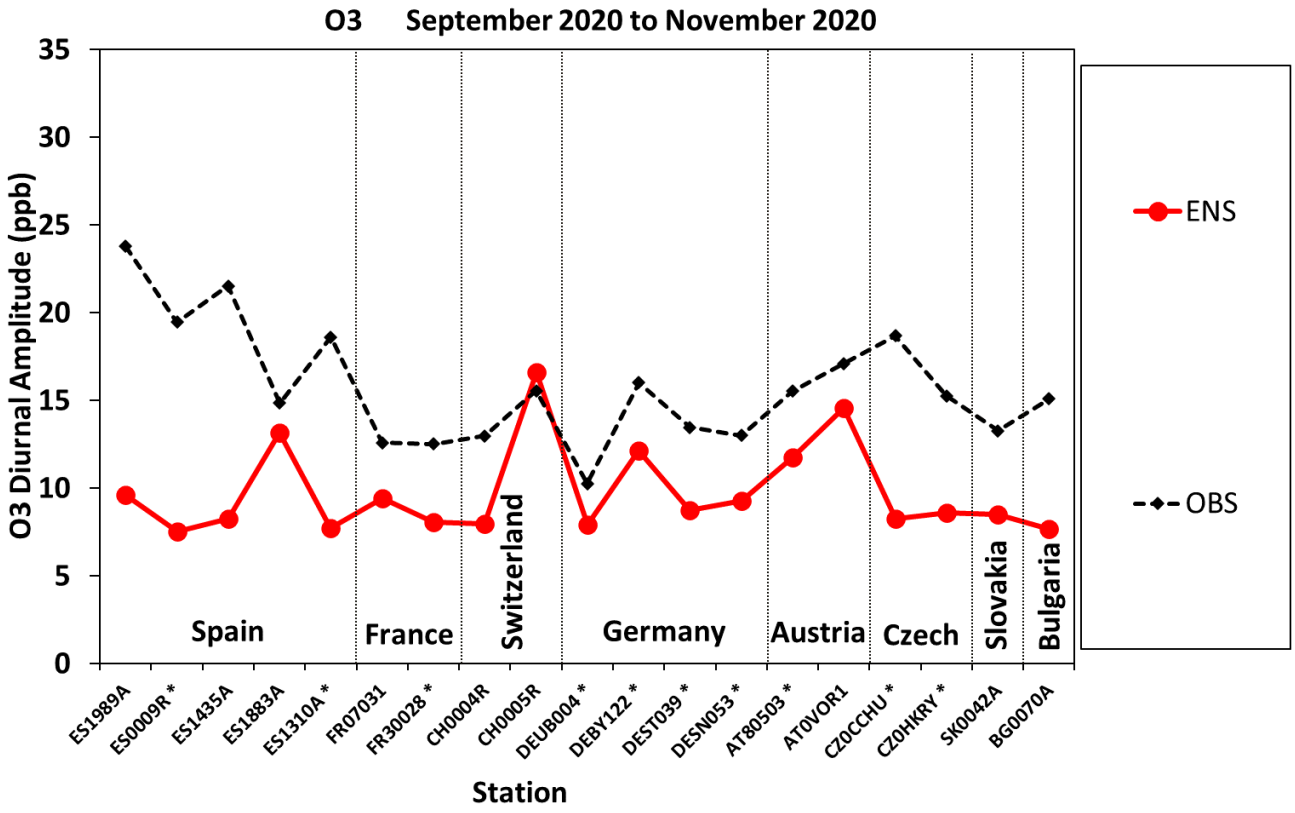


Figure 8.1. Amplitude of the diurnal cycle as measured (ppb) from stations observations (black diamonds) and as calculated from the ENSEMBLE forecast D+0 (red circles). With asterisks are denoted stations used in the assimilation process.

Table.8.1: Background-Rural EEA Air Quality e-reporting Stations (with NRT data) with elevation higher than 1000 m.

| Station Name | Stat_id | Longitude | Latitude | real Altitude | model Altitude | nearest Level | use in CAMS50 |
|---|---|---|---|---|---|---|---|
| Lario | ES1989A | -5.09 | 43.04 | 1140 | 1199 | 0 | validation |
| Capmisabalos | ES0009R | -3.14 | 41.27 | 1360 | 1124 | 2 | assimilation |
| Vilafranca | ES1435A | -0.25 | 40.42 | 1125 | 907 | 2 | validation |
| Torrelisa | ES1883A | 0.18 | 42.46 | 1005 | 1282 | 0 | validation |
| Ak- Pardines | ES1310A | 2.21 | 42.31 | 1226 | 1117 | 1 | assimilation |
| Chaumont | CH0004R | 6.98 | 47.05 | 1136 | 727 | 3 | - |
| Rageade | FR07031 | 3.28 | 45.11 | 1040 | 944 | 2 | validation |
| Schlucht | FR30028 | 7.01 | 48.05 | 1200 | 520 | 3 | assimilation |
| Schauinsland | DEUB004 | 7.91 | 47.91 | 1205 | 554 | 3 | assimilation |
| Rigi-Seebodenalp | CH0005R | 8.46 | 47.07 | 1031 | 997 | 1 | validation |
| Sulzberg im Bregenzerwald | AT80503 | 9.93 | 47.53 | 1020 | 961 | 1 | assimilation |
| Bad Hindelang/Oberjoch | DEBY122 | 10.40 | 47.52 | 1169 | 1150 | 0 | assimilation |
| Brocken | DEST039 | 10.62 | 51.80 | 1130 | 302 | 4 | assimilation |
| Fichtelberg | DESN053 | 12.95 | 50.43 | 1214 | 555 | 3 | assimilation |
| Vorhegg bei Kötschach-Mauthen | AT0VOR1 | 12.97 | 46.68 | 1020 | 1427 | 0 | validation |
| Churanov | CZ0CCHU | 13.62 | 49.07 | 1118 | 739 | 4 | assimilation |
| Krkonose-Rychory | CZ0HKRY | 15.85 | 50.66 | 1001 | 530 | 4 | assimilation |
| Bratislava - Jeséniova | SK0042A | 20.99 | 48.78 | 1244 | 445 | 5 | validation |
| Vitosha mountain | BG0070A | 23.24 | 42.64 | 1321 | 863 | 4 | - |

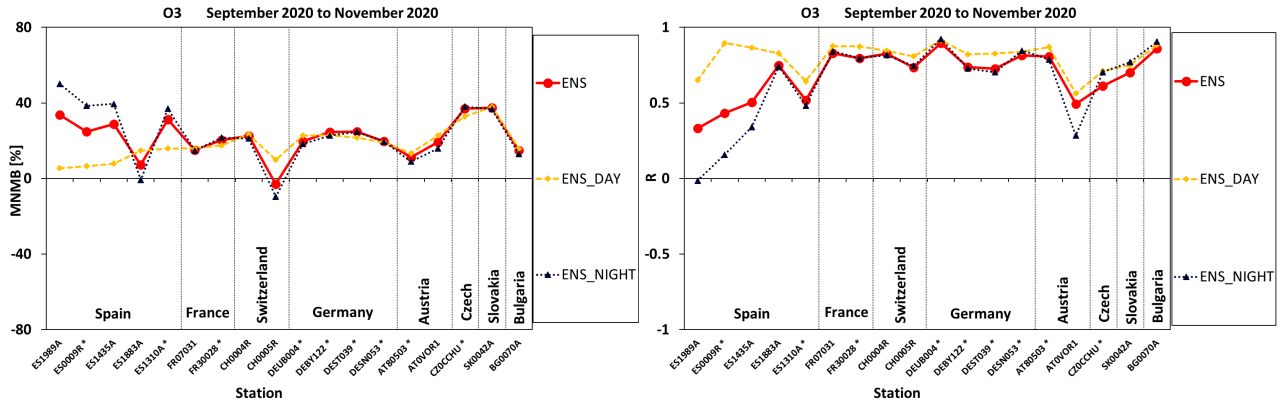


Figure 8.2. MNMBs [%] (left) and temporal correlations (right) calculated for the ENSEMBLE model for during daytime (orange) night-time (dark blue) as well as for the whole day (red) for the SON 2020 period. With asterisks are denoted stations used in the assimilation process.

For the validation, hourly $O_3$ concentration values (µg/m$^3$) are extracted from the nine models as well as for the regional ENSEMBLE. It should be noted that, in the EEA Air Quality e-reporting network the $O_3$ measurements that were made by the instrument in ppb were converted from ppb to µg/m$^3$, following the EU directive 2008/50, i.e., by multiplying by 2. This conversion is approximately correct for low altitude stations. However, at high altitude stations pressure and temperature should be taken into account when converting from ppb to µg/m$^3$ and vice versa. As hourly pressure and temperature data were not available for all EEA Air Quality stations the comparison between observed and modelled ozone was done by re-converting both modelled and observed hourly $O_3$ concentration in ppb. For modelled ozone values the conversion was done by applying the following ideal gas equation with the model's estimates of temperature (T) and pressure (P) (from CAMS-global):

$$O3\ (\text{in ppb}) = O3\ (\text{in mg/m3}) * \left(\frac{R * T}{p_m * M_{o3}}\right)$$

## 8.3 Regional ENSEMBLE results

In the previous report it was shown that comparing the observed and modelled amplitude of the diurnal variation of ozone at each high-altitude station could provide a criterion concerning the exposure suitability of the stations. We found out in this report that an additional criterion is needed to differentiate stations as to their suitability in exposure. The additional criterion is the correlation coefficients between the amplitude of the diurnal cycle as observed and modelled to be statistically significant roughly higher than 0.3. Figure 8.1 shows the observed and modelled diurnal amplitude of ozone at each station, moving from Spain to Bulgaria. Figure 8.2 shows the MNMBs and the correlation coefficients calculated for the ENSEMBLE model during daytime, at night-time as well as for the whole day. We can see that the 2 criteria of diurnal amplitude and day and night MNMBs and correlation coefficients differentiate the 3 stations in Spain from all other stations. For the above-mentioned findings these 3 high altitude stations will be excluded from our analysis. It should also be noted that daytime correlations have very small variations from stations to station and are higher than those calculated for night-time as well as for the 24-h daily means.

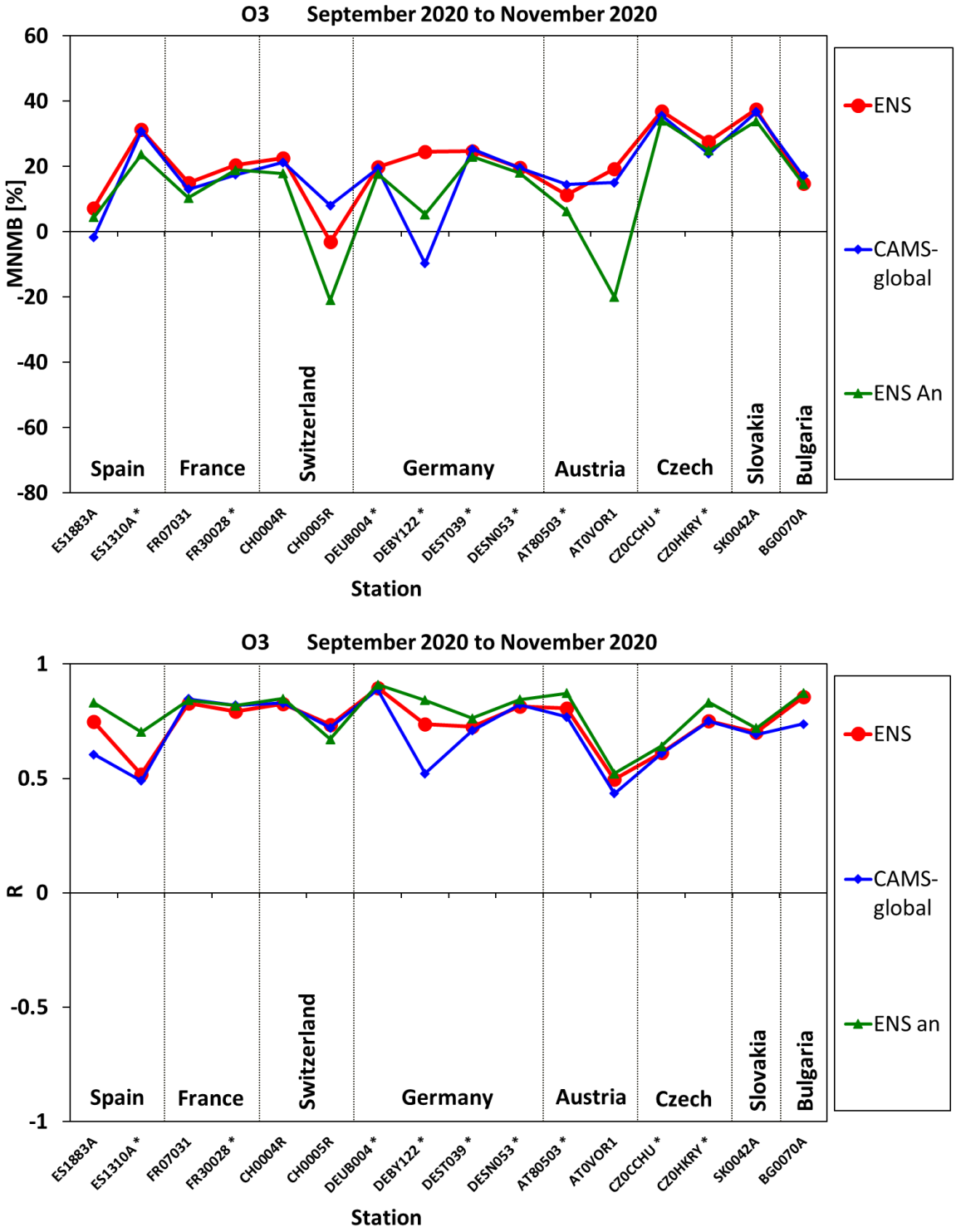


Figure 8.3. $O_3$ MNMBs [%] (top) and correlation coefficient (bottom) for the regional ENSEMBLE (forecast D+0; red circles and analysis; green triangles) as well as for CAMS-global (forecast D+0; blue diamonds) for the period SON2020. With asterisks are denoted stations used in the assimilation process.

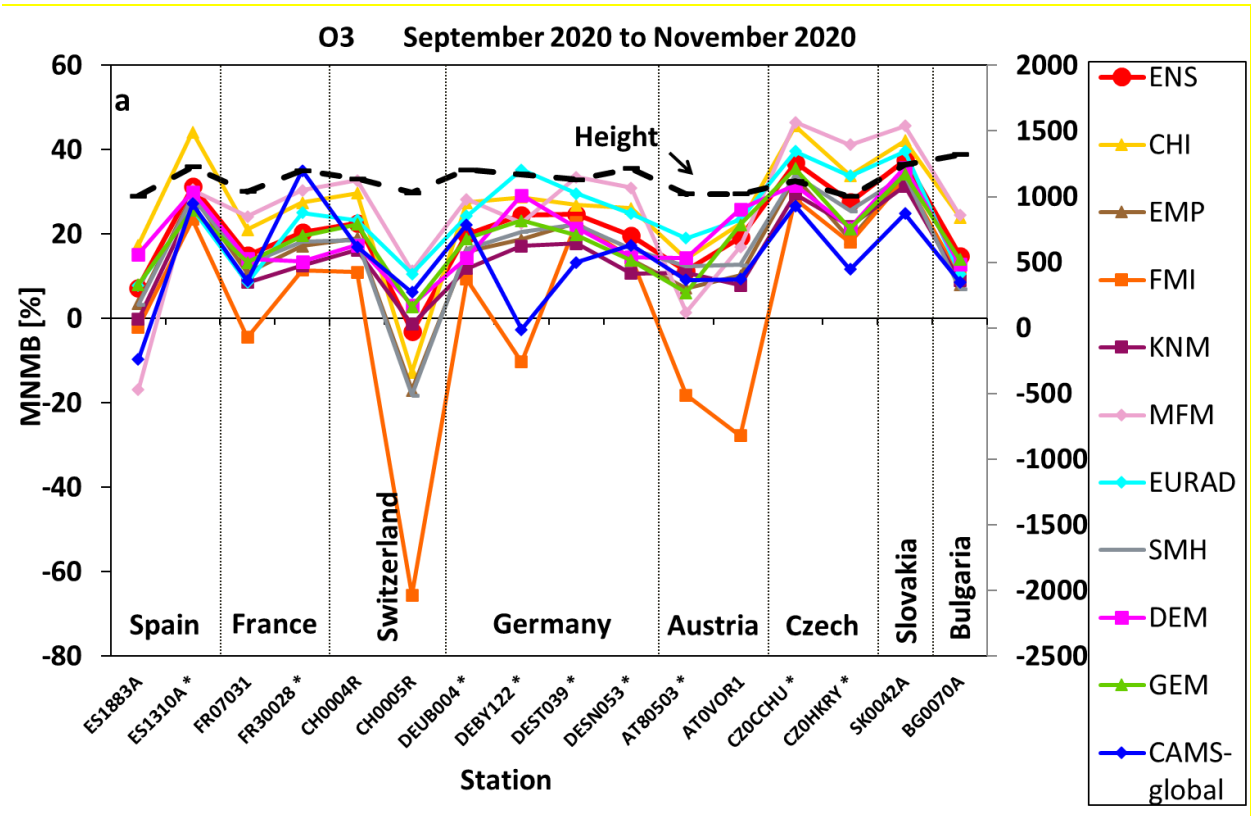


Fig. 8.4. Ozone MNMBs [%] for each one of the 9 models and CAMS-global (September to November 2020) for stations above 1000m altitude. With asterisks are denoted stations used in the assimilation process.

Figure 8.3 shows the Modified Normalized Mean biases (top) and correlation coefficients (bottom) at each of the remaining stations, moving from Spain to Bulgaria (i.e., from West to East) pertaining to the median of the regional ENSEMBLE forecast (D+0) and analysis (D+0) as well as CAMS-global (D+0). The ensemble median overestimates ozone levels during the period September 2020 to November 2020. Depending on the station the range of MNMB for the ENSEMBLE median D+0 forecast was found to be between 0% and 35%. From Figure 8.3 (bottom panel) it is obvious that the regional ENSEMBLE reproduces well the ozone variability. As it appears from Figs 8.3 (bottom panel) the correlation coefficients are highly significant (0.5<r<0.9). It should be noted that for the period September to November 2020, the ENSEMBLE analysis performs better than the ENSEMBLE D+0 forecast in terms of correlations. Additionally, over the majority of the selected stations, CAMS ENSEMBLE D+0 forecast shows higher correlations than CAMS Global D+0 forecast.

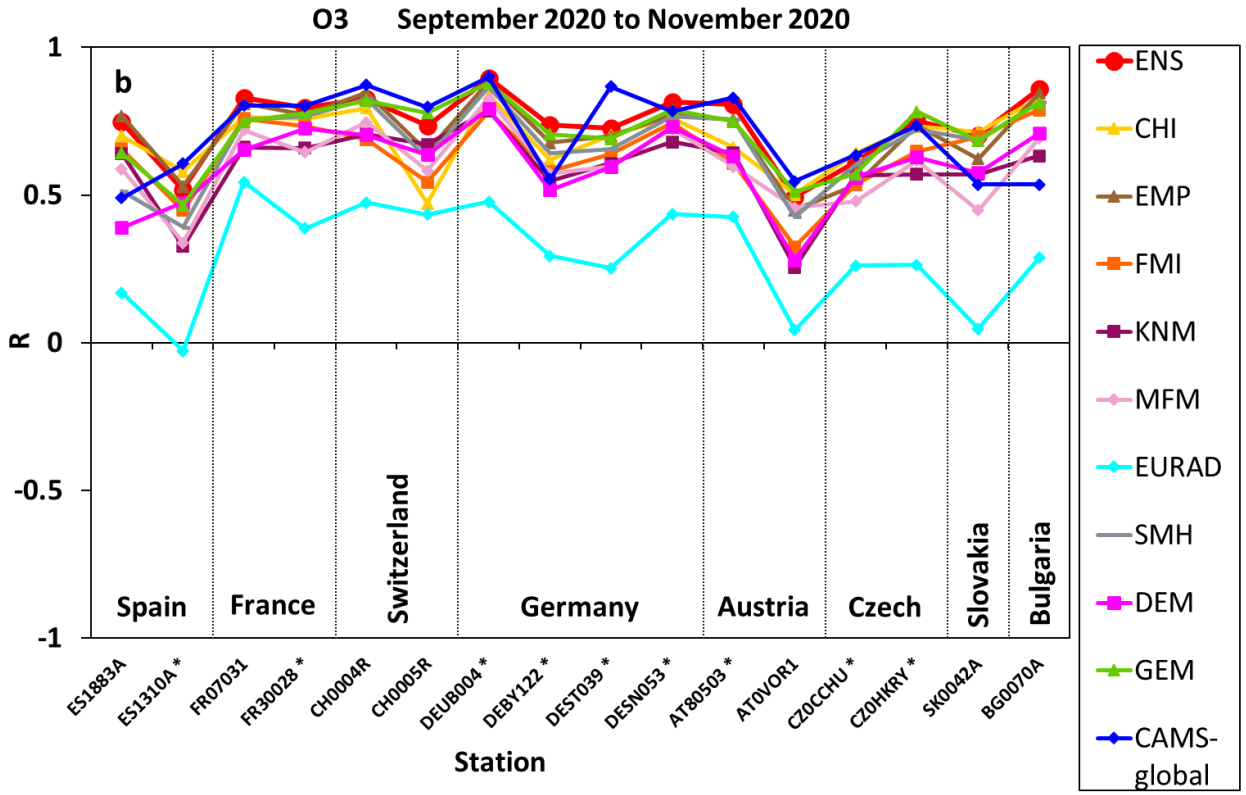


Fig. 8.5: Correlation coefficients (from hourly values) between observed and modelled $O_3$ from all models of the ENSEMBLE and CAMS-global (o-suite) for September to November 2020. With asterisks are denoted stations used in the assimilation process.

## 8.4 Results for the nine regional models

Figure 8.4 shows Modified Normalized Mean biases at each station with elevation greater than 1000 m above mean sea level, moving from Spain to Bulgaria (from West to East) pertaining to each one of the 9 model calculations, the regional ENSEMBLE as well as CAMS-global. All results are based on the forecast D+0 elevated ozone values. On top of the graph shown is the elevation of the station. Depending on the station the observed ozone levels are reproduced to within 0% and 35% from the regional ENSEMBLE. Figure 8.4 shows that CHIMERE and MOCAGE were deviating significantly from the ensemble median (strong positive offset up to 45%) while the remaining models show scores closer to the ENSEMBLE. However, SILAM deviates significantly from all ensemble members at 4 individual stations (namely CH0005R, AT0VOR1, AT80503, DEBY122) in Switzerland, Austria, and Germany respectively, with strong negative biases down to -60% in Switzerland and down to -30% in Austria.

Finally, Figure 8.5 shows the correlations between observations and each model. It is clear that the regional ENSEMBLE reproduces well the ozone variability and has a better score than any of the individual models. The EURAD and the MOCAGE models show lower correlation while the remaining models show scores closer to the ENSEMBLE.

# 9 Comparison with ozone sonde observations

## 9.1 Summary

Free tropospheric ozone (<850 hPa) could be reproduced by the ENSEMBLE forecast and analysis with MNMBs between 6% and 10% during SON 2020. The other models show MNMBs between -14% and 13% (forecasts and analysis).

## 9.2 Comparison approach

For the validation, the sonde profiles are compared to the model data closest in time. The model data is provided at the geographical coordinates of the sonde stations, the horizontal drift during the ascend of the sonde is considered negligible.

The model concentrations at the different height levels (0, 50, 250, 500, 1000, 2000, and 5000m above the ground) are matched to the respective sonde observations and are converted to mass mixing ratios. Pressure and temperature values needed for the conversion are taken from the sonde observations. For each station and all individual launches, the differences between observation and model are calculated. In order to be able to compare the profiles of different stations, this is done for fixed altitude levels between 0 and 6000m (interval for the surface 50m, above 100m, interval 100m). The sonde and model values are then aggregated to monthly means for each station and altitude level. For each month mean modified normalized biases (MNMB) are then calculated over all European stations for the free troposphere (<850 hPa).

## 9.3 Results for the ENSEMBLE

For the period November 2019 to November 2020, the ENSEMBLE forecast shows MNMBs between 3% and 15%. The ENSEMBLE analysis shows a similar behaviour with MNMBs between 3% and 14%, see Fig. 9.1.

Table 9.1: Sonde stations used in the validation for SON2020

| Station/location | Lat | lon | alt [m] |
|---|---|---|---|
| De Bilt | 52.1 | 5.2 | 4 |
| Hohenpeissenberg | 47.8 | 11.2 | 976 |
| Jokioinen | 60.8 | 23.5 | 103 |
| Legionow | 52.4 | 20.97 | 96 |
| Lerwik | 60.14 | -1.19 | 84 |
| Madrid Spain | 40.5 | -3.8 | 631 |
| Prag | 50 | 14.4 | 302 |
| Sodankyla | 67 | 27 | 180 |
| Uccle Belgium | 51 | 4 | 100 |

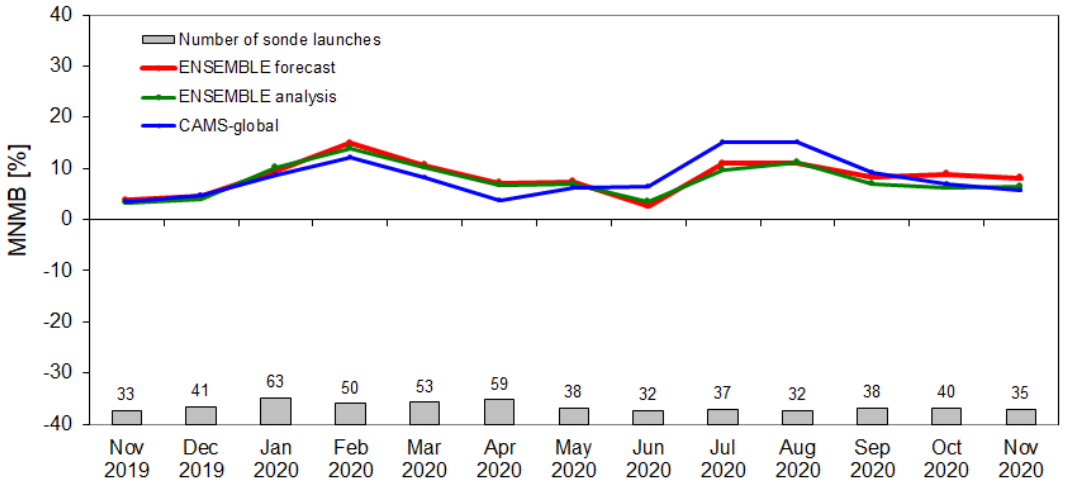


Figure 9.1 - MNMBs for the regional ENSEMBLE and CAMS-global between November 2019 and November 2020 for the free troposphere region (<850 hPa).

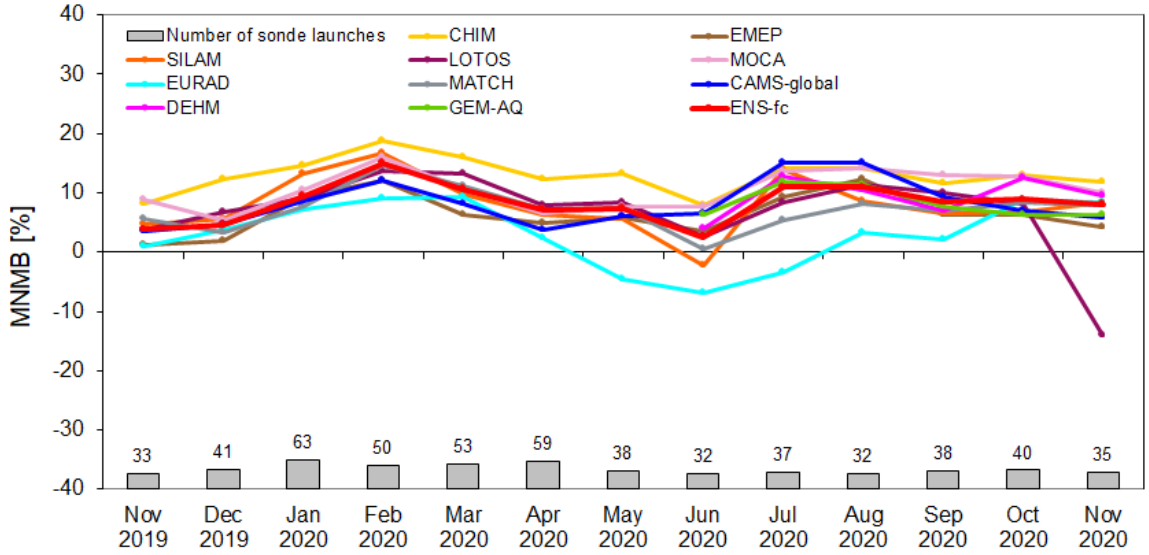


Figure 9.2. MNMBs for the individual regional model forecasts between November 2019 and November 2020 for the free troposphere region (pressure < 850 hPa).

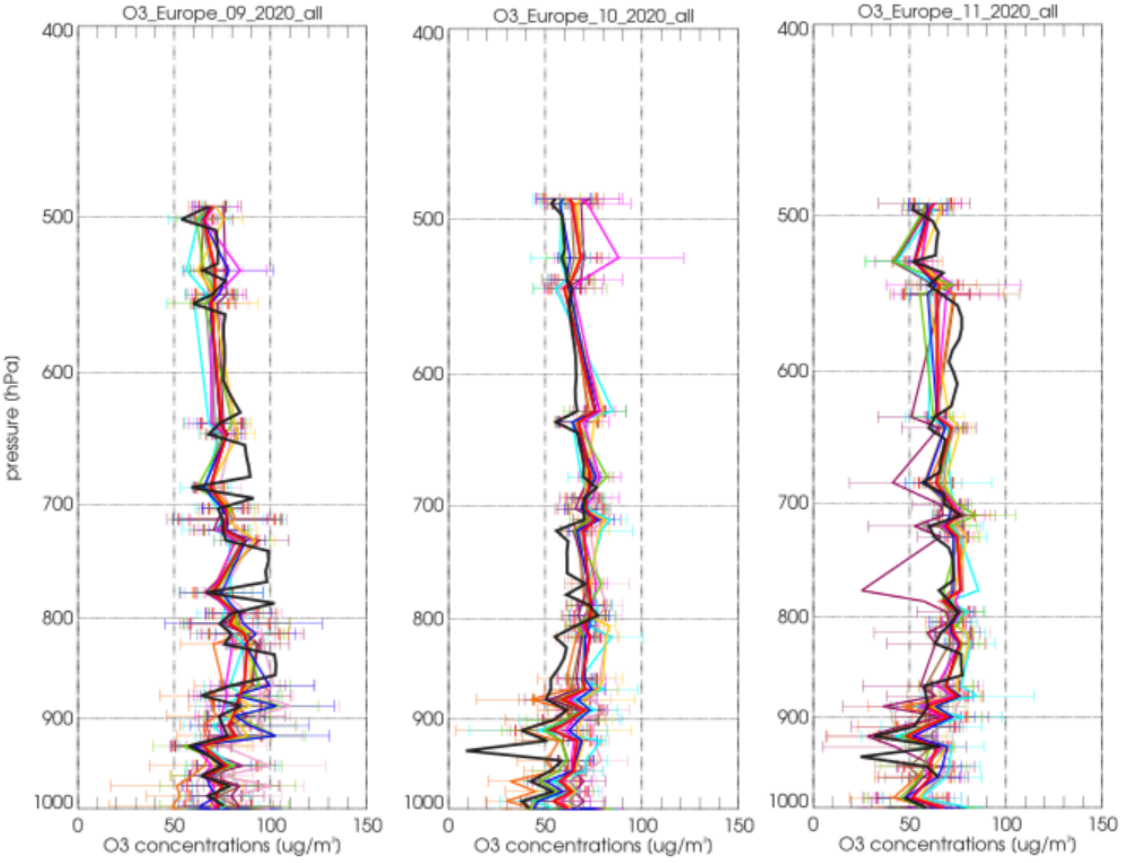


Figure 9.3 Averaged monthly profiles from the model forecast and sonde comparisons over European sonde stations for September, October, and November 2020 (red: ENSEMBLE, blue: CAMS-global, yellow: CHIMERE, brown: EMEP, orange: SILAM, purple: LOTOS-EUROS, cyan: EURAD-IM, pink: MOCAGE, grey: MATCH, fuchsia: DEHM, light green: GEM-AQ).

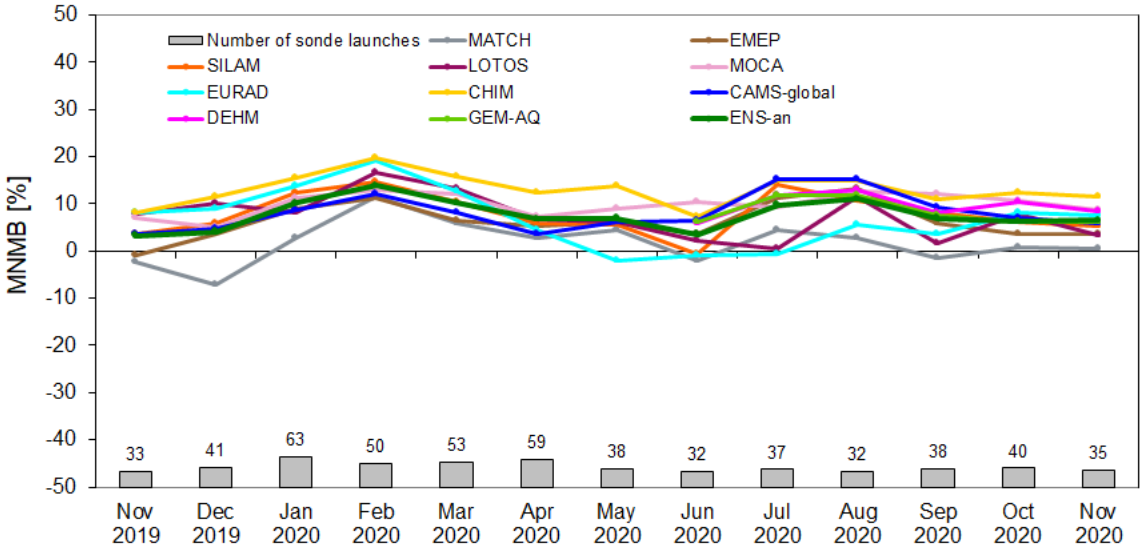


Figure 9.4. MNMBs for the regional model analyses between November 2019 and November 2020 for the free troposphere region (pressure < 850 hPa).

## 9.4 Results for individual regional models

Between November 2019 and November 2020 regional model forecasts show MNMBs in the range of -14 % and 19%, see Fig. 9.2.

*Results for the regional model analyses*

Similar to the results of the individual models' forecasts, the analyses show MNMBs between -7% and 20% (Fig. 9.4).

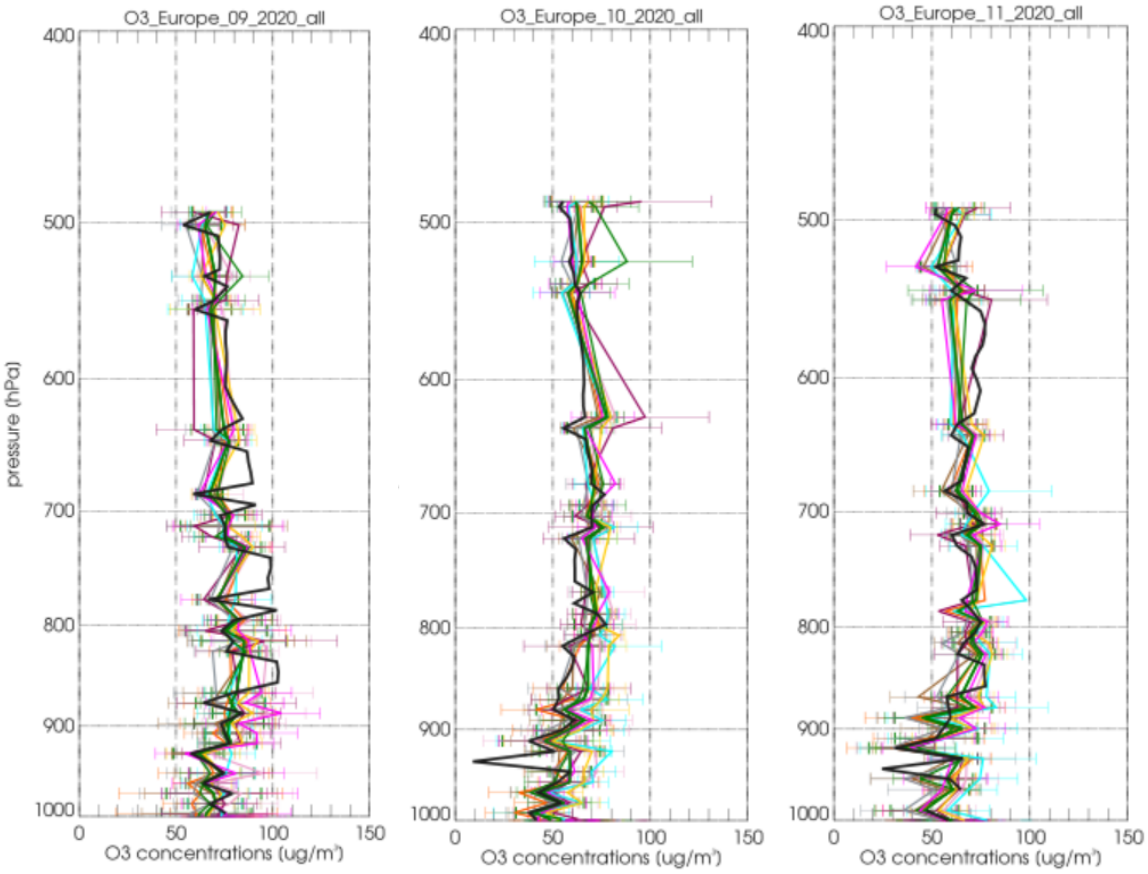


Figure 9.5. Averaged monthly profiles from the model analysis and sonde comparisons over European sonde stations for September, October, and November 2020 (green: ENSEMBLE, blue: CAMS-global, yellow: CHIMERE, brown: EMEP, orange: SILAM, purple: LOTOS-EUROS, cyan: EURAD-IM, pink: MOCAGE, grey: MATCH, fuchsia: DEHM, light green: GEM-AQ).

# 10 Comparison with GAW stations

## 10.1 Summary

The model concentrations of $O_3$ and CO at higher model levels were compared with five GAW high-altitude stations in mountainous terrain. As for the EEA air quality e-reporting stations, differences between the regional model orography and the true altitude of the station were used for this model level selection. Good results were obtained for the ENSEMBLE for ozone with relatively small biases and good correlations (except for Hohenpeissenberg station). The CHIMERE model shows larger MNMBs in both the analysis and the forecast and the MATCH model shows different behaviour compared to the other models in analysis (negative bias). For CO, especially the ENSEMBLE corresponds well to the observations, however, small underestimates are found. The CHIMERE model shows larger MNMBs in both the analysis and the forecast. The MATCH model shows very high bias in the analysis. The time series and correlation he coefficients for CO and $O_3$ show that the ENSEMBLE reproduces for a large part the variability observed.

## 10.2 Comparison method

Hourly $O_3$ and CO concentration values in µg/m$^3$ are extracted from the seven models and are compared to the GAW measurements, which were converted from volume mixing ratios (ppb) into concentrations by using pressure and temperature values at the respective pressure levels from the CAMS-global model.

The altitude of the stations Hohenpeissenberg (HPB), Jungfraujoch (JFJ), Monte Cimone (CMN), Sonnblick (SNB) and Zugspitze (ZUG) in the model has been extracted from the orography as used in the LOTOS-EUROS model, see Table 10.1. For the level choice, the GAW stations' altitudes together with the best correlation of the corresponding levels were taken into account. Uncertainties due to the choice of level (calculated as mean differences between the chosen level and one up/down for the period SON 2020 for the ENSEMBLE) are up to ±11 µg/m$^3$ for CO and up to ±9 µg/m$^3$ for $O_3$.

Table 10.1 - Validation set-up for September – November 2020.

| station | altitude station [m] | altitude model [m] | level choice (range 0-7) | altitude at level [m] |
|---|---|---|---|---|
| HPB | 985 | 813 | 2 | 1063 |
| JFJ | 3580 | 1837 | 5 | 3837 |
| CMN | 2165 | 602 | 4 | 1602 |
| SNB | 3105 | 1687 | 3 | 2187 |
| ZUG | 2670 | 1348 | 4 | 2348 |

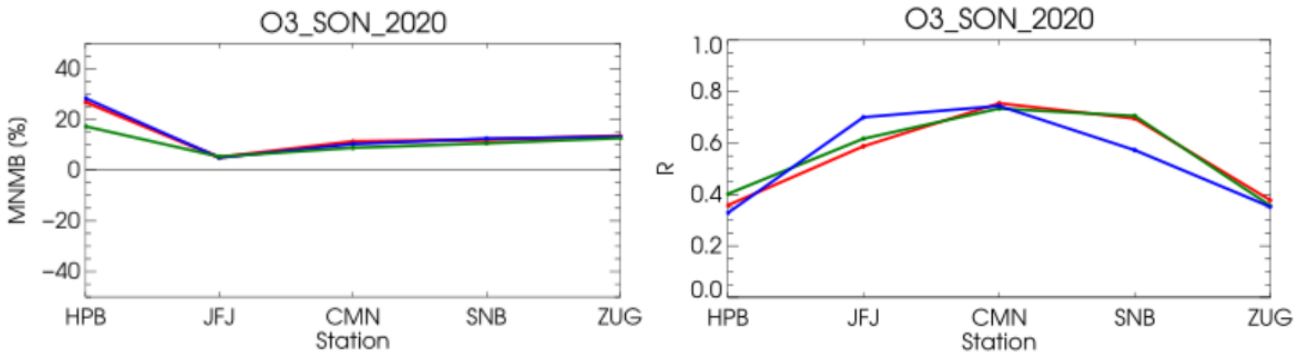


Figure 10.1. MNMBs [%] (left) and correlation coefficients (right) for ozone (red: ENSEMBLE forecast, green: ENSEMBLE analysis, blue: CAMS-global) for the period September 2020 to November 2020.

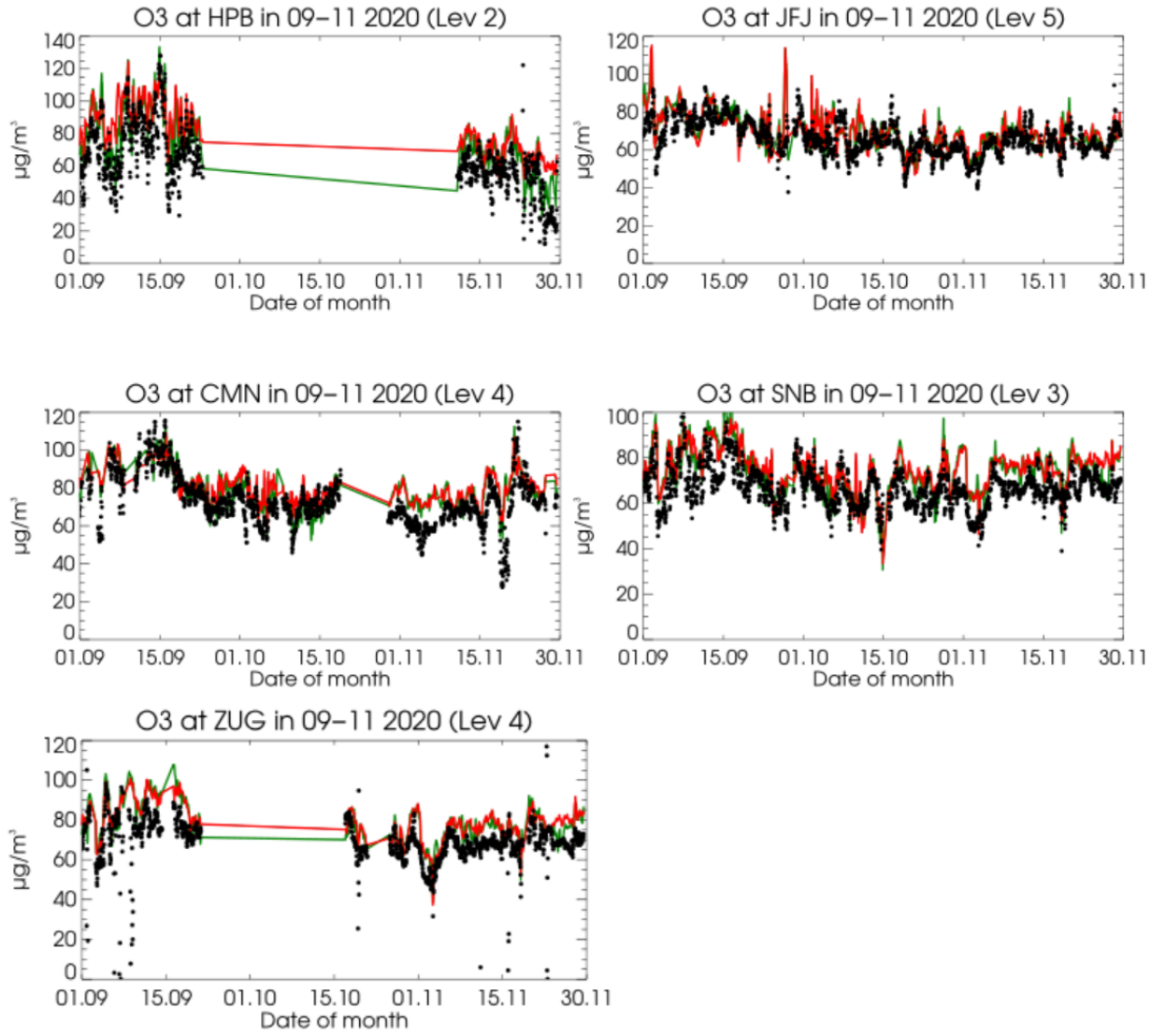


Figure 10.2. Time series plots for the ENSEMBLE forecast (red) and ENSEMBLE analysis (green) for surface $O_3$ in comparison with high altitude stations for the period September 2020 to November 2020.

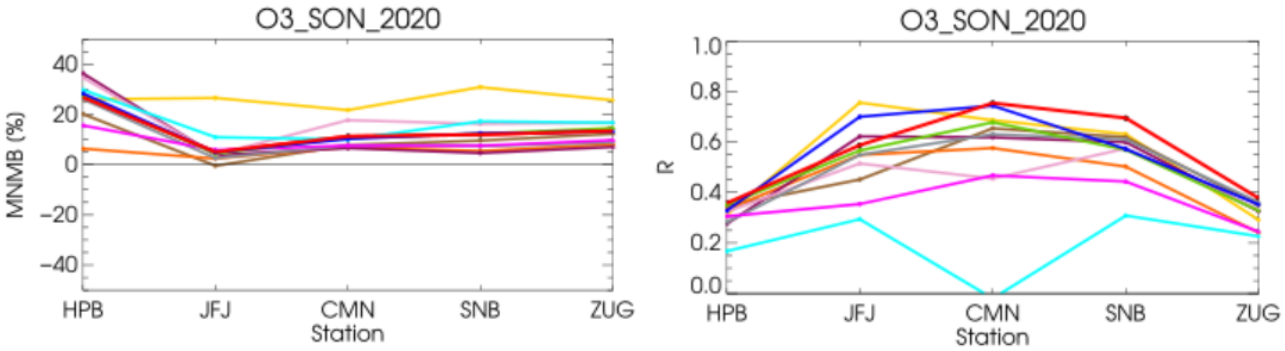


Figure 10.3. MNMBs [%] (left) and correlation coefficients (right) for all model forecasts for ozone (red: ENSEMBLE, blue: CAMS-global, yellow: CHIMERE, brown: EMEP, orange: SILAM, purple: LOTOS-EUROS, cyan: EURAD-IM, pink: MOCAGE, grey: MATCH). Altitudes are listed in Table 10.1.

## 10.3 Ozone

The ENSEMBLE forecast shows positive MNMBs between ~6% and 25% and correlation coefficients ranging between 0.35 and 0.76 for the period September 2020 to November 2020. The ENSEMBLE analysis shows smaller MNMBs (between 6% and 17%) and slightly better correlation coefficients ranging from 0.4 and 0.75 (see Fig. 10.1).

The time series plots show relatively good correspondence between model and observations (Fig. 10.2).

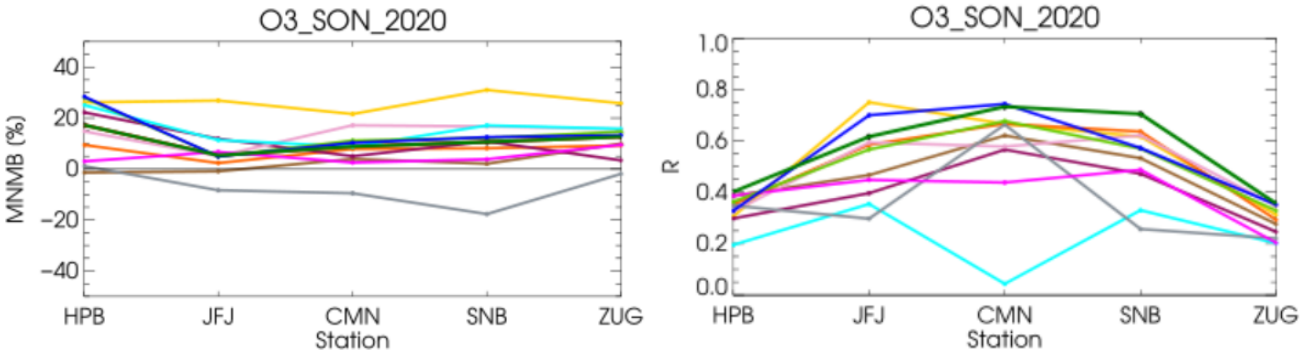


Figure 10.4. MNMBs [%] (left) and correlation coefficients (right) for all models analyses for ozone (green: ENSEMBLE, blue: CAMS-global, yellow: CHIMERE, brown: EMEP, orange: SILAM, purple: LOTOS-EUROS, cyan: EURAD-IM, pink: MOCAGE, grey: MATCH, fuchsia: DEHM, light green: GEM-AQ). Altitudes are listed in Table 10.1.

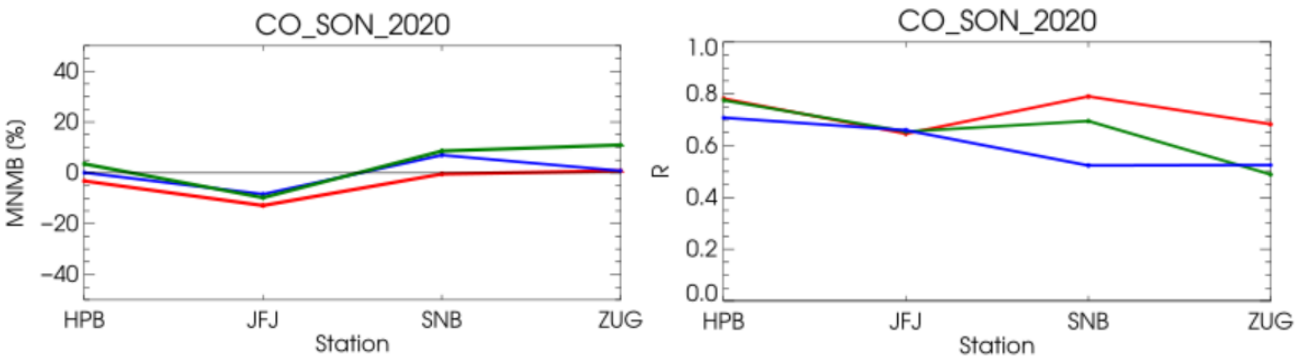


Figure 10.5. MNMBs [%] (left) and correlation coefficients (right) for the ENSEMBLE for CO (red: ENSEMBLE forecast, green: ENSEMBLE analysis, blue: CAMS-global).

*Results for individual model forecasts:*

The models show MNMBs in the range of 35% and -1% for the period September to November 2020 (Fig. 10.3). The CHIMERE model shows larger positive MNMBs than the other models. During SON 2020, correlation coefficients vary between 0.22 and 0.78. An exception is the EURAD model with low correlation coefficients (below 0.3).

*Results for the individual model analyses:*

For the individual model analyses (Fig. 10.4), MNMBs range between 33% and -2% and are very similar to the forecast (except MATCH). The MATCH model shows negative MNMBs (up to-19). Same as for the forecast, correlation coefficients range between 0.22 and 0.78, except for the EURAD model, which shows lower correlation.

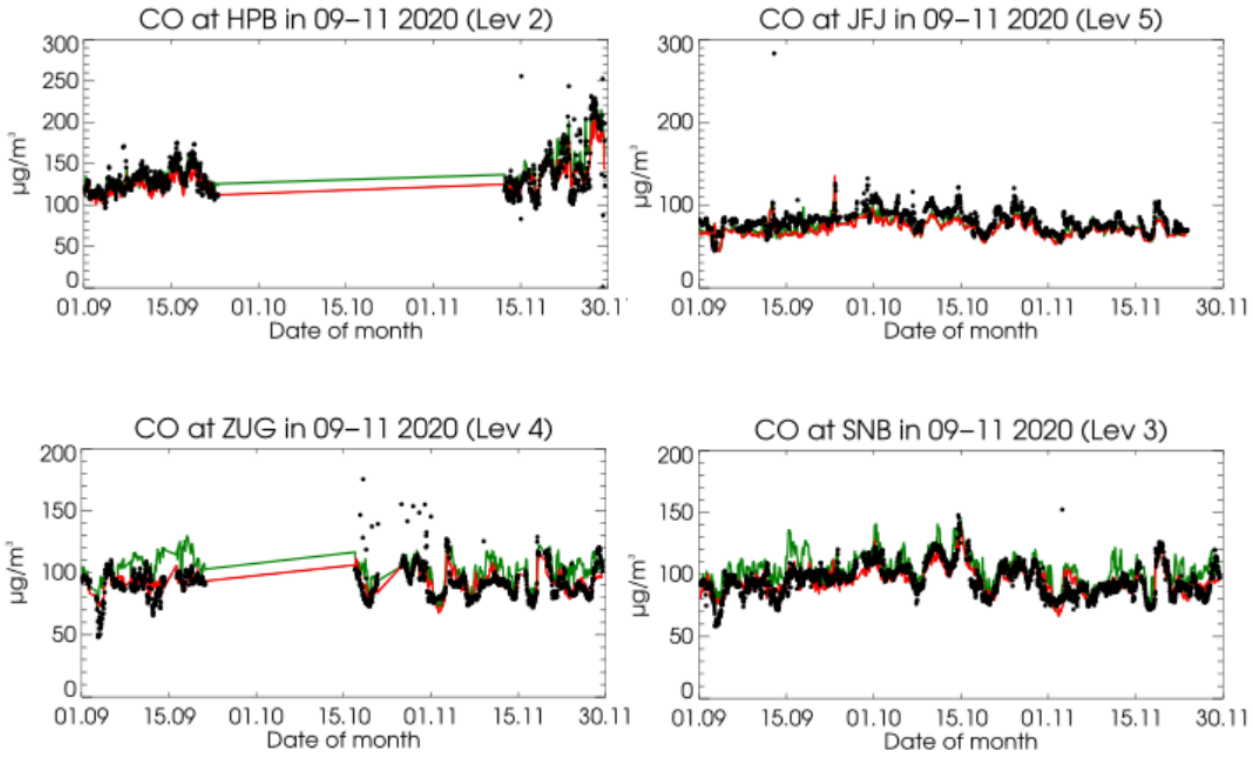


Figure 10.6. Time series plots for the ENSEMBLE forecast (red) and ENSEMBLE analysis (green) for surface CO in comparison with high altitude stations.

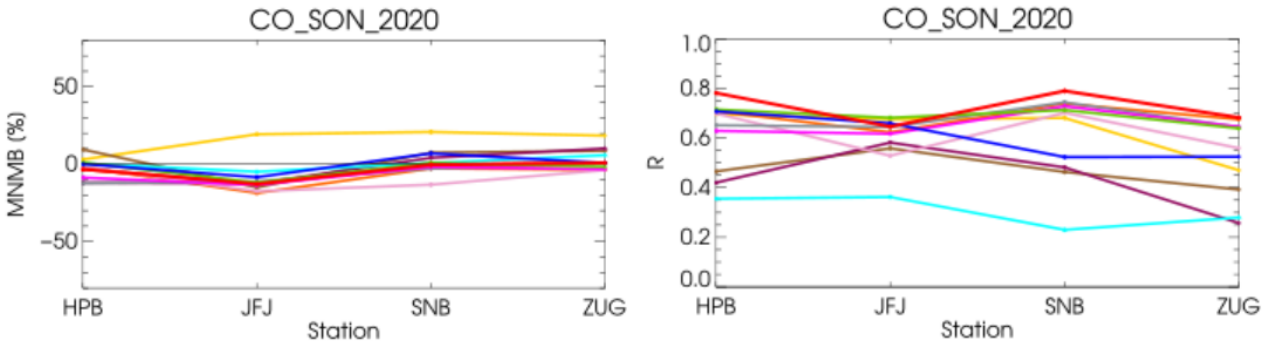


Figure 10.7. CO MNMBs [%] (left) and correlation coefficients (right) for all regional model forecasts, the ENSEMBLE and CAMS-global (red: ENSEMBLE forecast, blue: CAMS-global, yellow: CHIMERE, brown: EMEP, orange: SILAM, purple: LOTOS-EUROS, cyan: EURAD-IM, pink: MOCAGE, grey: MATCH, fuchsia: DEHM, light green: GEM-AQ). Altitude ranges are listed in Table 10.1.

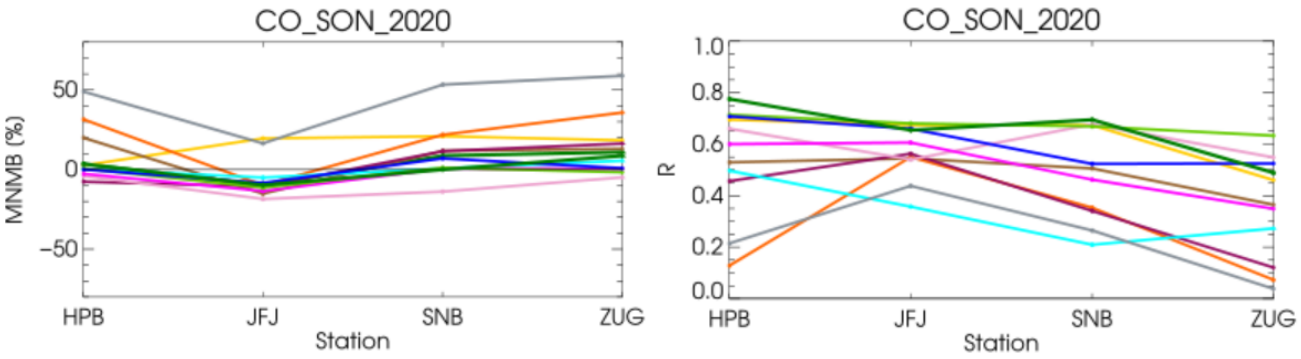


Figure 10.8. CO MNMBs [%] (left) and correlation coefficients (right) for all regional model analyses, the ENSEMBLE and CAMS-global (green: ENSEMBLE analysis, blue: CAMS-global, yellow: CHIMERE, brown: EMEP, orange: SILAM, purple: LOTOS-EUROS, cyan: EURAD-IM, pink: MOCAGE, grey: MATCH, fuchsia: DEHM, light green: GEM-AQ). Altitude ranges are listed in Table 10.1.

## 10.4 Carbon monoxide

For CO, the ENSEMBLE analysis and forecast MNMBs range between -8% and 10% for the analysis and between -12% and 1% for the forecast during September 2020 - November 2020. Correlation coefficients are between 0.5 and 0.79 for the analysis and between 0.7 and 0.8 for the forecast (Fig. 10.5). The time series plots (Fig. 10.6) show mostly a very good agreement between model and observations, except for a small vertical offset for some stations.

*CO results for individual model forecasts:*

CO show MNMBs between -17% and 20% (Fig. 10.7). The CHIMERE model shows the largest positive MNMBs of all models. Correlation coefficients are between 0.23 and 0.8 for the forecasts. The EURAD model mostly shows the weakest performance.

*Results for the individual model analyses:*

CO show MNMBs between -16% and 30%, except for the MATCH model, which shows large positive MNMBs (up to 60%) (Fig. 10.8). Correlation coefficients between the models vary significantly and range between 0.1 and 0.78.

# 11 Comparisons with MOPITT CO

## 11.1 Summary

MOPITT satellite data show relatively high CO values in September over several northern regions of Europe (e.g., Norwegian Sea, north of Germany, Lithuania). In October and November, the values are relatively low, especially over Spain in November. The ENSEMBLE forecast data show good agreement with the satellite observations. The bias is within 20% in September and within 10% in October and November. The bias shows mostly underestimations during September and October. In November, slight overestimation can be seen over the most terrestrial part of domain. The analysis data are very similar to the forecast data.

## 11.2 Method

CO total column forecasts over Europe from nine regional models and the model ENSEMBLE are compared with CO total column retrievals from MOPITT Version 8(thermal infrared radiances) (Emmons et. al., 2009). Modelled CO data were converted from µg/m³ to VMR by using temperature obtained from CAMS-global (o-suite) model. Pressure at the middle of the layers was also interpolated from the global model. Regional model data are available from the surface up to altitude of 5 km. For the comparison with satellite retrievals, the averaging kernels were applied to the modelled data.

Regional model data up to 5 km were merged with CAMS-global data above 5 km in order to minimize uncertainty error. We performed several confidence tests to establish the method. To check the error due to coarse sampling of the profiles up to 5 km as provided by the regional models, CAMS-global data were sampled at the height levels of the regional models up to 5 km and merged with the CAMS-global original levels above 5 km. Comparison of this results with the original CAMS-global data showed that the errors due to coarse sampling of the profiles up to 5 km were very small. Both results showed slight underestimation of the MOPITT data. CAMS-global values up to 5 km sampled at the height levels as the regional models and ENSEMBLE data without merging with the levels above 5km show overestimation of the satellite data over almost entire region. From this we concluded that error due to missing values above 5 km is significant and merging the regional data with CAMS-global values above 5 km is necessary for the proper comparison.

MOPITT satellite data show relatively high CO values in September over several northern regions of Europe (e.g., Norwegian Sea, north of Germany, Lithuania). In October and November, the values are relatively low, especially over Spain in November. The ENSEMBLE forecast data show good agreement with the satellite observations. The bias is within 20% in September, showing underestimation over the regions with high CO values. In October and November, the bias is within 10%. The bias shows mostly underestimations during September and October. In November, slight overestimation can be seen over the most terrestrial part of domain. All the models have very similar patterns to ENSEMBLE with some exceptions. CHIMERE shows smaller negative bias in September and bigger positive bias in October and November (up to 20%). LOTOS-EUROS have a negative bias up to 30% over Norwegian Sea in November. The analysis ENSEMBLE data are in general very similar to the forecast data with slightly smaller negative bias, though the individual models show some deviations. MATCH has an

extended area with a positive bias up to 30% over the central part of domain for all months. SILAM shows overestimation by about 20% over the several spots in central part of domain.

MOPITT

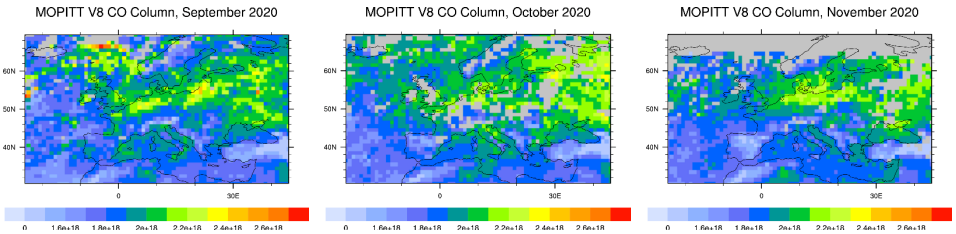


ENS-MOPITT
Forecast (0H24H)

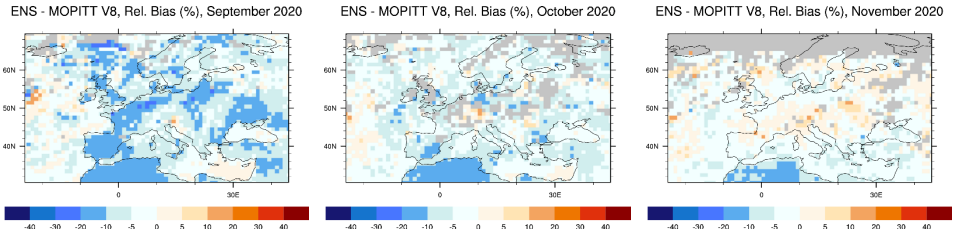


EMEP-MOPITT
Forecast (0H24H)

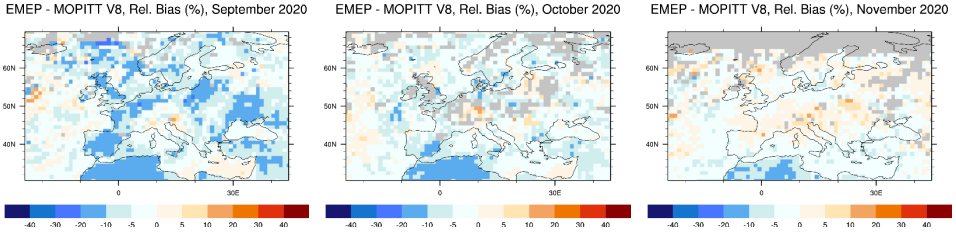


EURAD-MOPITT
Forecast (0H24H)

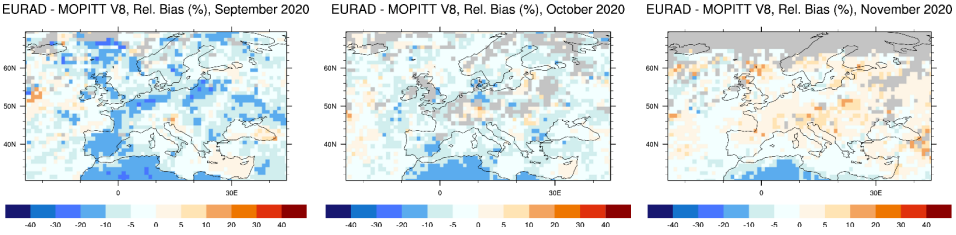


CHIMERE-MOPITT
Forecast (0H24H)

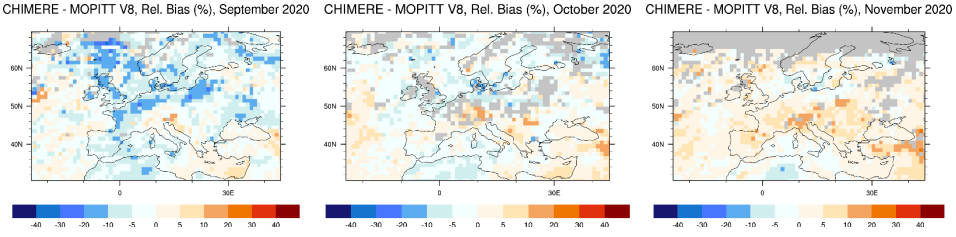


LOTOS-EUROS-MOPITT
Forecast (0H24H)

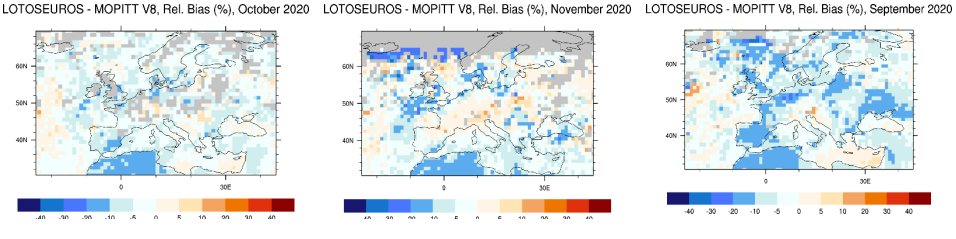

SILAM-MOPITT Forecast (0H24H)

MATCH-MOPITT Forecast (0H24H)

MOCAGE-MOPITT Forecast (0H24H)

GEMAQ-MOPITT Forecast (0H24H)

DEHM-MOPITT Forecast (0H24H)

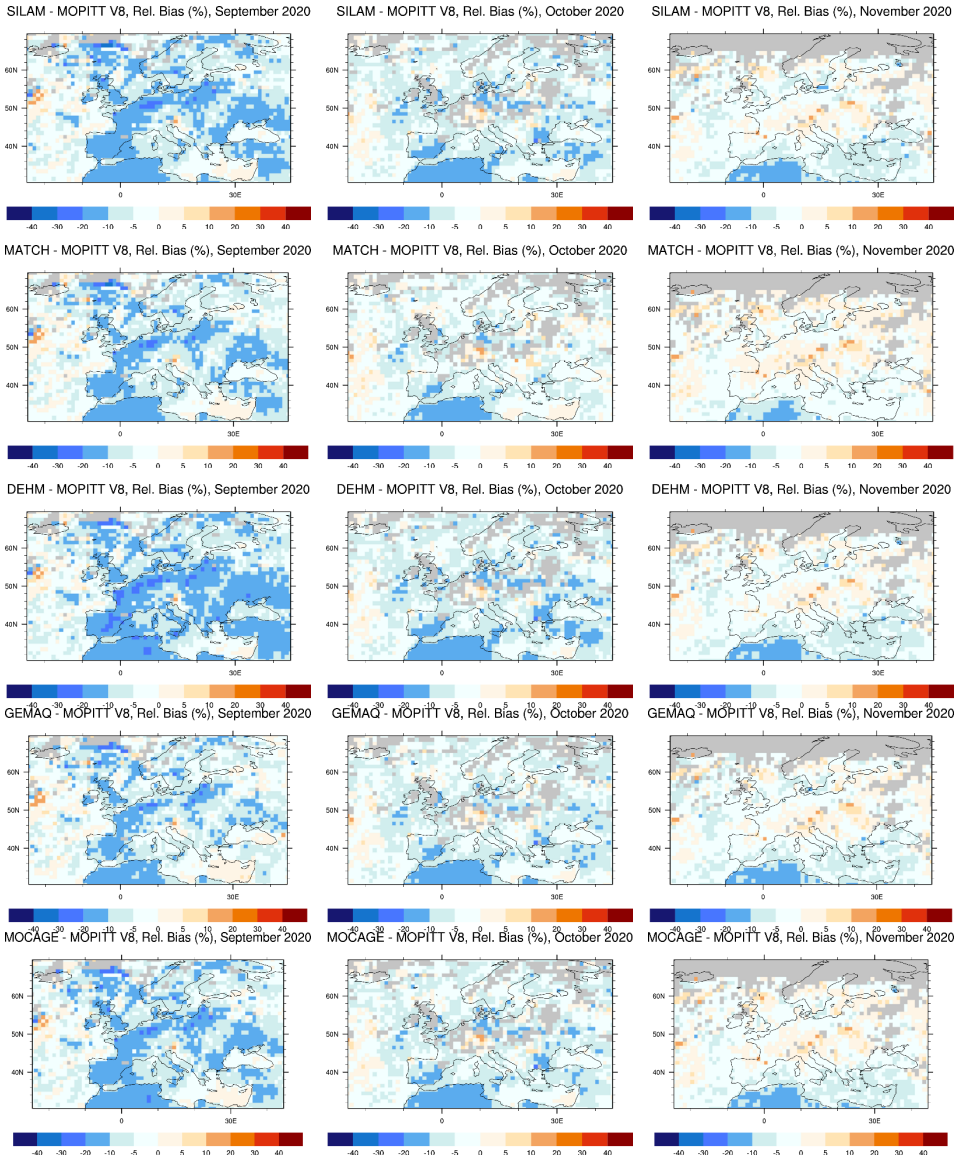


Figure 11.1. CO total column for MOPITT V8 satellite retrievals (top row, in molecules/cm$^2$), relative difference between the regional forecasts of the nine models and the ENSEMBLE and MOPITT (other rows) for September (left column), October (middle column) and November 2020 (right column). Grey colour indicates missing values.

MOPITT

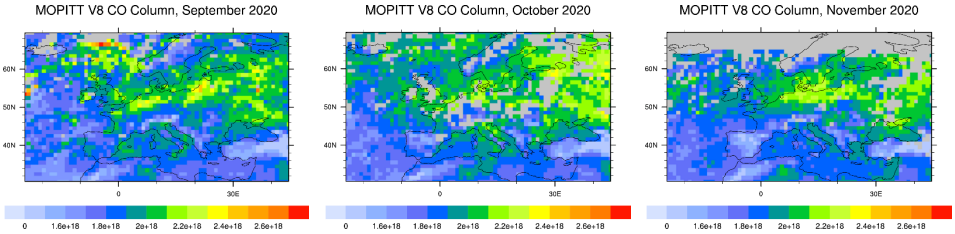


ENS-MOPITT
Analysis (-24H-1H)

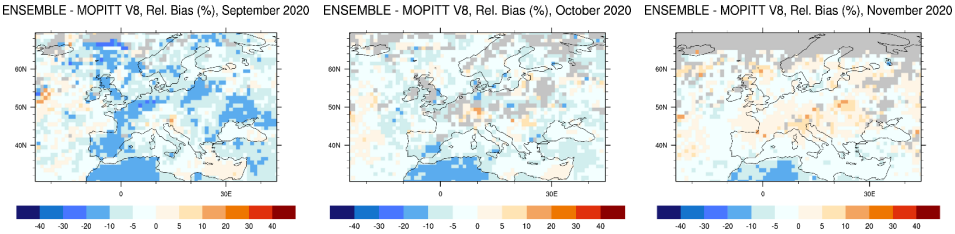


EMEP-MOPITT
Analysis (-24H-1H)

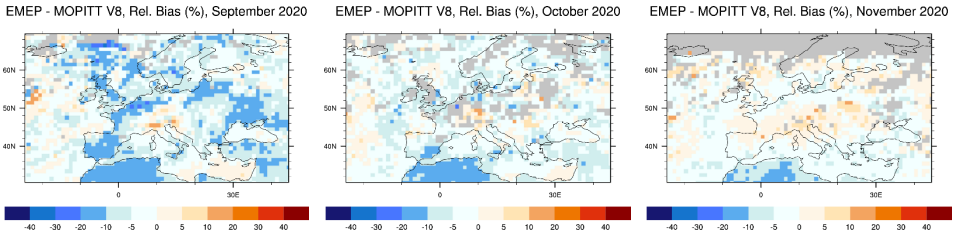


EURAD-MOPITT
Analysis (-24H-1H)

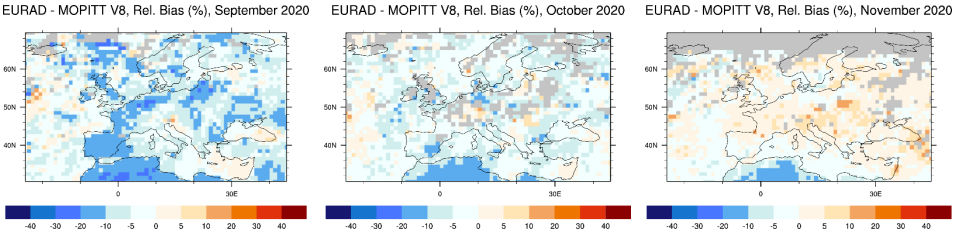


CHIMERE-MOPITT
Analysis (-24H-1H)

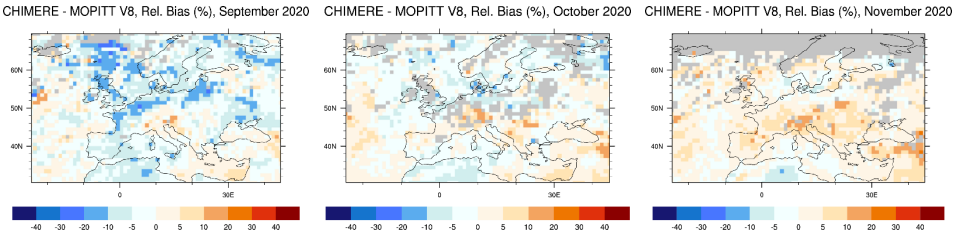


LOTOS-EUROS-MOPITT
Analysis (-24H-1H)

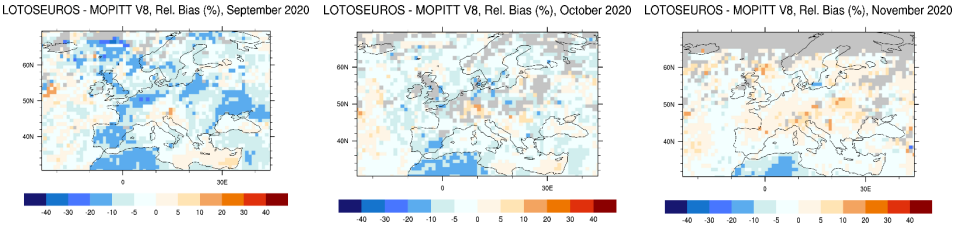

SILAM-MOPITT Analysis (-24H-1H)

MATCH-MOPITT Analysis (-24H-1H)

MOCAGE-MOPITT Analysis (-24H-1H)

GEMAQ-MOPITT Analysis (-24H-1H)

DEHM-MOPITT Analysis (-24H-1H)

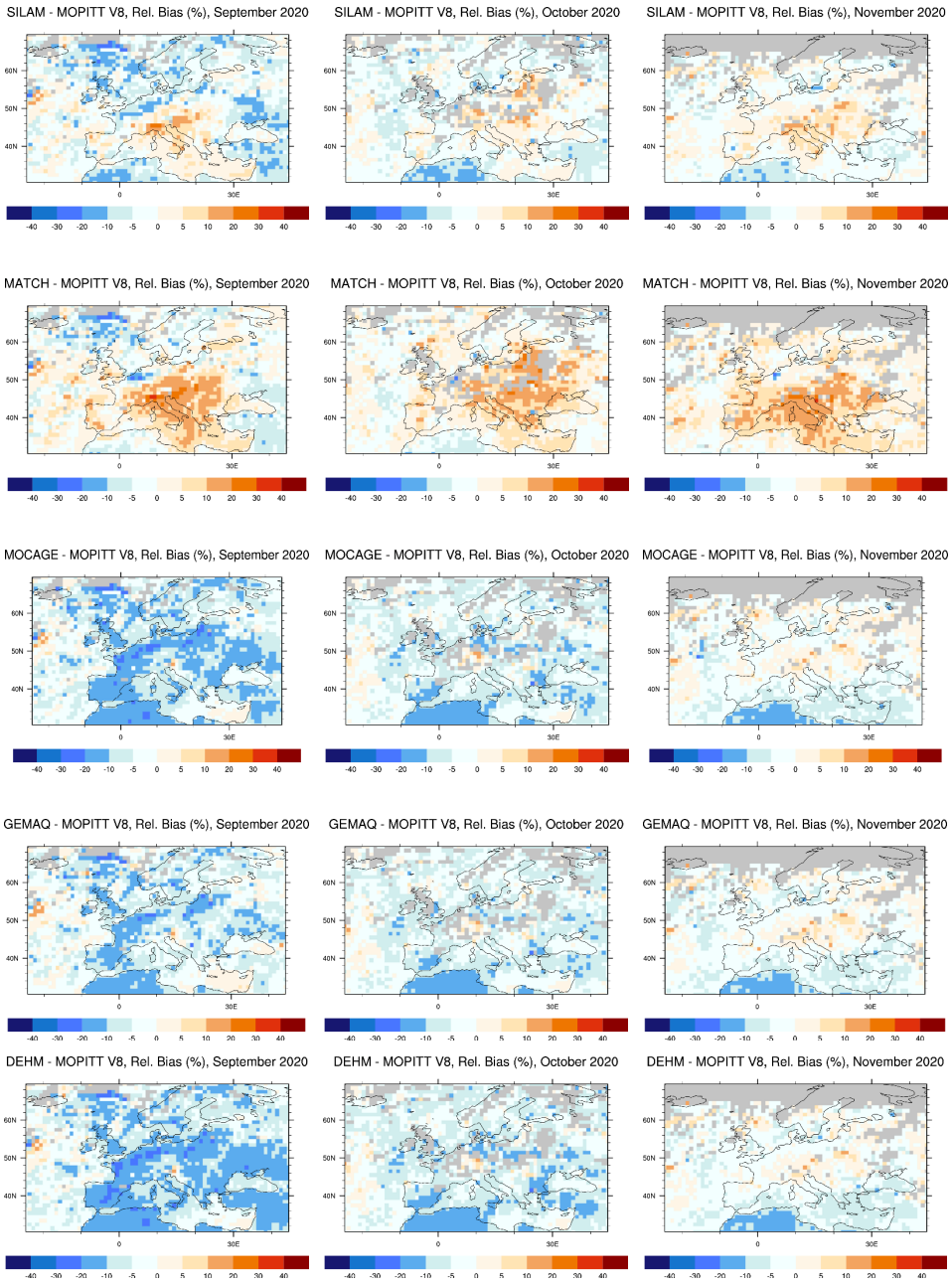


Figure 11.2. CO total column for MOPITT V8 satellite retrievals (top row, in molecules/cm$^2$), relative difference between the regional analyses of the nine models and the ENSEMBLE and MOPITT (other rows) for September (left column) October (middle column) and November 2020 (right column). Grey colour indicates missing values.

# 12 Summary of issues identified in individual models

This section provides a short overview of the main, model specific issues of this report.

*CHIMERE*

Ozone and CO cross sections at the lateral boundaries show features that are not in line with what is seen in CAMS-global or the other models (figs 3.13 and 3.14). This indicates a possible issue with the CAMS-global boundary conditions implementation. Comparison with the high altitude and GAW stations also indicates relatively high MNMBs for ozone (figs 8.4 and 10.3) and CO (fig 10.7).

*EURAD*

Ozone correlation coefficients at high altitude and GAW stations are much lower than for CAMS-global and the other models in both forecasts and analyses (figs 8.5, 10.3 and 10.4). Similar results are found in the correlation coefficients for CO based on comparisons at the GAW stations for the forecasts (fig 10.7).

*LOTOS-EUROS*

The model has exhibited a drop in the concentrations of most species at the beginning of November (fig 3.11). This is also visible in the MNMBs from the ozone sondes (fig. 9.2). The reasons behind this behaviour have not been yet identified. Differences between forecasts and analyses for ozone at 5000m seem to be large compared most other models and exhibit some unexpected spatial features (fig 3.18).

*MATCH*

Similar to past findings, the Benelux area appears to be introducing a correction in the analysis for CO that is strongly to the opposite direction of that in the rest of the domain (fig 3.19). This may be indicative of issues in the pre-processing of the observations that are assimilated in the model. The model generally seems to be still over-correcting for CO concentrations as evidenced by the MNMBs at the GAW stations (fig 10.8) and MOPITT (fig 11.2)

*MOCAGE*

High PM10 concentrations are spotted over the Atlantic, up to 250m above the surface (fig 3.9). The western boundary for PM10 is also quite high, while the southern boundary is low (fig 3.13), indicating possible issues with the implementation of the CAMS-global boundary conditions.

SILAM

Comparison with high-altitude EEA Air Quality e-reporting surface stations for ozone, reveal large negative biases at alpine stations, which are not observed in the rest of the models (fig 8.4).

# 13 Acknowledgements

The authors acknowledge all EARLINET and European ACTRIS/Aeronet data providers for providing aerosol lidar profiles and sun photometer data available from the ACTRIS data portal (http://actris.nilu.no), and the Aeronet NRT data dissemination system respectively (https://aeronet.gsfc.nasa.gov). The ACTRIS 2 project (http://www.actris.eu) has received funding from the European Union's Horizon 2020 research and innovation program under grant agreement No 654109.

We wish to acknowledge the provision of GAW hourly NRT station data by: the National Air Pollution Monitoring Network (NABEL) (Federal Office for the Environment FOEN and Swiss Federal Laboratories for Materials Testing and Research EMPA) for Jungfraujoch station, the Umweltbundesamt (UBA, Germany) for Zugspitze (Schneefernerhaus) station, the Umweltbundesamt (Austria) for Sonnblick station, the Observatory Hohenpeissenberg (Deutscher Wetter Dienst, DWD) for Hohenpeissenberg station, and the Institute of Atmospheric Sciences and Climate (ISAC) of the Italian National Research Council (CNR) for Monte Cimone station.

We wish to acknowledge the provision of ozone sonde data by the World Ozone and Ultraviolet Radiation Data Centre established at EC in Toronto (http://woudc.org), by the Data Host Facility of the Network for the Detection of Atmospheric Composition Change established at NOAA (http://ndacc.org), and by the Norwegian Institute for Air Research (http://nilu.no).

We acknowledge the EEA Air quality e-reporting Network (https://www.eea.europa.eu/data-and-maps/data/aqereporting-8) for the provision of hourly NRT station observations.

We wish to acknowledge the Department of Labour Inspection - Ministry of Labour and Social Insurance, of Cyprus (http://www.airquality.dli.mlsi.gov.cy/) for the provision of hourly NRT ozone data from Mountain Troodos station.

The programmes MOZAIC and CARIBIC, and the current Research Infrastructure IAGOS are operated with support from the European Commission, national agencies in Germany (BMBF), France (MESR), and the UK (NERC), and the IAGOS member institutions (http://www.iagos.org/partners). The participating airlines (Lufthansa, Air France, Austrian, China Airlines, Iberia, Cathay Pacific, Air Namibia, Sabena) supported IAGOS by carrying the measurement equipment free of charge since 1994. The data are available at http://www.iagos.fr thanks to additional support from AERIS (CNRS and CNES).

GOME2 lv1 radiances and irradiances were provided by EUMETSAT.

We acknowledge the NASA Langley Research Center Atmospheric Science Data Center for providing the MOPITT data.

AUTH acknowledges the AUTH Scientific Computing Centre (https://it.auth.gr/en/services) for providing technical and infrastructure support for data analysis performed in this WP.

# 14 References

*Richter, A., Begoin, M., Hilboll, A., and Burrows, J. P.: An improved NO2 retrieval for the GOME-2 satellite instrument, Atmos. Meas. Tech. , **4**, 1147-1159, doi:10.5194/amt-4-1147-2011, 2011.*

*Ackermann, J. (1998). The extinction-to-backscatter ratio of tropospheric aerosol: A numerical study. Journal of atmospheric and oceanic technology, 15(4), 1043-1050.*

*ACTRIS Deliverable WP6/D6.21,*
*http://www.actris.net/Portals/97/deliverables/PU/WP6_D6.21_M45v2.pdf*

*Cattrall, C., Reagan, J., Thome, K., & Dubovik, O. (2005). Variability of aerosol and spectral lidar and backscatter and extinction ratios of key aerosol types derived from selected Aerosol Robotic Network locations. Journal of Geophysical Research: Atmospheres, 110(D10).*

*Chin, M., Ginoux, P., Kinne, S., Torres, O., Holben, B. N., Duncan, B. N., ... & Nakajima, T. (2002). Tropospheric aerosol optical thickness from the GOCART model and comparisons with satellite and Sun photometer measurements. Journal of the atmospheric sciences, 59(3), 461-483.*

*Eskes, H.J., S. Basart, A. Benedictow, Y. Bennouna, A.-M. Blechschmidt, S. Chabrillat, Y. Christophe, E. Cuevas, H. Flentje, K. M. Hansen, J. Kapsomenakis, B. Langerock, M. Ramonet, A. Richter, M. Schulz, N. Sudarchikova, A. Wagner, T. Warneke, C. Zerefos, Observation characterisation and validation methods document, Copernicus Atmosphere Monitoring Service (CAMS) report, CAMS84_2018SC2_D6.1.1-2020_observations_v5.pdf, January 2021. Available from: http://atmosphere.copernicus.eu/user-support/validation/verification-global-services*

*Eskes, H., Huijnen, V., Arola, A., Benedictow, A., Blechschmidt, A.-M., Botek, E., Boucher, O., Bouarar, I., Chabrillat, S., Cuevas, E., Engelen, R., Flentje, H., Gaudel, A., Griesfeller, J., Jones, L., Kapsomenakis, J., Katragkou, E., Kinne, S., Langerock, B., Razinger, M., Richter, A., Schultz, M., Schulz, M., Sudarchikova, N., Thouret, V., Vrekoussis, M., Wagner, A., and Zerefos, C.: Validation of reactive gases and aerosols in the MACC global analysis and forecast system, Geosci. Model Dev., 8, 3523-3543, doi:10.5194/gmd-8-3523-2015, 2015.*

*Flemming, J., Huijnen, V., Arteta, J., Bechtold, P., Beljaars, A., Blechschmidt, A.-M., Diamantakis, M., Engelen, R. J., Gaudel, A., Inness, A., Jones, L., Josse, B., Katragkou, E., Marecal, V., Peuch, V.-H., Richter, A., Schultz, M. G., Stein, O., and Tsikerdekis, A.: Tropospheric chemistry in the Integrated Forecasting System of ECMWF, Geosci. Model Dev., 8, 975-1003, doi:10.5194/gmd-8-975-2015, 2015.*

*Joly, Mathieu, and Vincent-Henri Peuch, Objective classification of air quality monitoring sites over Europe, Atmospheric Environment 47, 111-123, 2012.*

*Katragkou, E., Zanis, P., Tsikerdekis, A., Kapsomenakis, J., Melas, D., Eskes, H., Flemming, J., Huijnen, V., xsxcInness, A., Schultz, M. G., Stein, O., and Zerefos, C. S.: Evaluation of near-surface ozone over Europe from the MACC reanalysis, Geosci. Model Dev., 8, 2299-2314, doi:10.5194/gmd-8-2299-2015, 2015.*

*Marécal, V., Peuch, V.-H., Andersson, C., Andersson, S., Arteta, J., Beekmann, M., Benedictow, A., Bergström, R., Bessagnet, B., Cansado, A., Chéroux, F., Colette, A., Coman, A., Curier, R. L., Denier van der Gon, H. A. C., Drouin, A., Elbern, H., Emili, E., Engelen, R. J., Eskes, H. J., Foret, G., Friese, E., Gauss, M., Giannaros, C., Guth, J., Joly, M., Jaumouillé, E., Josse, B., Kadygrov, N., Kaiser, J. W., Krajsek, K., Kuenen, J., Kumar, U., Liora, N., Lopez, E., Malherbe, L., Martinez, I., Melas, D., Meleux, F., Menut, L., Moinat, P., Morales, T., Parmentier, J., Piacentini, A., Plu, M., Poupkou, A., Queguiner, S., Robertson, L., Rouïl, L., Schaap, M., Segers, A., Sofiev, M.,*

*Tarasson, L., Thomas, M., Timmermans, R., Valdebenito, Á., van Velthoven, P., van Versendaal, R., Vira, J., and Ung, A.: A regional air quality forecasting system over Europe: the MACC-II daily ensemble production, Geosci. Model Dev., 8, 2777-2813, doi:10.5194/gmd-8-2777-2015, 2015.*

*Morcrette, J.-J., O. Boucher, L. Jones, D. Salmond, P. Bechtold, A. Beljaars, A. Benedetti, A. Bonet, J. W. Kaiser, M. Razinger, M. Schulz, S. Serrar, A. J. Simmons, M. Sofiev, M. Suttie, A. M. Tompkins, and A. Untch: Aerosol analysis and forecast in the ECMWF Integrated Forecast System. Part I: Forward modelling, J. Geophys. Res., 114, D06206, doi:10.1029/2008JD011235, 2009.*

*Mortier, A., Goloub, P., Derimian, Y., Tanré, D., Podvin, T., Blarel, L., ... & Ndiaye, T. (2016). Climatology of aerosol properties and clear-sky shortwave radiative effects using Lidar and Sun photometer observations in the Dakar site. Journal of Geophysical Research: Atmospheres.*

*Müller, D., Ansmann, A., Mattis, I., Tesche, M., Wandinger, U., Althausen, D., & Pisani, G. (2007). Aerosol-type-dependent lidar ratios observed with Raman lidar. Journal of Geophysical Research: Atmospheres, 112(D16).*

*Omar, A. H., Winker, D. M., Vaughan, M. A., Hu, Y., Trepte, C. R., Ferrare, R. A., ... & Kuehn, R. E. (2009). The CALIPSO automated aerosol classification and lidar ratio selection algorithm. Journal of Atmospheric and Oceanic Technology, 26(10), 1994-2014.*

*Pappalardo, G., A. Amodeo, A. Apituley, A. Comeron, V. Freudenthaler, H. Linne, A. Ansmann, J. Bösenberg, G. D'Amico, I. Mattis, L. Mona, U. Wandinger, V. Amiridis, L. Alados-Arboledas, D. Nicolae, and Wiegner, M.: EARLINET: towards an advanced sustainable European aerosol lidar network, Atmos. Meas. Tech., 7, 2389–2409, www.atmos-meas-tech.net/7/2389/2014/, doi:10.5194/amt-7-2389-2014, 2014.*

*Richter, A., Begoin, M., Hilboll, A., and Burrows, J. P.: An improved NO2 retrieval for the GOME-2 satellite instrument, Atmos. Meas. Tech. , **4**, 1147-1159, doi:10.5194/amt-4-1147-2011, 2011.*

*Vinken, G. C. M., Boersma, K. F., van Donkelaar, A., and Zhang, L.: Constraints on ship NOx emissions in Europe using GEOS-Chem and OMI satellite NO2 observations, Atmos. Chem. Phys., 14, 1353-1369, doi:10.5194/acp-14-1353-2014, 2014.*

*Wagner, A., M. Schulz, Y. Christophe, M. Ramonet, H. J. Eskes, S. Basart, A. Benedictow, Y. Bennouna, A.-M. Blechschmidt, S. Chabrillat, E. Cuevas, A. El- Yazidi, H. Flentje, K.M. Hansen, U. Im, J. Kapsomenakis, B. Langerock, A. Richter, N. Sudarchikova, V. Thouret, T. Warneke, C. Zerefos, Validation report of the CAMS near-real-time global atmospheric composition service: Period September - November 2019, Copernicus Atmosphere Monitoring Service (CAMS) report, CAMS84_2018SC2_D1.1.1_SON2019_v1.pdf, February 2020, doi:10.24380/xzkk-bz05.*

Copernicus Atmosphere Monitoring Service

ECMWF - Shinfield Park, Reading RG2 9AX, UK

Contact: info@copernicus-atmosphere.eu